MULTI-CAMERA HIGH-THROUGHPUT PLANT ROOT PHENOTYPING SYSTEM

A Thesis presented to

the Faculty of the Graduate School

at the University of Missouri

In Partial Fulfillment

of the Requirements for the Degree

Master of Science

---

by

Anand Seethepalli

Dr. Alina Zare, Thesis Supervisor

DEC 2016

The undersigned, appointed by the Dean of the Graduate School, have examined the thesis entitled:

MULTI-CAMERA HIGH-THROUGHPUT PLANT
ROOT PHENOTYPING SYSTEM

presented by Anand Seethepalli,
a candidate for the degree of Master of Science and hereby certify that, in their opinion, it is worthy of acceptance.

Dr. Alina Zare

Dr. Felix Fritschi

Dr. Scott Kovaleski

To my parents

ACKNOWLEDGMENTS

First, I would like to thank Dr. Alina Zare, my thesis advisor, who guided me giving constructive criticism in the research directions, presentations participated in seminars and discussions.

I would like to sincerely thank Dr. Felix Fritschi and Dr. Scott Kovaleski, my thesis committee, for their invaluable suggestions to further improve my research.

I would also like to thank Almtarfi, Hussien and Dr. Larry Matthew York, who gave invaluable suggestions on improving the experimental system used in this study for the years 2015 and 2016 respectively. I would also like to thank all the lab members in Dr. Fritschi lab who helped me operating the setup system through the years 2014, 2015 and 2016.

I am very grateful to Xiaoxiao Du for helping me collect data from field for the year 2014. I am also thankful to my lab members for their support in TigerSense lab.

Finally, I would like to express my deepest gratitude to my parents motivating me and continuously encouraging me through my years of study. Without their continuous support, this study would not have been possible.

TABLE OF CONTENTS

LIST OF TABLES

Table Page

LIST OF FIGURES

Figure Page

ABSTRACT

Plant root phenotyping is a key component in plant breeding and selection for desireable root properties. Preferable root traits can not only help a plant to grow faster but also allow for more dense and deep root system architectures (RSA) that aid in making the plant resistant to drought conditions. In this thesis, an efficient high-throughput plant root phenotyping system that can take the images of RSA from various angles using multiple cameras is presented. This system needs to be a high-throughput system such that is can be used to phenotype up to hundreds or thousands of plant roots quickly.

In this research, a novel multi-camera root imaging system and a phenotyping procedure, which can extract traits that correlate better than a single-camera root imaging system, is introduced. The system consists of a set of six cameras that take images of a plant root from six different directions. A segmentation procedure using the Expectation-Maximization (EM) algorithm is developed and employed to iteratively distinguish plant root pixels from background pixels. It is also shown that this proposed method provides a better segmentation results of plant root images when compared to the thresholding methods used in previously published research. Another novel contribution in this thesis is the automated extraction of root traits from the imagery collected. It is shown that these automated traits correlate to manually measured traits that have been previously shown to have strong relationships with genes associated with RSA. Results also show that merging of the autonomously extracted traits from multiple cameras provide higher correlation with the manual traits as opposed to traits measured from only one camera. The data for the plant

roots are collected over a period of 3 years, each year improving the imaging system and the underlying software used to control the system. Further, it is shown that the traits are extracted with a much faster implementation using the multi-camera imaging system when compared to a previous plant root phenotyping platform.

Chapter 1

Introduction

Climate change around the world affects the agricultural output throughout the world [2]. Increase in global warming and sea levels cause global average temperatures to raise and water tables under the soil to go more deeper. This may lead to a period of prolonged shortage of water supply including rain leading us to drought. The existence of drought may further lead us to several consequences such as hunger, malnutrition, mass migration, reduced electricity production. Hence, it is in our hands to cut the reasons that cause the adverse climate change and also at the same time develop technologies in agriculture to cultivate plants that can tolerate drought situations. This study aims to address the second problem. For this, we need to understand the RSA of the genes related to the plant roots that contribute to drought resistance. In order to identify the genes controlling the RSA, we need to efficiently phenotype the plant roots. These phenotypic traits are later used in future, for identifying the underlying genotypes that control plant root growth. For example, larger root depth of a plant root helps the plant to attach to the soil and hence become flood resistant.

Thus, the root depth can be taken as a trait that can be used to compare with other plants with different root depths. This comparison methods may be used further to separate the genotypes in a specific plant species that have larger root depth. Although many plant root phenotyping systems exist today, these systems either involve manual feature trait extraction or trait feature extraction from single cameras [3, 1, 4, 5]. When extracting traits from single cameras, the complete root topology may not be captured in the image, which may lead to less reliable trait values. When a single camera system is used with a turn-table, to capture the RSA from various angles, the imaging system may not be useful for high-throughput applications as it would take several minutes for the system to completely image the plant root.

This study proposes a multi-camera high-throughput plant root phenotyping system, that can efficiently take images of the plant roots, perform image segmentation and extract features of Root System Architectures (RSA) that have high correlation with the manually extracted features. We designed the phenotyping system consisting of multiple cameras that take images of a plant root from different angles. These cameras are connected to a USB hub which is in turn connected to a PC. These cameras are programmed using Canon Hacker Development Kit (CHDK) ([6, 7, 8]) to take photos of the plant roots from different angles simultaneously. Once the images were taken, they were downloaded to the PC and segmentation was performed on them. The segmentation consists of EM algorithm that separates root pixels from the background images. After acquiring a binary image for every original image, feature extraction is performed on the binary image by performing line scanning and skeletonization operations. The extracted traits in the feature extraction are further used in correlation analysis with the manually extracted features to verify the consistency

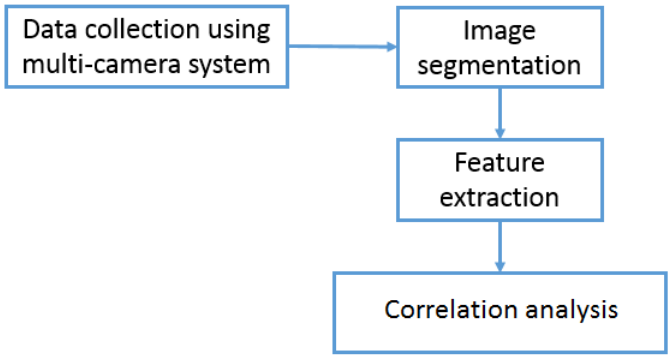

Figure 1.1: Procedure for plant root phenotyping

of automatically extracted traits from the images.

1.1 Goals of the study

The primary goal of this study is to make a automatic working system that can extract the traits from the photographed images of plant roots using camera programming, image processing and segmentation algorithms. The extracted traits from the images should correlate to the manually extracted traits of the plant roots. The advantage of such a system is that it completely eliminates the need for manual feature extraction which is prone to errors and excessive time consumption. Another goal of this study is that the features extracted should be reliable enough for future analysis for identification of genotypes. This is made possible using the multi-camera system that takes images of plant roots from different angles. This multiple angle perspective of the same plant root enables us to extract the best features that can be used in future research. For example, the plant root width from one perspective may be smaller, whereas the same plant seen from a different perspective may show larger root width.

Hence, for the phenotypic trait called maximum width, we can take the maximum width of the root across images from multiple cameras. The final goal of this study is to show that it is a high-throughput system. That is, unlike the phenotyping systems that take multiple images using a turn table [4, 5], we take images from multiple cameras simultaneously. The advantage is that the speed of imaging the plant roots can be very fast. Further, we implemented the algorithm for segmentation that makes use of hardware acceleration. We show that with this combined setup, we can image and process hundreds of images per day.

1.2 Assumptions

When designing the experimental setup box for imaging the roots, it is necessary for us to determine the size of the box in order to record the image of the root completely. For this reason, we assumed that the maximum width and height of the root systems to be imaged will be 20 inches or less. When segmenting the images, the root pixels are assumed to be darker than background. This is because usually the plant roots have a color ranging from light brown to black. The roots may sometimes be red in color. The color of the roots just after digging, look darker because they are wet and are washed to remove dirt. Further, when imaging the plant roots, some lateral roots may cast a shadow on other roots, which leads us to note that the roots appear even darker. If we select the background to be black, it would be hard for the segmentation algorithms to separate the root pixels from the background. Hence, we select a bright colored background such as light blue. Thus the segmentation algorithms also assume that the background has a lighter color than the root.

Chapter 2

Literature Review

This section describes the related work done in high-throughput root phenotyping. We first discuss about the recent work in modeling root systems, which is used by some of the available open source softwares for phenotyping. We then discuss the imaging and phenotype extraction methods and finally describe the recent work in discriminating the genotypes given the phenotypic data.

2.1 Identification of root topology

Recent advances in imaging and computing technologies had enabled us to efficiently analyze plant root images [9, 10]. These methods use complex algorithms such as the EM algorithm [11] with multiple clusters and assign some clusters to plant root or perform simpler ways to generate the segmented image such as intensity thresholding [1, 3, 12, 13]. The segmented image may then be analyzed for further analysis for extraction of phenotypic traits. For example, Janusch and Busch [14] proposed to

identify root topology using Reeb graphs. Chen et al. (2006) [15] describes method to determine the branching structure in wheat using Markov chains [16]. However, this methods need to have simpler root system to extract traits with higher accuracy.

Recently modeling plant roots by performing 3-D reconstruction is gaining traction. In 2012, Mairhofer et al. [17] described a procedure to determine root topology from x-ray CT images containing root cross-sections by scanning the image stack vertically and predicting the possible location of root in the next image using the location of the root in the current image. RooTrak process on the volume generated by inverse radon transform on the x-ray CT images taken from the side view of the plant root. The visual tracking was achieved using level-set functions. Although complex root architectures were successfully identified by the tool, the procedure is still computationally intensive to perform any high throughput phenotyping. Similarly, Zhou et al. [18] describes a method to perform 3-D reconstruction on x-ray CT images containing cross-sectional root images by using Marching Cubes algorithm [19]. Zheng et al. [20] performed reconstruction on RGB images, by first segmenting the images, performing reconstruction using visual hull followed by selecting nearest connected components as the final reconstruction.

Methods also exist that analyze the root growth such as KineRoot [21], ArchiSimple [22] and [23]. Variation in the root topology with varying environmental conditions were also studied. Balestri et al. [24] discusses the changes in the root topology when a seagrass is grown in different soil conditions quantitatively. Further studies include modeling of roots [25] and growth of roots [26] in time series. Studies also include imaging the roots by parts and stitch them [27] using SIFT keypoint matching procedure [28] and estimation of root system architecture by modeling root length or

number of roots per unit volume or root density [29].

2.2 Data collection and feature extraction

Recently, two novel strategies were proposed for high-throughput phenotyping of plant roots: Digital Imaging of Root Traits (DIRT) [3] and Root Estimator for Shovelomics Traits (REST) [1] systems. The procedures consist of a root imaging system for excavated roots followed by image processing, feature extraction and analysis of the extracted features.

In the DIRT system, each excavated root is first washed and a small portion of the root is excised. This excised root provides better understanding on the topology of the lateral roots. The root crown, its excised root along with a tag and a scale marker are imaged by placing them on a black background. The scale marker of fixed size is used in every image so as to accurate estimate the size of the root crown from the images. The background was selected to be black in order to easily obtain the segmented image. After segmenting and separating the image into several parts, the marker in the image is used to calibrate the feature measurements. A skeletal structure or Root Tip Path (RTP) is extracted to further extract features from not only the segmented image, but also from the medial axis such as the width of the roots. The features so extracted are within the standard deviation of 10% when testing the repeatability of the experimental system. 1445 cowpea roots representing 188 genotypes were imaged and a Pearson correlation of 0.49 is achieved from the image based features compared to manually extracted features. Statistical analysis was then performed on the extracted traits.

In the REST system, each rootstock is divided lengthwise into two halves. The larger half is used for root phenotyping from images. Angles were measured using a scoreboard and nodal roots were counted as manual traits. The rootstock was photographed in a custom made imaging tent. The other half is used for counting nodal roots for manually noting the branching density. This imaging system consists of a root imaging tent with cuboid shaped backside and prism shaped front side. The root crown with 25 cm stalk is hung from top. Uniform illumination is achieved using two reflector coils on the opposite of the flash lights. The images were taken with a 10 megapixel Canon EOS 400D camera with a focal length of 35 mm, aperture of 9.0, exposure time of 1 second. The root background color was selected to be black. The images were segmented using Otsu's thresholding method [30]. To reduce errors standing out of the bulk root stock, the evaluated area was reduced to 95% in width and height for further analysis. Some of the features extracted are root system filling factor as the ratio of root pixels by the number of pixels in the convex hull. Other features include area of the convex hull, maximum width and number of holes. The extracted features are then used in statistical analysis.

Recent work also include phenotyping plant roots that were placed in gel medium and images taken in different angles using a turn table. [4, 5]. Pantalone et al. [31] showed that drought resistance can be achieved if the roots are fibrous in nature. This work also tried to assign a rootscore to various root systems depending upon several factors such as the amount of fibrous content, size and number of nodules of the root. Topp et al. [32] extracts 2-D features from images and 3-D features from the reconstructed 3-D models. These extracted traits are used in Multivariate QTL analysis using a program called GiA Roots [33].

2.3 Statistical analysis

The idea behind performing statistical analysis is to identify the underlying genotypes. For this we need to have a high quality traits that reflect the effects caused by the underlying genotypes. Hence, to identify these effects, many studies use methods such as Analysis-of-Variance (ANOVA), Quantitative Trait Loci (QTL) [3, 1, 5, 4, 5, 32]. Advanced methods are also employed such as Support Vector Machine (SVM) [34, 35, 36] to classify the genotypes. Recently, due to the increase in the processing power of computers, we now tend to perform the feature extraction automatically using algorithms instead of manual methods. In order to ensure that the traits extracted from the images are as reliable as the manual features, we need to check if the extracted features from images correlate well to the manually extracted features. It may be the case that automated features are more accurate than manual features. Thus, these methods also provide Pearson and Spearman correlation coefficients to demonstrate that the features extracted from the image correlate to the manual features. The REST system performed correlation and heritability analysis to show that the image features are valid and are silimar to the traits inherited from the parent plant roots. The following text describes the method used by DIRT system to determine if the genotypes are well separated.

The statistical analysis tools such as Relative Phenotypic Variation (RPV) and Heritability (H) are used for cluster separability analysis and identifying most heritable traits in the genotypes. RPV is a heuristic that determines how much the genotypes are separated using the extracted features. For a given trait, it is defined as the ratio of variance V_d of the trait of all the roots of the data and the average variance per genotype V_{avg}.

$$RPV = \frac{V_d}{V_{avg}} \tag{2.1}$$

The authors describe that the RPV value of 1 indicates that the trait is evenly distributed over all the genotypes. The DIRT system shows an RPV of above 2.5 for traits such as root density, median/maximum width and spatial root distribution, which shows that these traits can differentiate between genotypes. Although RPV may be used to describe the features, this heuristic may not accurately describe the cluster separability of the genotypes. More analysis can be found the next section.

The broad-sense Heritability (H) is defined as the variation in the phenotypic trait in all the genotypes (V_d) to the average variance per genotype (V_{avg})

$$H^2 = \frac{V_d}{V_{avg} + V_d} \tag{2.2}$$

The most heritable traits was the average root density in image features.

Chapter 3

Data Collection Procedure

Collection of data involves acquiring images of different plant roots using a multi-camera system that has the following properties. The system should take images of the same plant root in different angles so that the shape of the root can be recorded from all angles for better trait extraction. Another property needed for efficient design of the multi-camera setup system is to make it less laborious for the people operating it and to easily transport it from one place to another. This involves a robust design of the setup box so that the plant roots can be replaced easily after taking the images, take into consideration that neither the roots nor the multi-camera system in setup box do not move easily for external disturbances such as strong winds. Finally, the cameras in the multi-camera system should be able to record good quality images, that enable the segmentation algorithms to extract complete root topology of the plant roots.

For a system with aforementioned properties, in this study, we designed the multi-camera system with the help of Larry Matthew York [37, 38], consisting of a setup

box, in which a plant root is suspended and images are taken from the cameras mounted on a wooden plank inside the setup box. Multiple cameras are mounted on a horizontal wooden plank which take images of plant root at various angles. An extra camera is placed at the bottom of the setup box facing the ceiling so that the camera may capture the plant root from the lower side. The cameras on the wooden plank are placed on the plank so that these cameras form an arc, in such a way that the cameras are equidistant from the suspended plant root and that this arc subtends an angle of 90° at the suspended plant root. Each arc-segment between adjacent cameras are equal in length and subtend equal angles at the suspended root. There are a total of 5 cameras on the wooden plank. Throughout this study, the images from the extra camera at the bottom were manually observed, but no image processing and segmentation was performed due to excessive noise in the background which is present in the ceiling of the setup box. The wooden plank on which the cameras are mounted can be moved forwards or backwards so that the mounted cameras are at a distance of approximately 0.61 meters (2 feet) away from the plant root. This distance is selected based on the focal length being used in different experimentations, so that the roots can be recorded clearer. In this study, we imaged soybean plant roots which are sufficiently smaller than the maize roots and a distance of 0.61 meters suits for imaging the roots so that cameras can capture smaller lateral roots. A distance bigger than 0.61 meters may result in bigger setup box dimensions which may be difficult to transport to the field for data collection. In case of bigger roots such as maize roots, the cameras need to be further away from the root because the root occupies significantly larger space in the recorded images. A distance of 0.914 meters (3 feet) would be sufficient to image the maize roots. In the implementation for this study, we

designed a smaller experimental setup box just to take the images for soybean roots. In order for the data acquisition to be efficient, the setup system is closed in all faces of the box from external lighting caused by the sunlight such as by current weather of the day, time of the day. We isolated external lighting in our implementation by closing all the faces of the setup box with wooden planks. We painted the wooden plank that covers the background with light blue color and placed 4 daylight colored bulbs facing opposite of the background in the experimental setup box, so that the light gets diffused by the time it reaches the background. This makes sure that the shadows due to the lighting inside the box is minimized. The front open face of the setup box is closed with a white shower fabric which can diffuse the light inside the setup box in all directions inside the box. The use of fabric to close the front face of the setup box allows us to turn on the cameras, adjust them properly before starting the data collection process.

All the cameras are powered by a generator in the field. The power is fed through AC to DC adaptors for each camera instead of batteries. This allows the cameras to work the whole day long without having to replace the batteries. All the cameras are also connected to a USB hub which is in turn connected to a PC. A special software is installed on the SD cards of the cameras called Canon Hacker Development Kit (CHDK). CHDK allows us to programmatically control the camera functions by sending commands from USB using Picture Transfer Protocol (PTP). The commands include changing the optical zoom, aperture, exposure time, ISO speed, taking images of the plant root and downloading the images to the PC from the USB connection. A client program called chdkptp [39] allows us to send commands to the canon cameras that have CHDK installed on their SD cards. For information on how to install CHDK

on Canon cameras and control the cameras using the client program, please refer to Appendix A. In our implementation for camera control, of all the 6 cameras (5 on the wooden plank and one at the bottom of the setup box) we have used 3 Canon G1X cameras and 3 Canon S110 cameras. Each camera is given a unique number and is placed at a specific position in the setup box so that whenever we refer to the camera number we get an idea as to which angle the image is taken at. For example, we have selected the camera at the bottom is the camera number 1. All the Canon G1X cameras have numbers from 1 to 3 and all the Canon S110 cameras have numbers from 4 to 6. In our implementation, when we are looking at the front side of the setup box, we have selected the cameras from left to right to have the following numbers 4, 2, 5, 3, 6. This order is selected because we want different camera models to take images from different angles. Canon G1X cameras are more robust in image quality and hence a G1X camera is placed at the bottom of the setup box. The Canon S110 cameras are placed at the middle and at either ends, so that we can compare visually the images at different angles because these images come from cameras with same image sensors.

We want the multi-camera setup system to contain all the cameras which are sufficiently far away from the suspended plant root and at the same time we need to make sure the setup box is compact enough for us to easily transport to the field for data collection. For this we need to determine the minimum width of the setup box which is also the length of the wooden plank on which the cameras are mounted. Since, the cameras are placed in an arc we also need to determine the width of the wooden plank so as to place the cameras. In other words, we need to determine the dimensions of the setup box. The following section describes it in detail.

3.1 Dimensions of Experimental Setup Box

The following Figure 3.1 shows the top view of the setup box. The plant root is held at the vertex R and the five cameras are placed along the arc from A through B, equidistant from the corresponding adjacent cameras. All the cameras are equidistant from the root R.

$$AR = CR = DR = ER = BR = d \tag{3.1}$$

The total width of the setup box is given by the line segment AB. Our goal is to find the width (w) of the setup box, given the distance from the cameras to the root (d). Since, the cameras are equidistant from the root and from the adjacent cameras, we have

$$\angle ARC = \angle CRD = \angle DRE = \angle ERB = \theta \tag{3.2}$$

Also, since

$$\angle ARD = \angle ARO = 2\theta \tag{3.3}$$

we have from Figure 3.1,

$$ARsin(2\theta) = AO \tag{3.4}$$

Since AR is the camera distance from the root, AR = d. Hence,

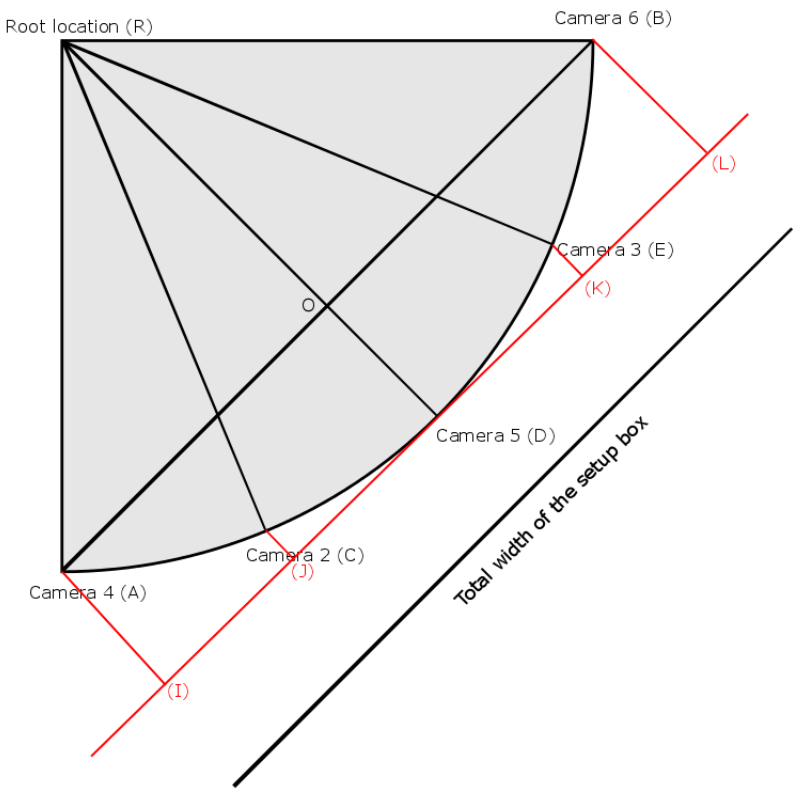

Figure 3.1: Top view of the camera setup box.

$$\begin{aligned} AO &= d\ sin(2\theta) \\ or \qquad AB &= 2AO = 2d\ sin(2\theta) \end{aligned} \tag{3.5}$$

Hence, total width f the box should be 2 $sin(2\theta)$ times the distance between the root and the cameras. Since, in this study, we are implementing the setup box to image soybean plant roots, the distance between the cameras and the root is 0.61 meters would be sufficient. Also, since the arc of the cameras subtend 90 deg at the root and the cameras are equidistant from each other, we have $\theta = 22.5$ deg. If the distance between the cameras and the root is 0.61 meters, then AB = 0.862 meters. If instead we want to increase the camera to root distance to 0.914 meters to image

large maize roots and keeping the same angle $\theta = 22.5\,\text{deg}$, then the width is AB = 1.293 meters.

The following equations provide the distance of each camera to the line segment IL (marked in red color) in Figure 3.1 and the distance of each camera from the line segment RD. We have

$$ID = LD = ARsin(2\theta) = d\ sin(2\theta) \tag{3.6}$$

$$IA = LB = AR - ARcos(2\theta) = d - d\ cos(2\theta) \tag{3.7}$$

$$JD = KD = CRsin(\theta) = d\ sin(\theta) \tag{3.8}$$

$$JC = KE = CR - CRcos(2\theta) = d - d\ cos(\theta) \tag{3.9}$$

In case of imaging soybean plant roots, we select d = 0.61 meters and $\theta = 22.5\,\text{deg}$, then the distances above are

$$ID = LD = 0.431\ meters \tag{3.10}$$

$$IA = LB = 0.179\,meters \tag{3.11}$$

$$JD = KD = 0.233\,meters \tag{3.12}$$

$$JC = KE = 0.046\, meters \tag{3.13}$$

If instead we wanted to image maize roots, we select d = 0.914 meters, and $\theta = 22.5\,\text{deg}$, then the distances above are

$$ID = LD = 0.647\, meters \tag{3.14}$$

$$IA = LB = 0.268\, meters \tag{3.15}$$

$$JD = KD = 0.350\, meters \tag{3.16}$$

$$JC = KE = 0.070\, meters \tag{3.17}$$

The calculation of experimental setup box dimensions for maize roots are given here so that we have a idea of how that size of the experimental setup box changes when larger roots are to imaged. Throughout out this study, we implemented and used the setup box designed for imaging soybean plant roots. The final setup box for imaging the soybean plant roots is shown in the Figure 3.2. The images of one plant root taken by all the cameras in the same order as shown from left to right in the 3.2a is shown in the Figure 3.3.

(a) Setup box interior as seen from the open front face.

(b) Setup box interior as seen from the opening used to replace plant roots after imaging.

Figure 3.2: The interior of experimental setup box

(a) Camera 1

(b) Camera 2

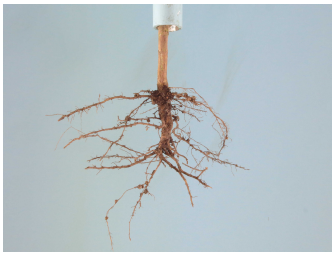

(c) Camera 3

(d) Camera 4

(e) Camera 5

Figure 3.3: Sample images from each of the cameras shown in Figure 3.2a from left to right.

Chapter 4

Image Segmentation

Image segmentation is needed for acquiring information on the plant root pixels located in the image. The images are first cropped so that it contains only background and the plant root pixels before performing segmentation. This involves cropping the clip or pipe used to clamp the plant root at the time of imaging. The images produced as the output of the segmentation further help in extracting variety of features. In this study, we implemented two methods, tested and compared for efficient segmentation. The first method involves preprocessing the input image and passing the preprocessed RGB pixels to the Relevance Vector Machine (RVM) classifier [40, 36]. The training data was kept the same for all the images that were collected.

In the second method, the segmentation is performed using Expectation Maximization (EM) algorithm [11, 36], by modeling the pixels as originating from two 3D gaussian distributions. One gaussian distribution models background (blue color) pixels whereas the other distribution models the plant root pixels. The image does not undergo any preprocessing before running the EM algorithm. Figure 4.1 shows

various stages in the segmentation procedure. The original image is passed to the EM algorithm to generate a basic segmented image (Figure 4.1b). This intermediate output contains a lot of background pixels miss-classified as foreground pixels. This is due to the noise content in the image, which makes the variance in the red, green and blue pixel values higher leading to classifying a dark blue pixel to be classified as plant root pixel. This problem may be fixed by removing miss-classified root pixels using connected component analysis. Hence in the next step, we select the largest connected component from the intermediate segmentation and save it as the final segmentation output.

We implemented the EM algorithm in C/C++ that can accelerate the algorithm on NVIDIA GPUs with Compute Capability 3.0 or higher. On systems that do not have NVIDIA GPUs, the program can parallelize the algorithm on multi-core CPUs using pthreads. The CPUs must have support for Intel's Advanced Vector Extensions 2.0 (AVX2) and Fused Multiply and Add (FMA) instruction sets for the program to run. On a typical quad-core CPU, the program takes 25 seconds to segment a 4000 x 3000 pixel image. Whereas on GPU, the program takes just 10 seconds to segment the same image.

Unlike most of the earlier work which threshold the image to separate root pixels from background, we use EM algorithm as it auto-tunes the parameters based on the image taken during different lighting conditions. The following sub-sections describe in detail, the need for using a non-linear background separation techniques, these two methods of segmentation step-by-step and also discusses advantages of EM based segmentation over the supervised RVM segmentation.

(a) Original Image

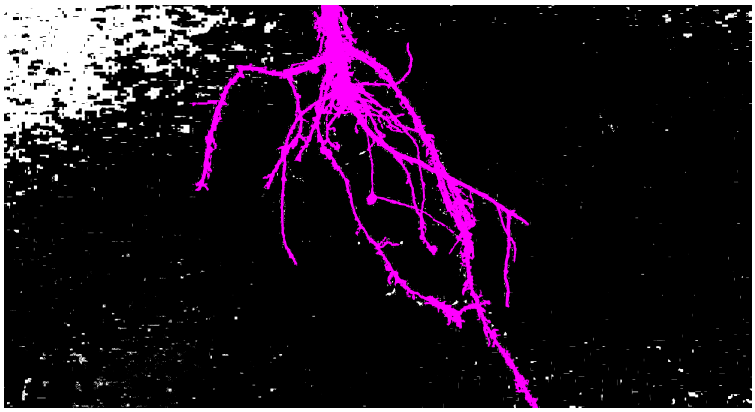

(b) Segmented Image showing largest connected component.

(c) Largest connected component

Figure 4.1: Image segmentation procedure

4.1 Need for Non-Linear Background Subtraction

The Figure 4.2b shows the DIRT segementation [3] output for the image shown in Figure 4.1a. The image is first converted to grayscale image (shown in Figure 4.2a) before passing it to DIRT program. The DIRT segmentation procedure separates the background by using Otsu's thresholding. This method of thresholding may not work because the image is converted to grayscale from the color image which mixes the intensity values across all the channels. Otsu's thresholding essentially finds a threshold that separates two classes so that the between class variance is maximized while minimizing the within class variance. EM, on the other hand, maximizes the combined likelihood for samples from both foreground (root) and the background. Also, RVM makes a probability map of the two classes using the training data by drawing a non-linear surface in the 3-dimensional feature space (red, green and blue). Both the algorithms work multivariate data. A scatter plot of the root and the non-root pixels of the input image shown in Figure 4.1a can be seen in the Figure 4.3. The scatter plot shows that the background pixels have higher intensity of blue channel compared to other channels. We also observe that the variance of the non-root pixels are smaller than the variance of the root pixels in all the color channels, which meets our expectation. This is because we chose a single blue background color to be able to easily identify root from non-root in the image. The variance of root pixels in all the color channels is high because several portions of the root can have light brown, brown and dark brown pixel intensities. Further, when we observe a tiny root with its background blue in color, the root pixels of the tiny root are also in blue color, but darker. This is due to the fact that the light reflecting from the background was bent near the tiny root, which makes it look in dark blue in color.

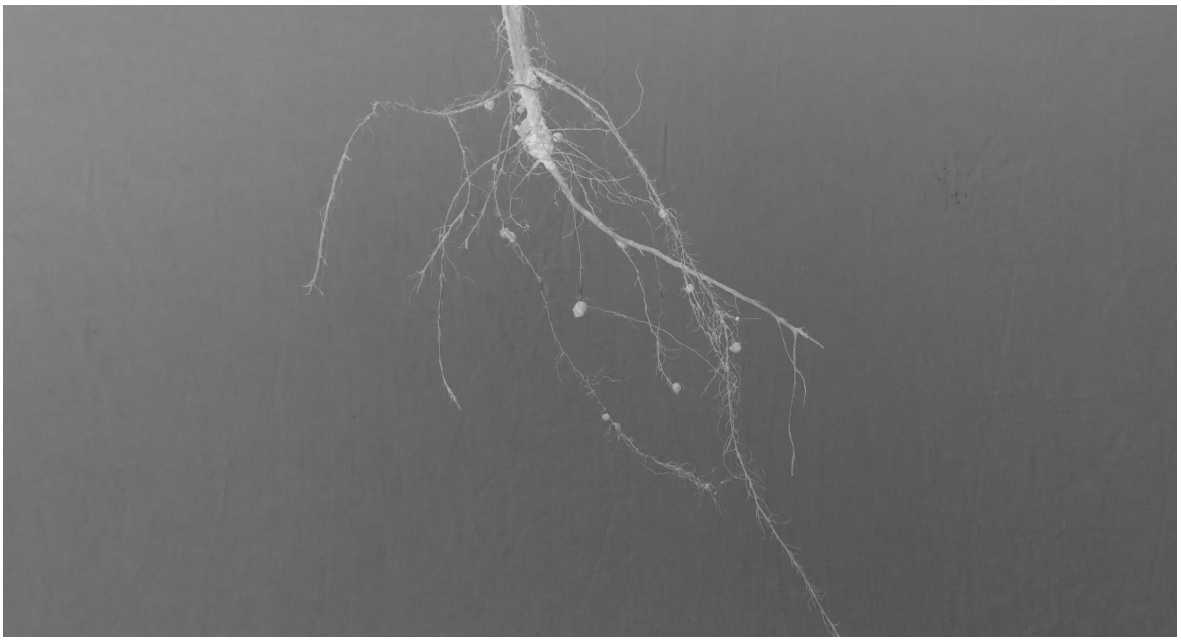

(a) Color inverted grayscale image passed as input to DIRT system

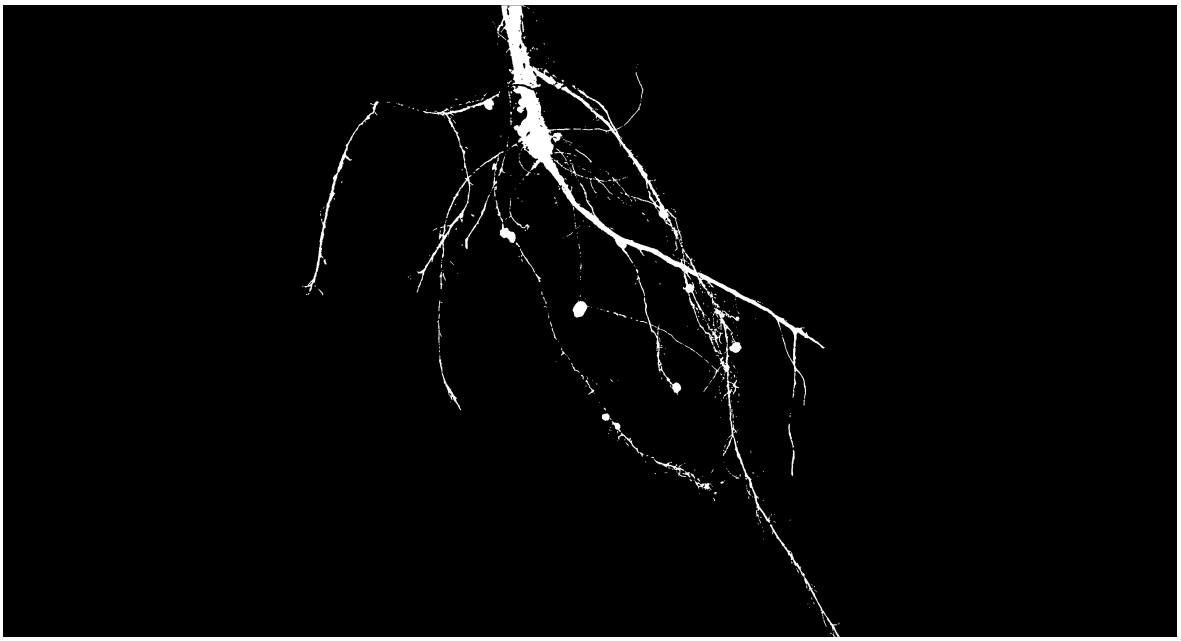

(b) DIRT segmented image output.

Figure 4.2: Dirt Output

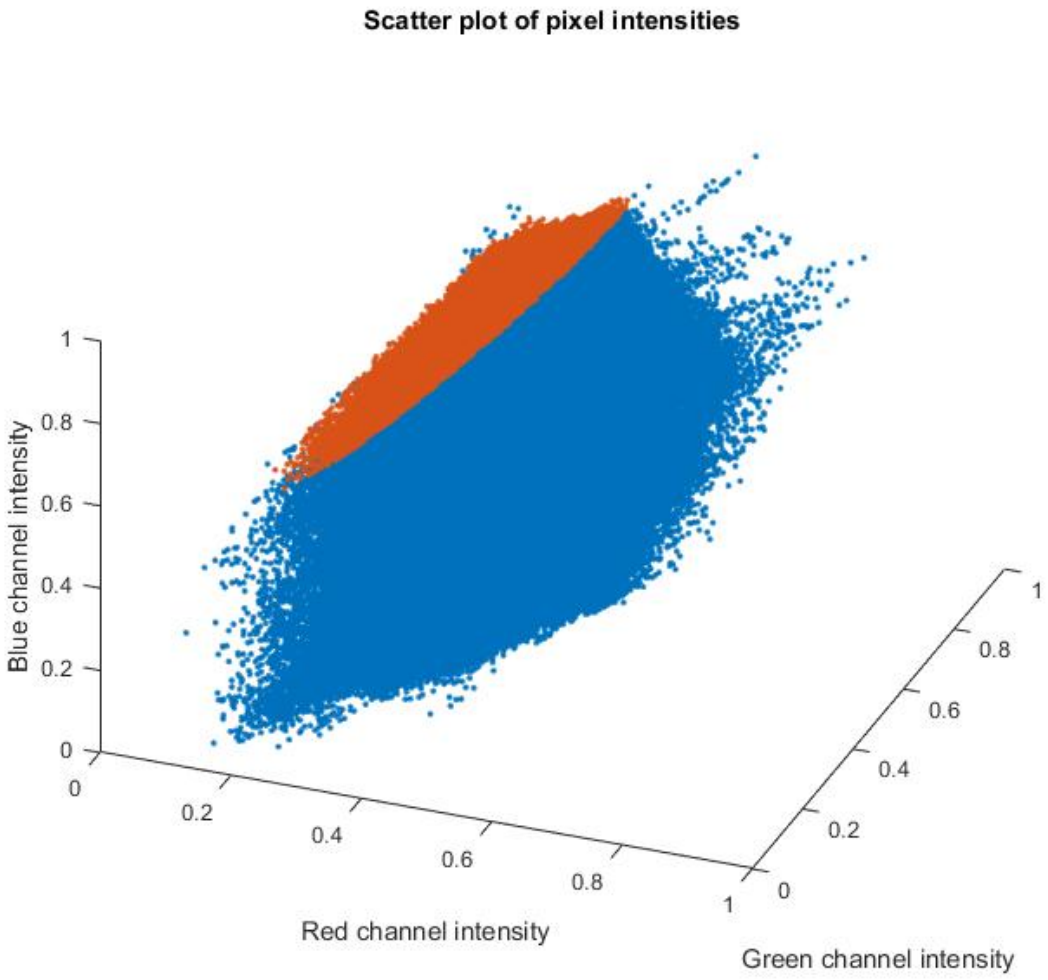

Figure 4.3: Scatter plot of pixel intensities. The blue dots represent the root pixels in the RGB colorspace. The orange dots represent the background pixels.

4.2 Segmenting Images by RVM

In this study, we used Relevance Vector Machine (RVM) [40, 36] for regression to segment the image into foreground and background. RVM algorithm involves computing posterior probabilities for each of the input pixel of the entire pixels from the input image. This section describes in detail, the RVM algorithm followed by the

implementation details that consist of preprocessing the image followed by classification using trained RVM classifier. We also discuss the problems involved in using this algorithm over large set of plant images, that led us to select a different approach to segmentation - EM algorithm.

The RVM algorithm for regression finds the parameters of the following linear function

$$y(\mathbf{x}) = \sum_{i=1}^{N} w_i^T \phi(x_i) + b = \mathbf{w}^T \phi(\mathbf{x}) + b \tag{4.1}$$

ϕ is the non-linear basis function, w_i is the coefficient in the linear model for each $\phi(x_i)$ and b is the bias parameter. The basis functions are specified in the form of kernel functions K to express the inner product of the samples in the function space given by the design functions. The linear model now becomes

$$y(\mathbf{x}) = \sum_{i=1}^{N} w_i^T k(\mathbf{x}, \mathbf{x_i}) + b \tag{4.2}$$

The total number of parameters including bias b is $M = N + 1$. In this study, we used the Gaussian Radial Basis Function (RBF) kernel as the kernel function for training the RVM classifier. The kernel is given by

$$k(\mathbf{x}, \mathbf{x_i}) = \exp\left(-\frac{||\mathbf{x} - \mathbf{x_i}||^2}{2\sigma^2}\right) \tag{4.3}$$

The conditional distribution of obtaining a target value t for a given input data, the weight coefficients w_i and the noise precision β is modeled as follows

$$p(t|\mathbf{x}, \mathbf{w}, \beta) = \mathcal{N}(t|y(\mathbf{x}), \beta^{-1})) \tag{4.4}$$

The $\mathbf{X}$ denotes the set of N input observations. The likelihood is given by

$$p(\mathbf{t}|\mathbf{X}, \mathbf{w}, \beta) = \prod_{i=1}^{N} \mathcal{N}(t|y(\mathbf{x}), \beta^{-1})) \tag{4.5}$$

We also define a hyperparameter α_i for each parameter w_i that denotes the precision in the prior distribution given below.

$$p(\mathbf{w}|\boldsymbol{\alpha}) = \prod_{i=1}^{M} \mathcal{N}(w_i|0, \alpha_i^{-1})) \tag{4.6}$$

Thus, the posterior distribution for coefficients of the linear model is given by

$$p(\mathbf{w}|\mathbf{t}, \mathbf{X}, \boldsymbol{\alpha}, \beta) = \mathcal{N}(\mathbf{w}|\mathbf{m}, \boldsymbol{\Sigma})) \tag{4.7}$$

where the mean $\mathbf{m}$ and the covariance $\boldsymbol{\Sigma}$ are given by

$$\mathbf{m} = \beta \boldsymbol{\Sigma} \boldsymbol{\Phi}^{\mathbf{T}} \boldsymbol{\Phi} \tag{4.8}$$

$$\boldsymbol{\Sigma} = \left(\mathbf{A} + \beta \boldsymbol{\Phi}^{\mathbf{T}} \boldsymbol{\Phi}\right)^{-1} \tag{4.9}$$

where A is a matrix that contains α_i along the diagonal. The hyperparameters α_i and β are updated using the following equations

$$\alpha_i^{new} = \frac{\gamma_i}{m_i^2} \tag{4.10}$$

$$(\beta^{new})^{-1} = \frac{\|\mathbf{t} - \boldsymbol{\Phi}\mathbf{m}\|}{N - \Sigma_i \gamma_i} \tag{4.11}$$

where $\gamma_i = 1 - \alpha_i \Sigma_{ii}$. The algorithm starts with initializing α and β with 0.5 in the implementation. It then computes the mean $\mathbf{m}$ and the covariance $\boldsymbol{\Sigma}$ using

the equations 4.8 and 4.9 followed by recalculation of hyperparameters uaing the equations 4.10 and 4.11. After some iterations, many α_i values tend towards infinity and their corresponding w_i coefficients tend towards zero. The remaining set of α_i values tend towards zero and the corresponding w_i coefficients tend towards non-zero values. The training samples corresponding to these non-zero coefficients are stored as relevance vectors. The algorithm 1 summarizes the steps used in training the RVM classifier.

Having computed the $\boldsymbol{\alpha_{final}}$ and β_{final} values along with the parameters w_{final} for the relevance vectors, we now use the equation 4.2 to obtain the target variable for the new test variable x. The bias parameter is present in the w_{final}, that was already determined in the training algorithm. The variable $\mathbf{x_i}$ in the equation 4.2 is the set of the relevance vectors that was obtained earlier in the process of training.

Algorithm 1 RVM Training Algorithm

Require: Training set X = $\{X_n | 1 \leq n \leq N\}$, where N is the number of training samples and the corresponding target set t = $\{t_n\}$

$\boldsymbol{\alpha} \leftarrow 0.5$

$\beta \leftarrow 0.5$

while maximum iterations is not reached **do**

$\mathbf{m} \leftarrow \beta \boldsymbol{\Sigma} \boldsymbol{\Phi}^{\mathbf{T}} \boldsymbol{\Phi}$

$\boldsymbol{\Sigma} \leftarrow \left(\mathbf{A} + \beta \boldsymbol{\Phi}^{\mathbf{T}} \boldsymbol{\Phi}\right)^{-1}$

$\gamma_i \leftarrow 1 - \alpha_i \Sigma_{ii}$

$\alpha_i^{new} \leftarrow \frac{\gamma_i}{m_i^2}$

$\left(\beta^{new}\right)^{-1} \leftarrow \frac{\|\mathbf{t} - \boldsymbol{\Phi}\mathbf{m}\|}{N - \Sigma_i \gamma_i}$

Stop updating the parameters and hyperparameters for those samples having α_i^{new} values greater than 10000.

end while

$\boldsymbol{\alpha_{final}} \leftarrow \boldsymbol{\alpha}$

$\beta_{final} \leftarrow \beta$

$w_{final} \leftarrow w$

4.2.1 Preprocessing the Image

Individual color channels of the input image are taken separately and for each color channel, contrast enhancement, gamma correction and brightness correction is applied in order, so that the entire range of the color channel is used in the preprocessed image. The gamma correction is applied so that the background non-root pixels become more blue in color so that they can be classified easily using a learned classifier. The color channel images are now subjected to image sharpening. Image sharpening involves adding a fraction of the difference between the original channel and its smoothed image to the original channel. Here, the fraction of the difference is denoted as the amount of sharpness for the image. As most of the root can be identified using blue channel image, sharpening is performed at a greater amount for the blue channel, moderate amount for green channel and minimal amount for red channel. To further reduce the variation in the background pixels, each color channel is then subjected to Local Contrast Enhancement (LCE) [41, 42]. These stages of the preprocessing is shown step-by-step in the Figures 4.5, 4.6, 4.7, 4.8, 4.9 and 4.10.

4.2.2 Segmentation Output

The image preprocessing is a computationally intensive task involving lots of pixel operations. Hence, running RVM classification for each pixel after the image preprocessing involves takes even larger amounts of processing time. Hence, we identify common parts of the root image which, we are sure, are not a part of plant root. This involves blue background, green beans (some plant root images may contain shoot system), pink clip (used to clamp the root to a metallic bar for imaging or mark the root) and dark brown colored glove (In 2014, earlier plant root images were taken

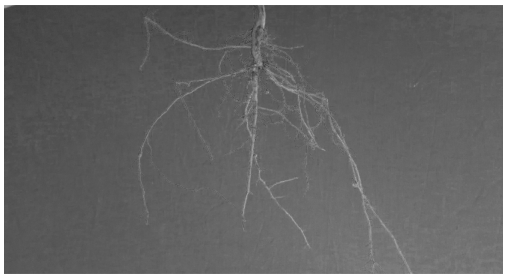

(a) Red channel

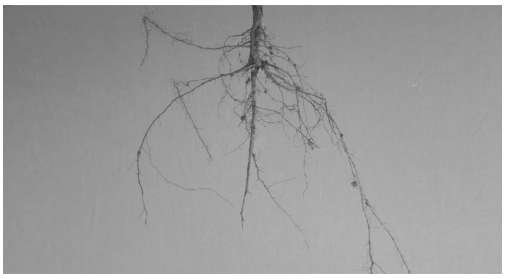

(b) Green channel

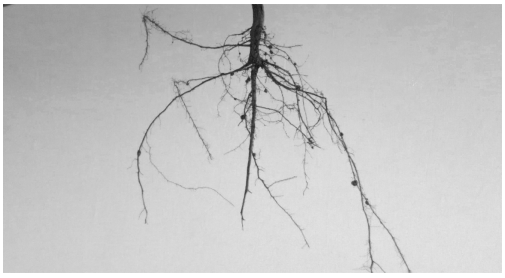

(c) Blue channel

Figure 4.4: Original image channels

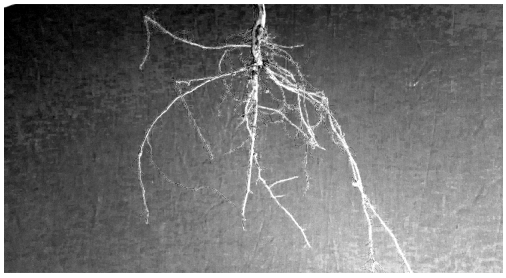

(a) Red channel contrast stretched

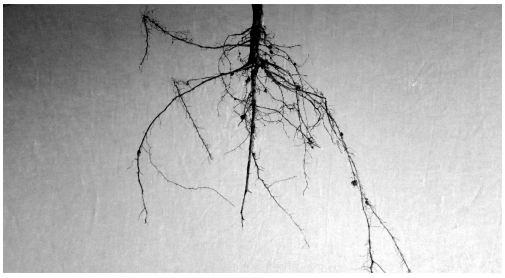

(b) Green channel contrast stretched

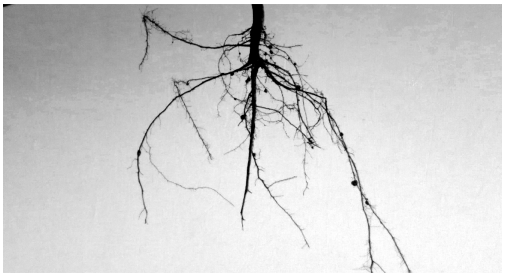

(c) Blue channel contrast stretched

Figure 4.5: Image channels after contrast stretching

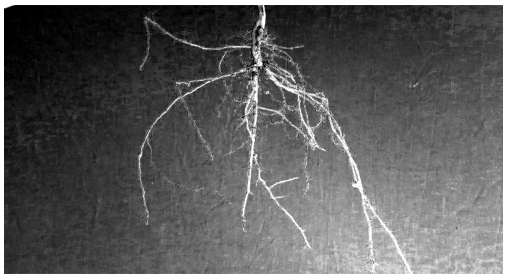

(a) Red channel gamma corrected

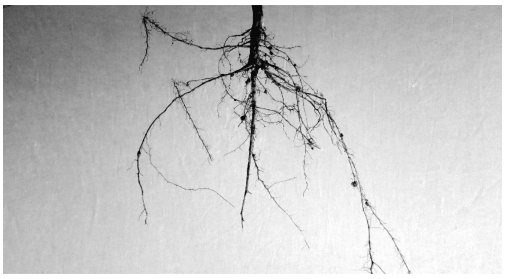

(b) Green channel gamma corrected

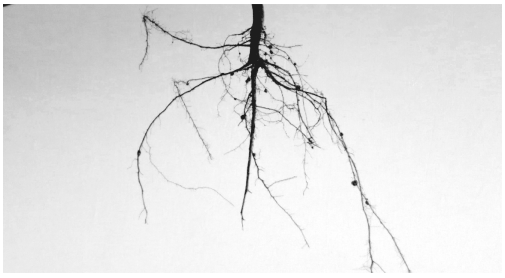

(c) Blue channel gamma corrected

Figure 4.6: Image channels after gamma correction

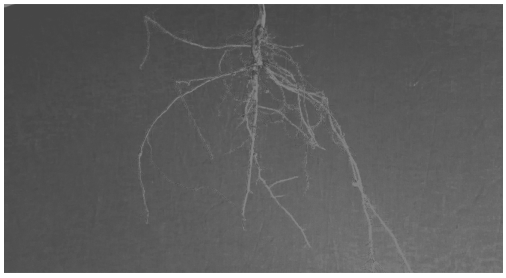

(a) Red channel brightness corrected

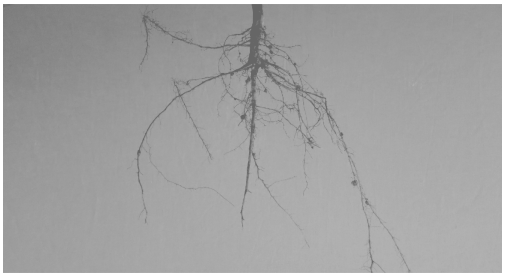

(b) Green channel brightness corrected

(c) Blue channel brightness corrected

Figure 4.7: Image channels after gamma and brightness correction

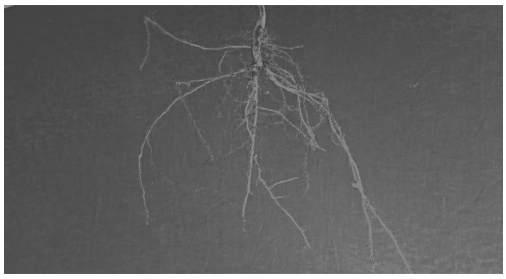

(a) Red channel sharpened

(b) Green channel sharpened

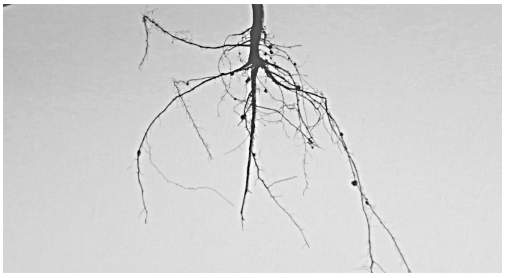

(c) Blue channel sharpened

Figure 4.8: Image channels after gamma, brightness correction and sharpening

manually in open air by handling the root with gloves at the time of imaging). These portions are identified by applying a high threshold at specific locations of the image. For example, green beans always come at the top of the image before the plant root. After these portions are removed, we are left with few thousands of pixels that can be easily passed for RVM classification. The results from the RVM classifier are then combined with the manually removed image portions to construct the final segmented image. The RVM segmented output is shown in the Figure 4.11.

Problems for using RVM as a reliable classifier involves collection of data for training the algorithm. That is because, the RVM classifier is a supervised learning algorithm. For example, consider the image shown in the Figure 4.12. When we train the RVM classifier using the pixels from original image in the Figure 4.1, and then use it to classify pixels from the image having poor lighting, it may result in

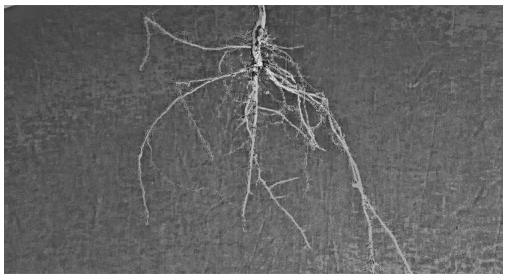

(a) Red channel local contrast enhanced

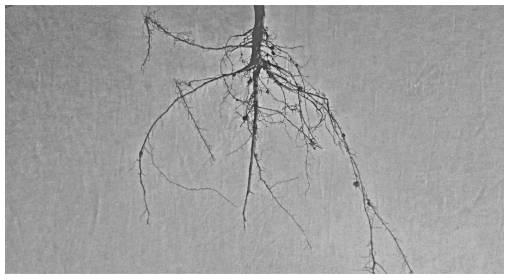

(b) Green channel local contrast enhanced

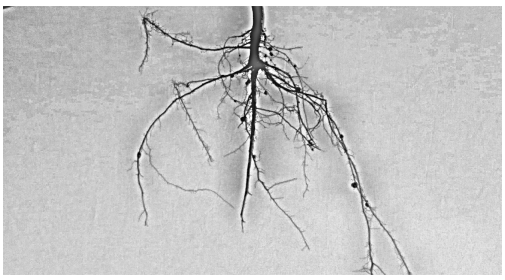

(c) Blue channel local contrast enhanced

Figure 4.9: Image channels after gamma, brightness correction, sharpening and local contrast enhancing

the majority of the image to be classified as root pixels. Hence, we need to take the training data from multiple images having multiple background lighting conditions. Even though we get diverse training data from various images, we may still find problems in classification. This may be caused due to unbalance in the training data, as majority of pixels in the image are background pixels. Hence, we first perform computationally intensive preprocessing to achieve maximum class separation between root and non-root portions of the image. This further leads us to setting different parameters for image preprocessing, which may have to be changed from one input image to another depending upon the lighting conditions, weather on the day (sunny or cloudy). Hence, using this process involves hard manual labor of carefully collecting the training data, setting up parameters that work in general for all images for preprocessing the image. RVM segmentation is implemented in MATLAB and it

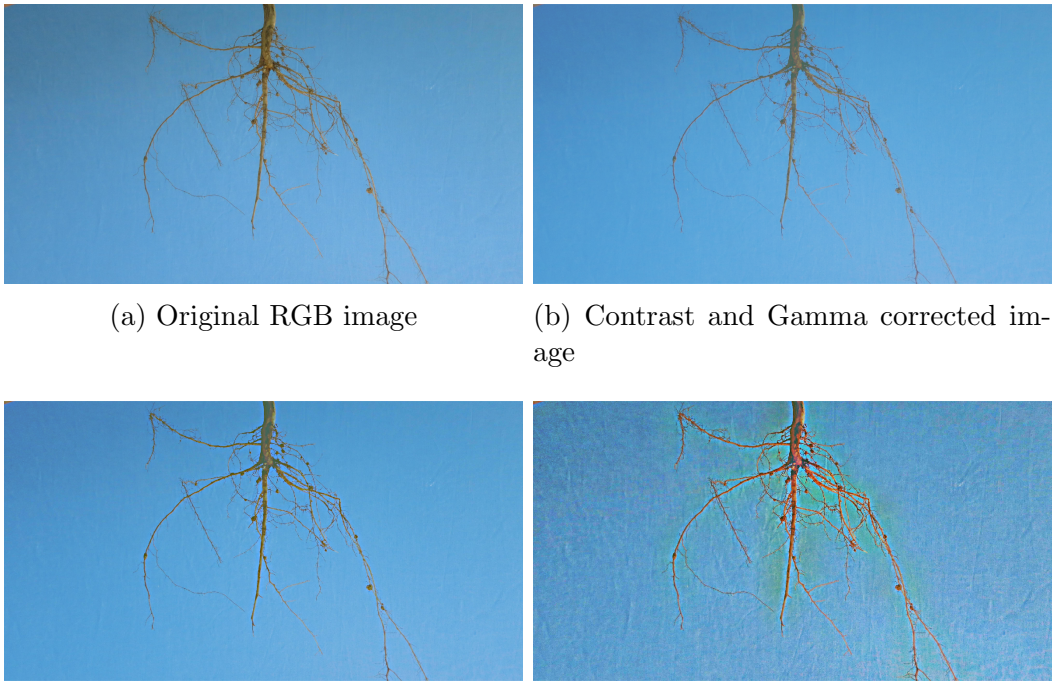

(a) Original RGB image

(b) Contrast and Gamma corrected image

(c) Sharpened image

(d) Local contrast enhanced

Figure 4.10: Image channels after gamma, brightness correction, sharpening and local contrast enhancing

takes about 1 minute 15 seconds to perform the pre-processing and RVM classification to generate the segmented image. In order to remove these laborious processes, we now discuss EM algorithm based segmentation.

4.3 Segmenting Images by EM

Expectation-Maximization [11, 36] is an iterative procedure for finding maximum a posteriori (MAP) estimate of parameters for mixture distributions. The pixel values in the input image are taken as 3-dimensional data points that is coming from a mixture of two gaussian distributions, one each for root and non-root pixels. The

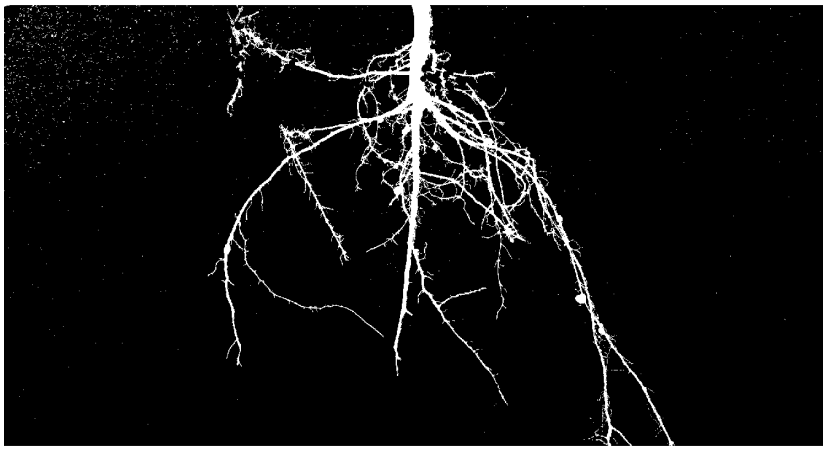

(a) RVM segmented image

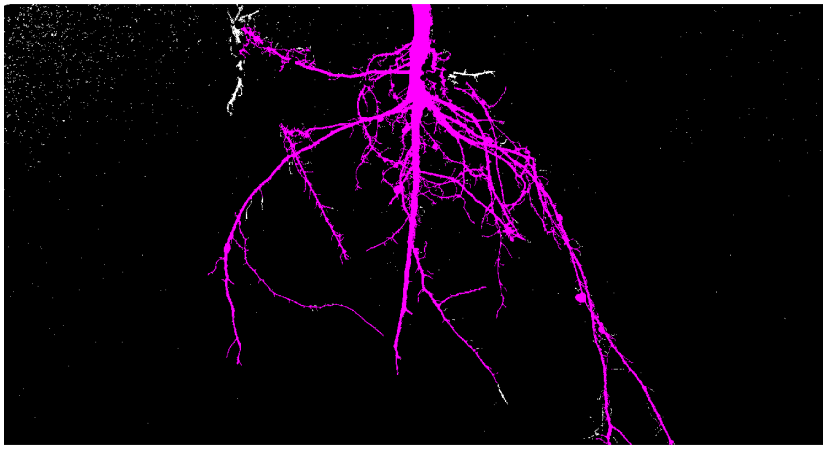

(b) Largest Connected Component of RVM Segmented image

Figure 4.11: RVM Output

EM algorithm finds the parameters of the Gaussian mixture model by maximizing iteratively the likelihood function of the given data samples ($\boldsymbol{X}$). Using the notation of $\boldsymbol{\mu}$ as the mean vectors, $\boldsymbol{\Sigma}$ as the covariance matrices and $\boldsymbol{\pi}$ as the prior probabilities for all the mixtures in the data samples, we now write the log likelihood function.

$$\ln p\left(\boldsymbol{X}|\boldsymbol{\mu},\boldsymbol{\Sigma},\boldsymbol{\pi}\right)=\sum_{i=1}^{N}\ln\left\{\sum_{j=1}^{M}\pi_j\mathcal{N}\left(\mathbf{x}_i|\boldsymbol{\mu}_j,\boldsymbol{\Sigma}_j\right)\right\} \tag{4.12}$$

Figure 4.12: Input image with dark lighting conditions

The E-step involves computation of the sum of conditional probabilities of a sample belonging to a mixture component given the sample.

$$\gamma_{i,j} = \frac{\pi_j \mathcal{N}\left(\mathbf{x}_i | \boldsymbol{\mu}_j, \boldsymbol{\Sigma}_j\right)}{\sum_{k=1}^{M} \pi_k \mathcal{N}\left(\mathbf{x}_i | \boldsymbol{\mu}_k, \boldsymbol{\Sigma}_k\right)} \tag{4.13}$$

N is the number of samples in the dataset and M is the number of mixture components. Having computed the membership probabilities $\gamma_{i,j}$, the M-step reestimates the parameters using the following equations.

$$
\begin{aligned}
\boldsymbol{\mu}_j^{'} &= \frac{1}{N_j}\sum_{i=1}^{N}\gamma_{i,j}\mathbf{x}_i \\
\boldsymbol{\Sigma}_j^{'} &= \frac{1}{N_j}\sum_{i=1}^{N}\gamma_{i,j}\left(\mathbf{x}_i-\boldsymbol{\mu}_j^{'}\right)\left(\mathbf{x}_i-\boldsymbol{\mu}_j^{'}\right)^T \\
\pi_j^{'} &= \frac{N_j}{N}
\end{aligned}
\tag{4.14}
$$

where N_j is given by

$$
N_j = \sum_{i=1}^{N}\gamma_{i,j} \tag{4.15}
$$

The algorithm is initialized using suitable values for the parameters of the mixture model, and then iteratively updated using the equations above until the parameters do not change or maximum number of iterations are reached.

When segmenting the plant root images, each pixel consisting of the red, green and blue color components, constitutes a data sample in the dataset.

4.3.1 Initialization using Histograms

Running the EM algorithm by randomly initializing the parameters often results in undesirable segmentation results. This is because, the percentage of root pixels are significantly lower than the background pixels. In that case, the EM algorithm may just separate the background pixels into brighter pixels and darker pixels as shown in Figure 4.13. The root pixels may be classified as brighter or darker based on their pixel intensities. Hence, we find better results in segmentation when the algorithm is initialized using the peaks of the histograms in the color channels. An example may be illustrated using the histograms as following. The histograms of the color channels

of the original image (Figure 4.1a) is shown in the Figure 4.14. The magnified version of histograms (Figure 4.15) is shown to highlight a small but wide peak to the left of the peak in red channel seen in the Figure 4.14. This peak corresponds to the plant root pixels. Depending on the lighting at the time of capturing the images, we find similar peaks in green and blue channels for other images. We observe that these peaks are so small that these are hard to find compared to other peaks that are located near to the global peaks of the histograms. This results in the EM algorithm to not recognize the root pixel cluster and instead segment the image into two parts depending on the lighting of the image in various parts of the image as shown in the Figure 4.13. Hence, in order to identify the peaks in the histograms, we need to smooth the histograms. The histograms are first smoothed using a median filter using a window size of 5 elements. This used to remove any sudden spikes or valleys in the histograms. The histograms are then smoothed with a gaussian filter using a larger window size of 11 elements. A larger window is used in latter case because we want to smooth out the peaks that are nearby each other so that the tiny peaks due to the presence of root pixels may be identified. The window sizes for smoothing are selected such that the major peaks in the histogram would be identified as a tall peak formed due to background and a short peak formed due to root.

Once, the histograms are smoothed, we find the peaks of the histograms. We expect to have a minimum of two peaks (one for each background and the root pixels) from the histograms of each color channel. The locations of the tall peaks for histograms in all the three channels are used for initializing the mean for the background cluster. The locations of the shorter peaks are used for initializing the mean for the root pixel cluster. Sometimes, the shorter peak for the root pixels may

not be identified because the peak may be smoothed out. If only one peak is present, we assume that the peak corresponds to the background pixels and we initialize the mean of the root pixels to be 0.05 (in the color range from 0 to 1). Sometimes, the input image is so dark that a majority of pixels may have the same value. In such a case, after smoothing the histogram with the median filter, the histogram almost looks flat. Hence, the histogram may not have a peak at all. In that case, the means for each color channel are initialized to be 0.25 and 0.75 for root pixels and the background pixels respectively (in the color range from 0 to 1). The EM segmented image for the original image 4.1a is shown in the Figure 4.16. Out of thousands of images segmented , some images still get badly segmented because of smooth variation in lighting when images were taken at extreme angles at either end of the experimental setup box. Such smooth variation leads to two large peaks in the histograms, which make the algorithm not recognize the root at all. Then the images were manually edited such that one of the peaks of the histogram is increased and the other decreased by copying some pixels in one peak to other pixels in other peak. That way the smaller peak is smoothed out allowing the algorithm to get the plant root structure. The Figure 4.17 show the EM segmented images for the sample images of the same root taken from the 5 cameras shown in the Figure 3.3. The images were cropped before performing the segmentation.

4.4 Advantages of EM algorithm Over RVM

One of the important reasons why RVM algorithm could fail is that since RVM is a supervised learning algorithm, we need to feed the algorithm with sufficiently large

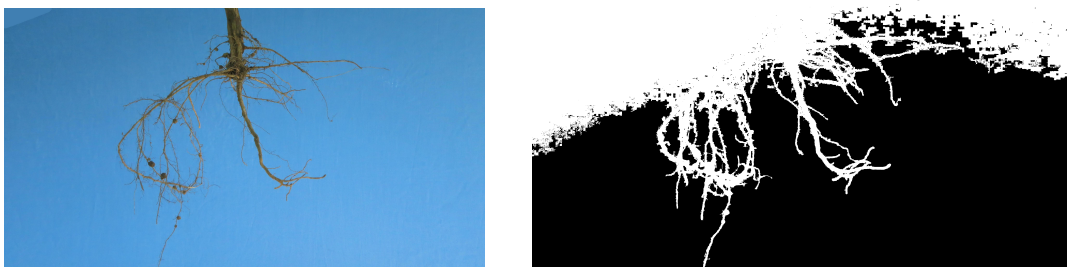

(a) Original image (b) Segmented image

Figure 4.13: Poor segmentation by EM algorithm due to random initialization

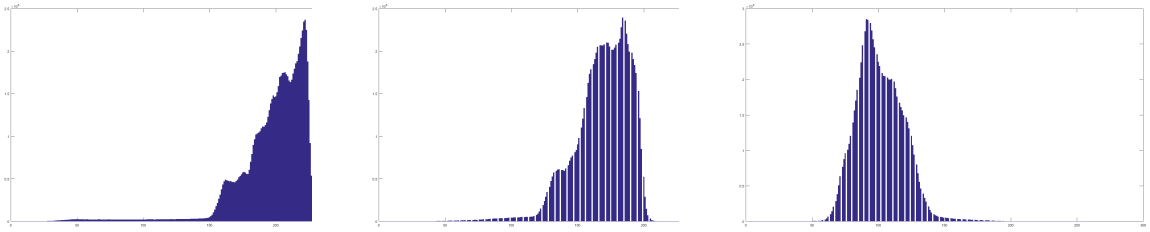

(a) Red channel histogram (b) Green channel histogram (c) Blue channel histogram

Figure 4.14: Histograms of color channels

training set. That includes pixel intensities in all the color channels from the images that are taken at different lighting conditions. Even though we provide a large training set, the algorithm may not work some images just because the pixels for that lighting condition were not trained 'sufficiently'. This makes us heavily rely on preprocessing methods such as contrast enhancement, gamma correction, image sharpening. Further, this adds to the computational processing needed to segment the image. Segmenting an image using RVM (MATLAB implementation) discussed in the study takes about 90 seconds whereas segmenting using EM (MATLAB implementation) takes 50 seconds. When EM is implemented in C++ with CPU threading and using Intel's AVX2 and FMA vector processing instruction sets, the program drammatically reduces the segmentation time to 25 seconds. Also, in this study, we implemented EM

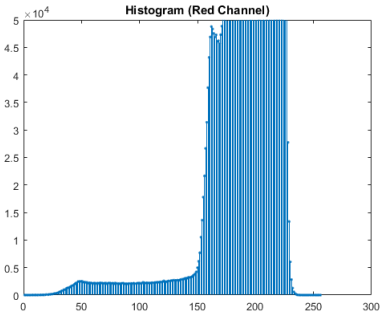

(a) Magnified red channel histogram

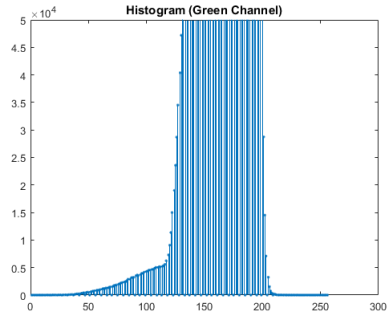

(b) Magnified green channel histogram

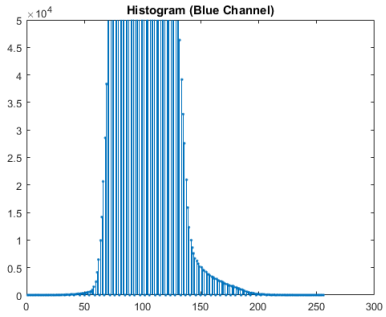

(c) Magnified blue channel histogram

Figure 4.15: Magnified histograms of color channels

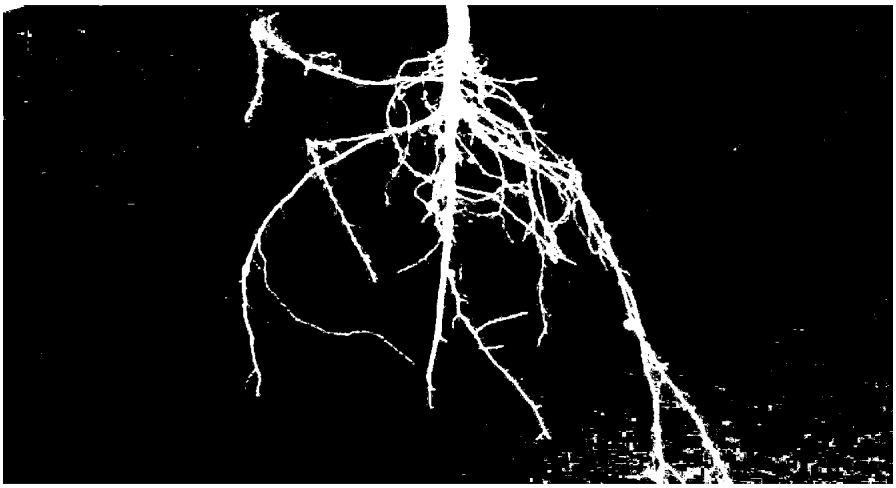

Figure 4.16: Segmentation output of EM algorithm

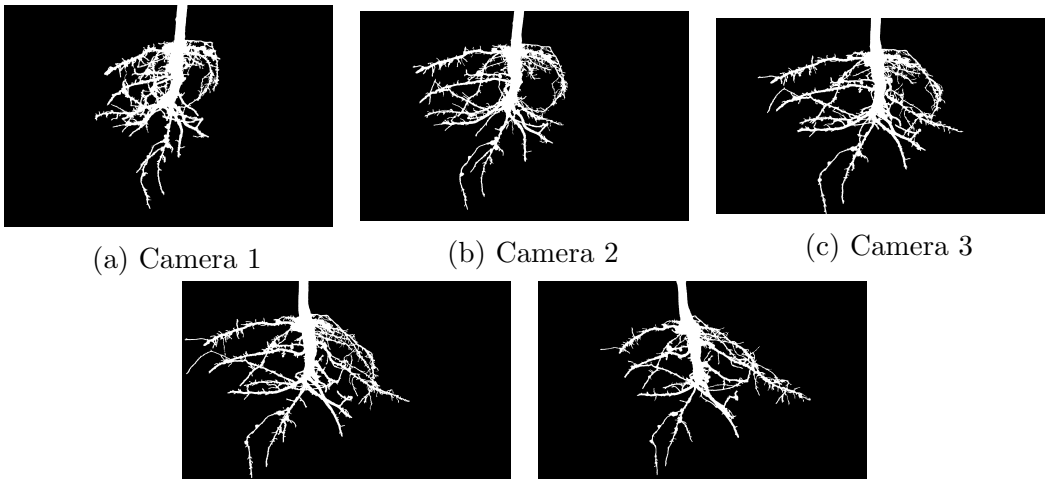

(a) Camera 1 (b) Camera 2 (c) Camera 3

(d) Camera 4 (e) Camera 5

Figure 4.17: Segmented images of sample images shown in the Figure 3.3.

algorithm to utilize NVIDIA GPUs, which can further reduce the segmentation time to 10 seconds. This makes EM algorithm suitable for high-throughput phenotyping system.

Chapter 5

Feature extraction

The feature extraction procedure involves performing operations on the segmented image to extract a set of phenotypic traits to be used for statistical analysis later. Before extracting features from a segmented image, we first crop the segmented image so that the image does not contain any blank rows or columns (that is without plant root). Throughout this chapter use the following naming convention to describe the features being extracted. The original image is denoted by I, the cropped segmented image is denoted by S, the skeletonized image is denoted by T and the image containing the perimeter of the segmented image is denoted by P. All the three images S, T and P are binary images. A subscript of i, j denotes the pixel at i^{th} row and j^{th} column. The segmented image shown in the Figure 4.16 was skeletonized using the MATLAB function `bwmorph()` to generate the image shown in the Figure 5.1. The image containing the perimeter P of the image S is shown in the Figure 5.2. The following sections describe each feature traits extracted in detail.

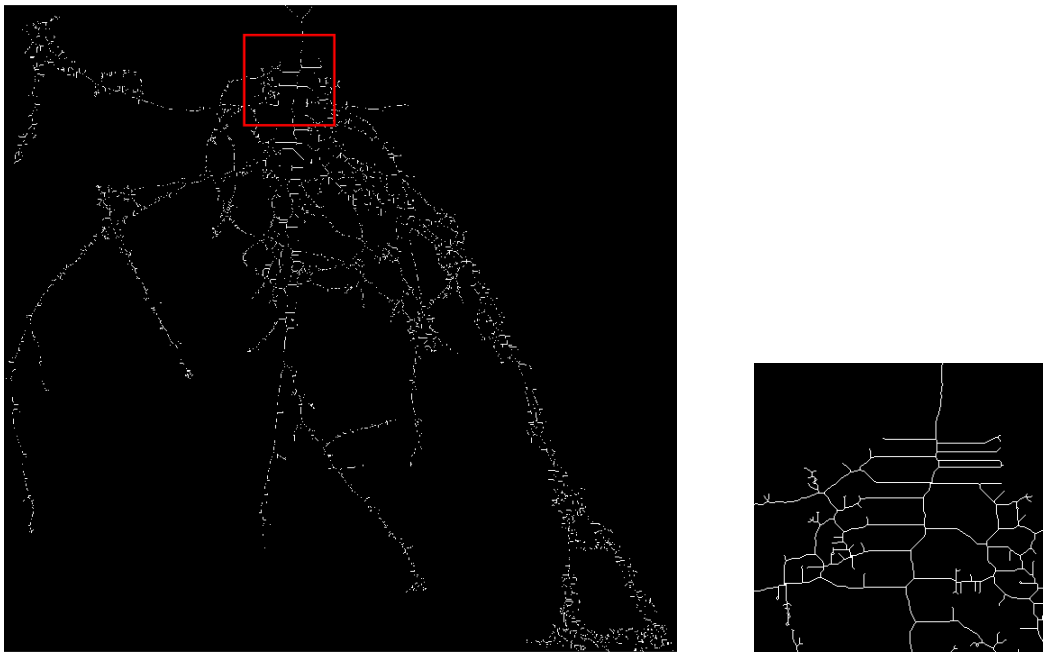

(a) Skeletonized image

(b) Magnified skeletonized image for the rectangular portion.

Figure 5.1: Skeletonized Image and a magnified portion of the skeletonized image

5.1 Median and maximum number of roots

We count the number of roots by performing horizontal line scans from left to right in each row through the segmented image S. In each of the line scan, we check if there is a pixel value transition from the previous pixel value $S_{i,j-1}$ to the current pixel value $S_{i,j}$. If the current pixel value changes from 0 to 1, we note that a root is present. This can be done efficiently by subtracting the segmented image that is right shifted to a pixel from the original segmented image. The resulting image contains the pixel locations that have the pixel transitions either from 0 to 1 or viceversa. The pixel transitions from 0 to 1 are marked with a value of 1 in the subtracted image, whereas the pixel transitions from 1 to 0 are marked with a value of -1. This procedure is shown

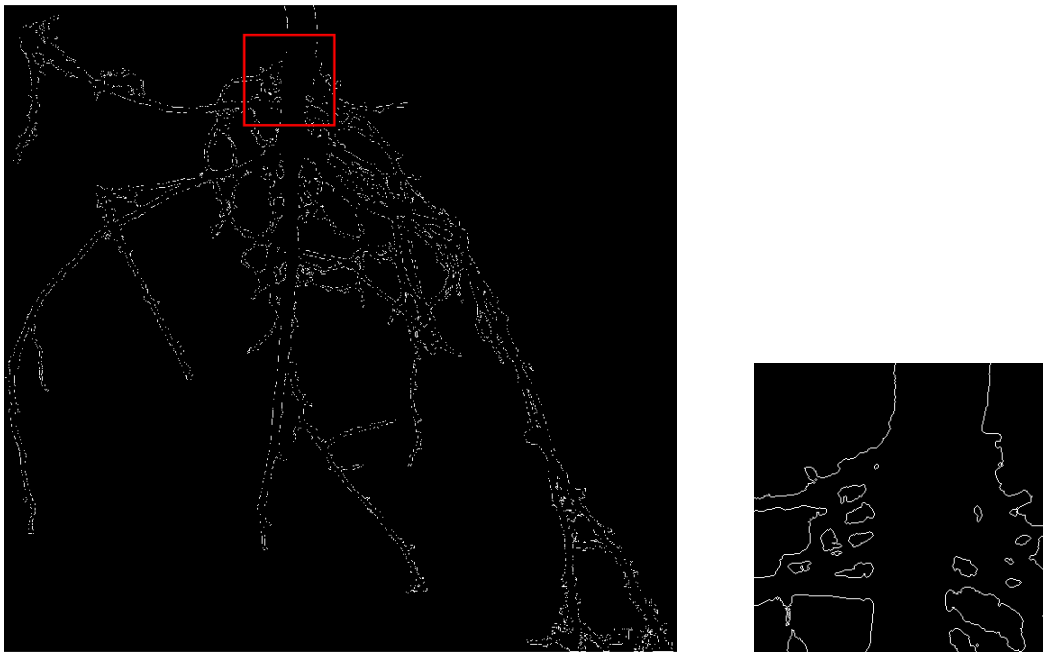

(a) Pixels showing perimeter of the segmented image S.

(b) Rectangular portion magnified showing the perimeter of the segmented portion of crown root..

Figure 5.2: Perimeter of the segmented image

mathematically as follows. Let S_1 denote the right-shifted segmented image made by prepending a column of zeros to the segmented image. Let S_2 denote the original segmented image appended by the column of zeros so as to make the dimensions of the images equal when subtracting. Then image containing pixel transitions are given by

$$S_t = S_2 - S_1 \tag{5.1}$$

The image containing only the pixel transitions from zero to one are given by

$$S_{01} = (S_t + 1)/2 \tag{5.2}$$

We can now add all the elements of the rows in S_{01} transition image to get a depth-wise profile of the number of roots denoted S_p. S_p is a vector containing the number of roots in each row as we go from the top to bottom part of the root. This profile gives a lot of information on how the root propagates as the depth increases. For this study, we extract to important traits from the profile. Given the list of the number of roots in every image row of the segmented image, we now sort these values and compute median and maximum number of roots. We still need to be cautious when measuring these traits. This is because when cutting the root part from the stem part, the root is not always cut at the same distance from the center of the root. This may lead to bad results in the statistical analysis. For example, when digging the roots from the soil, if the root is cut at higher altitude, then the image may have more stem part. Hence, the resulting profile of the number of roots S_p will have smaller root count for majority of elements, which may skew the median number of roots. Future studies include depth invariant features from this profile such as trying to fit a graph from the profile and use its coefficients as traits or merely threshold the S_p vector removing smaller root counts and take median for the rest of the elements in the vector.

5.2 Total root length

Total root length is computed by counting the total number of pixels in the skeletonized image T.

5.3 Depth, maximum width and width-to-depth ratio

The length of the profile vector S_p is taken as the depth of the plant root. Since, all the empty rows and empty columns of the segmented image were cropped before extracting the features, we can also take the height of the segmented image as the depth of the plant root. The width of the segmented image can be taken as the trait value for maximum width. The trait values for both depth and maximum width can be obtained by getting the dimensions of the segmented image in MATLAB using `size()` function. The ratio of maximum width to the depth of the image is noted as width-to-depth ratio.

5.4 Network area, convex area and solidity

Network area is the total number of pixels in the segmented image S. This may be determined summing the pixel values of all the pixels of the image S. This is mathematically expressed as

$$network\ area = \sum_{i=1}^{M} \sum_{j=1}^{N} S_{i,j} \tag{5.3}$$

The M and N denotes the number of rows and columns of the image respectively. The convex hull of a geometric shape is minimal sized convex polygon that can contain the shape. In case of the segmented image S, the convex hull image is obtained using the `bwconvhull()` MATLAB function. The convexhull image for the segmented image S in shown in the Figure 5.3.

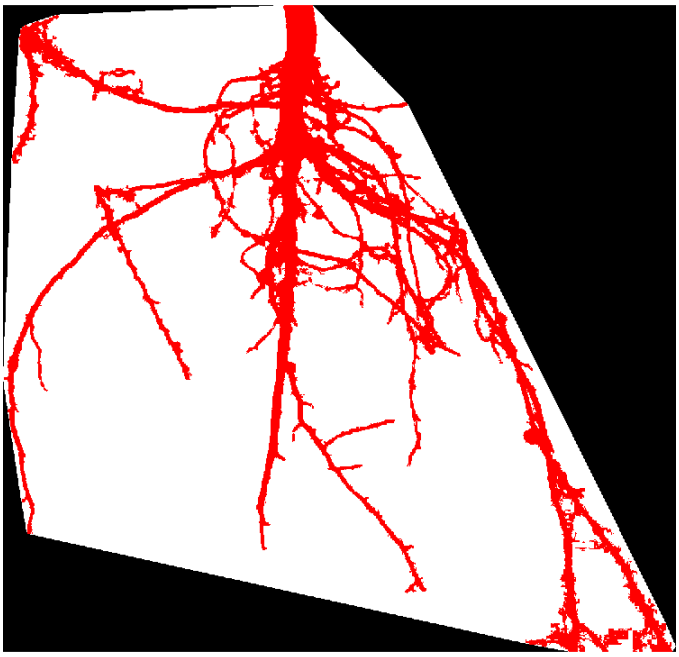

Figure 5.3: Convex hull polygon that contains the segmented image.

The convex area is the sum of the pixel values of the binary convex hull image C. This is given by the following expression

$$convex\ \ area = \sum_{i=1}^{M} \sum_{j=1}^{N} C_{i,j} \tag{5.4}$$

The ratio of network area and the convex area is noted as the solidity.

5.5 Perimeter

Perimeter is the count of total number of pixels in the perimeter image P. The image of the perimeter is obtained by the `bwperim()` MATLAB function. The perimeter is expressed by the following expression

$$perimeter = \sum_{i=1}^{M} \sum_{j=1}^{N} P_{i,j} \tag{5.5}$$

5.6 Average and maximum radius

Given the segmented image S, for each pixel on the plant root, we compute the nearest distance to a non-root pixel. We obtain a distance map denoted by D. Since, the skeletal image T is an image of zeros and ones, when we perform an element-by-element multiplication with D, we are left with the nearest distances to the non-root pixels from the medial axis pixels. In other words, we now have, the radius of plant root at every location. We take the list of radii and compute average, which is the average radius trait. The maximum value of the radii is noted as maximum radius trait.

5.7 Volume and surface area

Since, we now know the radius at every medial axis pixel, we can compute the cross-sectional area and perimeter of the root at a particular root location. The sum of all cross-sectional areas across all the medial axis pixels are noted as volume and the sum of the perimeter across all the the medial axis pixels are noted as surface area.

5.8 Lower root area

For every medial axis pixel, we know radius. Hence, we can find the location of the medial axis pixel which has the maximum radius. The lower root area is the area of the segmented image pixels that are located below the location of the medial axis pixel, that has the maximum radius. In other words, lower root area is the network area under the medial axis pixel having maximum radius.

5.9 Holes

Holes are the disconnected background components. They can be counted by inverting the segmented image S and performing connected component analysis. The connected component analysis is performed in MATLAB using the function `bwconncomp()`. we hypothesize that the number of holes correspond to the complexity of the plant root topology. As the root branches are more spread, the background pixels are further divided.

5.10 Histogram of radii at medial axis pixels

Since, we have the list of radii values at every medial axis pixel, we compute a histogram of 10 bins on these values. These bins are equally spaced and are same from each image to image. This makes us compare the histogram values between two segmented images. This histogram provides an insight into the root system and tells if the root system predominantly contains tinier roots or larger roots.

5.11 Histogram of orientations on the medial axis

Given the skeletal image T, for every pixel in the medial axis, we get the locations of the medial axis pixels in a 20x20 pixel locality and determine the orientation of these pixels in the locality. This orientation is noted for every medial axis pixel. Given these orientations, we compute the histogram of 6 bins. This histogram vector is reported as the extracted traits. This histogram of orientations give an idea of how spread the root system is. For example, if a majority of root pixels have a horizontal orientation, the root system is spread horizontally. This also means that the root has greater maximum width and greater width-to-depth ratio.

5.12 PCA components of histograms of radii and orientations

Sometimes, performing correlation analysis with the bins of histograms may not give good results as the radius and orientation changes from location to location in the same plant root. Hence, correlation may give a better result when the manually extracted features are compared with the projections of histogram vectors having highest variance. Hence, after extracting all the traits from all the plant roots, we run PCA separately on the histogram vectors from each camera. From the output of the PCA, we take scores from 3 most dominant directions, both for radii histograms and for the orientation histograms. We use these dominant directions in correlating manual features in the experiments.

5.13 Computational time

Although the high-throughput multi-camera phenotyping system is much faster compared to previous methods, we also extract the computational time required for every plant root image from each camera to extract all the feature traits. This time can also be regarded as an important trait as more the complexity of the root, more is the time taken to extract the traits.

5.14 Manually extracted feature traits

This section describes the manually feature traits extracted plant science group. This group extracted the following traits.

- **Stem diameter (SD)** It is the diameter of the stem that connects the root and shoot part of the plant.
- **Tap Root Diameter (TR)** It is the diameter of the main root of the plant root.
- **Overall complexity (OC)** Overall complexity is a complexity score assigned to a plant root by looking at the root. Several observations were made while looking at the root before assigning the complexity score such as the size of the root, number of lateral roots present in the root system, width of the root. The complexity scores are an integer rating between 1 and 5, 1 means very simple root and 5 means very complex root. The examples of different complexities are shown in Figure 5.4.

- **Number of upper roots (NUR)** Number of lateral roots that branch away from the main root from the starting of the plant root to the center of the plant root.

- **Lateral root density upper (LRDU)** Number of upper lateral roots divided by the length of the starting of the root to the center of the root.

- **Root angles of the upper lateral roots** Five dominant angles are selected in all of the lateral roots at the starting of the root and are reported as traits. Sometimes the lateral roots may be lesser than 5. Then the remaining angles are noted as missing data. When performing correlation analysis with these angles, we compute mean and median angles of the upper lateral roots. These are denoted as MEan of Upper Angles (MEUA) and MeDian of Upper Angles (MDUA).

- **Number of lower roots (NLR)** Number of lateral roots that branch away from the main root from the center of the plant root to the end of the main root.

- **Lateral root density lower (LRDL)** Number of lower lateral roots divided by the length of the center of the plant root to the end of the main root.

- **Root angles of the lower lateral roots** Five dominant angles are selected in all of the lateral roots at the lower part of the root and are reported as traits. Sometimes the lateral roots may be lesser than 5. Then the remaining angles are noted as missing data. When performing correlation analysis with these angles, we compute mean and median angles of the lower lateral roots. These

(a) Overall complexity 1 (b) Overall complexity 2 (c) Overall complexity 3

(d) Overall complexity 4 (e) Overall complexity 5

Figure 5.4: Sample images from each of the camera 5 (front facing) with increasing overall complexity from left to right.

are denoted as MEan of Lower Angles (MELA) and MeDian of Lower Angles (MDLA).

5.15 Merging feature traits from all the cameras

From the images shown in the Figure 3.3, traits such as maximum width, maximum number of roots change as we look at the same plant root from different perspectives. Another example is that a plant root may have lesser width when viewed from one angle and large width when viewed from another angle. Such a plant root may approximately be in a plane. In such a case, the extracted traits from some images do not correlate well with the manually extracted traits. To address this problem, we have come up with merging the features extracted from all the cameras by taking mean

of all the traits extracted across all the cameras. Correlation analysis is performed on these merged features and the results are compared with the features from individual cameras.

When collecting data from multiple cameras, all the Canon G1X cameras were set to a focal length 35.208 mm and all S110 cameras were set to a focal length of 13.586 mm. Since, these cameras were operated in different focal lengths, the size of the plant root recorded in the image may be different. Further, the sensor sizes of these cameras are different. Hence, the extracted features may also be different, which would make us difficult to directly take mean of the features from all the cameras. In order to compare the sizes of the plant root in images from different cameras, we convert the focal lengths for different image sensors [43, 44] to 35 mm equivalent focal lengths [45]. The length of the diagonal of the image sensor in Canon G1X is known to be 23.36 mm ([43]), whereas that of Canon S110 camera is known to be 9.3 mm ([44]). The 35 mm equivalent focal length is given by the following equation.

$$f_{35} = 43.3\frac{f}{d} \tag{5.6}$$

where f is the focal length of the camera, d is the diagonal of the camera image sensor. Both f and d are measured in millimeters. the value 43.3 is the length of the image sensor of a standard 35 mm film camera.

Using this formula, the 35 mm equivalent focal length of a Canon G1X camera operating at 35.208 mm focal length is 65.26 mm. Similarly, the 35 mm equivalent focal length of a Canon S110 camera operating at 13.586 mm focal length is 63.26 mm. These focal lengths are very similar to each other, that the size of the plant root taken using Canon G1X is just 1.032 times bigger than the size of the same

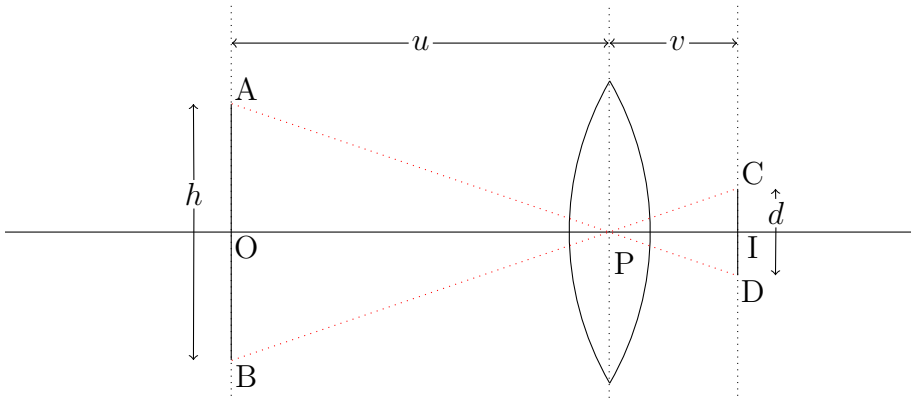

Figure 5.5: Estimation of real object size from the image.

plant root taken using Canon S110. We can resize the images using this ratio, extract the features and then merge the features. In such a case, we may not be able to understand how big a plant root is by looking at the trait values and may even be hard for us compare the traits from the image to manually extracted traits. Hence, for performing the correlations of merged features and for determination of inter-camera variances, we estimate the extracted traits of the plant root objects from the images, in physical units. Conversion of the extracted traits to physical units also allows us to get an idea about the size of the plant roots by looking at the traits. In this study, we converted the digital features Total root length, Depth, Maximum width, Network area, Convex area, Perimeter, Average radius, Volume, Surface area, Maximum radius and Lower Root Area from pixel units to physical units (in meters). We now describe the estimation of the physical lengths of plant roots from the images, in detail.

Consider the Figure 5.5. The object AB is at u units away from the camera lens, that has a focal length of f. The image is formed at v units on the camera sensor. h is the height of the object being imaged and d is the height of the image formed

on the image sensor. Our aim is to determine the height of the object given u, f, number of pixels of the object on the image n and the image sensor size s.

Using the lens formula,

$$\frac{1}{u} + \frac{1}{v} = \frac{1}{f} \tag{5.7}$$

$$1 - \frac{u}{f} = -\frac{1}{m} \tag{5.8}$$

where m is called Magnification given by (v/u). Also, from the Figure 5.5, triangles APO and CPI are similar. Hence, we have

$$\frac{h/2}{u} = \frac{d/2}{v} \tag{5.9}$$

$$h = \frac{ud}{v} \tag{5.10}$$

$$h = \frac{d}{m} \tag{5.11}$$

From the equations 5.8 and 5.11, we have

$$h = -\left(1 - \frac{u}{f}\right) d \tag{5.12}$$

$$h = \frac{(u - f)\, d}{f} \tag{5.13}$$

Since, d is the height of the image on the sensor, we can find its value using the

following calculation.

$$d = \frac{(image\ height\ in\ pixels,\ n_i)}{(sensor\ height\ in\ pixels,\ n)} \times (sensor\ height\ in\ physical\ units,\ h_s) \quad (5.14)$$

Using both the equations 5.13 and 5.14, we can determine the real height of the object (h) for one pixel in the image, by setting $n_i = 1$. We can then use this predetermined value as a multiplier to the number of pixels to compute the physical heights and widths of the image. All these calculations hold true even widths is used in place of heights in the analysis made above. The pixels have equal height and width. Hence, for images taken in an aspect ratio of 4:3, the number of pixels along width is 4/3 times the number of pixels along height of the image.

We now substitute the sensor sizes, the height in pixels of the sensor sizes and the distance of the real object from the lens of the camera to determine real height of the object (h) for one pixel in the image. In our implementation we set the distance from the cameras to the plant root to be 0.61 meters (or 610 mm) approximately. We use this value as u. For Canon G1X camera, having sensor height of 14 mm, sensor height in pixels of 3264 and operating with a focal length of 35.208 mm, the height of the real object is given by

$$h = \frac{(610\ mm - 35.208\ mm)}{35.208\ mm} \times \frac{1\ pixel \times 14\ mm}{3264\ pixels} \quad (5.15)$$

$$h_{g1x} = 0.07\ mm \quad (5.16)$$

Similarly, for Canon S110 camera, having sensor height of 5.58 mm, sensor height

in pixels of 3000 and operating with a focal length of 13.586 mm, the height of the real object is given by

$$h = \frac{(610\ mm - 13.586\ mm)}{13.586\ mm} \times \frac{1\ pixel \times 5.58\ mm}{3000\ pixels} \tag{5.17}$$

$$h_{s110} = 0.08\ mm \tag{5.18}$$

Here, h_{g1x} and h_{s110} are the heights of the real objects when their image is just one pixel size on the sensor. We can now count the pixels on the image and multiply with these values to estimate the real lengths of the traits, such as total root length. In case when the digital features represent area such as Network area, we multiply the trait with either h^2_{g1x} or h^2_{s110} to convert the trait value to physical units. Similarly, for the Volume trait, we multiply the trait value with h^3_{g1x} or h^3_{s110}.

In order to test the accuracy of estimation of the physical lengths using sensor sizes and focal lengths, we perform a simple experiment of estimating the size of an object, of known size, from its image. In this experiment, we take the image of a rectangular shape of length 212 mm and width 157 mm printed on an A4 size paper. The physical length of the diagonal is $h_{real} = 263.4\ mm$. Images of the rectangle shape were taken from both Canon S110 and Canon G1X cameras using the same camera parameters used for imaging the plant roots. From each of the image, we determined the lengths of diagonals and averaged them in order to remove the effects of unequal camera distortion along the diagonals. The average diagonal lengths of the rectangle in pixel units from the images are given as follows.

$$n_{i,g1x} = 3666.3\ pixels \tag{5.19}$$

$$n_{i,s110} = 3447.6\ pixels \tag{5.20}$$

Using these lengths from both the cameras, and the equations 5.13 and 5.14, we estimate the real length of the diagonal as follows.

$$h = \frac{(610\ mm - 35.208\ mm)}{35.208\ mm} \times \frac{3666.3\ pixels \times 14\ mm}{3264\ pixels} \tag{5.21}$$

$$h_{g1x} = 256.73\ mm \tag{5.22}$$

$$h = \frac{(610\ mm - 13.586\ mm)}{13.586\ mm} \times \frac{3447.6\ pixel \times 5.58\ mm}{3000\ pixels} \tag{5.23}$$

$$h_{s110} = 281.5\ mm \tag{5.24}$$

With the real length of the diagonal in physical units known to be $h_{real} = 263.4\ mm$, the accuracy of estimation of real length using the image from Canon G1X camera is 97.32%. Similarly, the accuracy of estimation of real length using the image from Canon S110 camera is 93.29%. These high accuracies tell us that we use this method to reliably convert the traits from pixel units to physical units.

After converting the traits to physical units, we then proceed towards merging the traits across all the cameras by taking means. When performing correlations between the DIRT features with the manually extracted features, the following features were

converted to physical units before merging the features from all the cameras: Stem Diameter, Tip Diameter median, Tip Diameter mean,Max diameter at 90% depth, median Width, maximum Width, D10, D20, D30, D40, D50, D60, D70, D80, D90, spatial root distribution X, spatial root distribution Y, CPD 25, CPD 50, CPD 75, CPD 90.

Chapter 6

Results and Analysis

The main goal of this study is to find an efficient, faster and an automated procedure for plant root phenotyping, requiring lesser effort. For this, we divide the experiments into the following parts.

- **Performance analysis** In this experiment we compare the running time taken at various stages of the data collection procedure. That is an average observed time is recorded at the time of imaging the plant root, followed by time taken to segment the image and finally extraction of the phenotypic traits features from the segmented image. We compare the performance in speed with that of the DIRT system.

- **Correlation with the manually extracted traits** It is necessary for a reliable phenotyping system to extract features that can be correlated with that of the manually extracted features. In this experiment, we take the phenotypic traits that we extracted from the images and compare them with the

manually extracted features using Pearson correlation. We also discuss how a simple merge of the features from all the cameras may result in a better Pearson correlation coefficient.

- **Average standard deviation of traits across cameras** Here we discuss how traits vary between each camera.

We now describe the data collected over a period of 3 years and ran the multi-camera high throughput phenotypic system. In 2014, a total of 6113 plant roots of soybean were photographed. These plant roots came from 230 genotypes, where each genotype consists of 3 plots, each plot having approximately 10 plant roots. The photos were taken in an open air multi-camera system that is susceptible to external lighting. The cameras were 1 meter away from the root. The background of the plant root was chosen to be light blue cotton cloth, so that the light does not shine from the surface and that the blue color is easier to remove from the segmentation. The data collection process had become difficult since, the setup was placed in open air, the background was not blue when sun rays were on the background or shadows were formed of the background due to other objects on a day with bright day light. Also, the presence of strong winds reduced the quality of images taken. The cameras were programmed to use the 'Auto' mode which automatically change various parameters such as focal length, aperture, exposure time and ISO speed when taking photos of plant roots. This made us even more difficult for us to process the images properly. The only set of images that were processed for 2014 data was from the front camera (or the camera number 5 as described in Chapter 3).

In 2015, we designed an experimental setup box with only one open side for changing the plant roots after imaging them. This time the setup box is less susceptible to

external lighting and the cameras were programmed to use a specific set of camera parameters. The plant roots were replaced by hooking the plant root to a metallic strip attached to an of a plastic rod. This plastic rod is suspended on two hooks of the ceiling of the setup box, so that the root is placed at the center of the background. This plastic rod is susceptible to movement in strong winds that blow near the open-faced setup box. This led to significant time taken to stop the movement, accompanied by replacement of rod from the suspension whenever we have to replace the root, which is physically taxing. Before taking images of the plant roots, we adjusted the position and angles of the cameras so that the cameras correctly focus the plant root. High quality images were taken using this setup but operating the setup box was laborious. Since, the setup box was more robust, we processed the images from all the 5 cameras facing the background. A total of 1221 plant roots were imaged consisting of 272 plots where each plot contains approximately 5 plants. Of these plant roots, 198 plants were cotton roots which have similar size as that of the soybean roots, with a simpler root system architecture and the remaining plant roots are soybean roots.

In 2016, we closed the setup box from all sides with one side closed using a cloth. This allowed us to check and correct the camera positions in the setup box. The setup box now has an opening at the top-rear part on the ceiling used to replace the roots after imaging. The lid that closes the opening has a PVC pipe of smaller diameter so as to push the root stem inside it and hold it when taking photos from all the cameras. This made the setup physically easier to operate and work. The time taken to image the plants significantly improved to an imaging speed of 5 plants in 3 minutes compared to the previous year imaging speed of 5 plants in 10 minutes. In

this year, we took a total of 1506 plant roots were imaged. These plant roots were divided into plots where each plot consists of approximately 5 plants. We now discuss the speed performance results at every stage of the phenotyping process.

6.1 Performance Analysis

The average imaging speeds of the high-throughput multi-camera phenotyping system in the three year period is shown in the Table 6.1. Further, these speeds can also be compared to the imaging speed of the REST system [1]. The initially designed setup system was very fast as it was just enough for us to hold the plant by hand while another person sends commands to the cameras to image the plant root. The replacing the root was also much faster as we did not have to remove the clamp to which the root is attached. While the initial system was fast, several problems can be observed regarding the quality of the images. Firstly, the images taken in 2014 contained lot of noise and unwanted objects in the background with colors other than light blue. These objects were hard to remove often requiring manual editing of images. Also since the roots were held by us while imaging, we may position the root at a different height, which leads to the plant root going out of focus of the cameras.Additionally, since the cameras were operated in automatic mode, we did not control the focal length, aperture, exposure time and ISO speed. Thus the images did not have good clarity and often resulted in bad segmentations which required us to manually edit the images to extract the root segmentations.

With the design of the experimental setup box in 2015, we made the system less susceptible to external lighting and the cameras were operated at a specific focal

Table 6.1: Speed of imaging the plant roots over the three year period and the REST system [1]. Higher is better.

Imaging Method	**Average imaging speed (#plant roots/minute)**
Experimental setup system as of 2014	2.4
Experimental setup system as of 2015	0.6
Experimental setup system as of 2016	1.2
REST Imaging System	1.5

lengths of 35 mm for Canon G1X cameras and 13.6 mm for Canon S110 cameras. The aperture was set to f/8.0 and the ISO speed was set at 800 for all the cameras, the exposure time was set to 1/40 seconds for Canon G1X cameras ans 1/100 seconds for Canon S110 cameras. This made the image quality very good compared to the image data collected in 2014. Since, the plant roots were replaced after imaging using a plastic rod, it took a lot of time to replace the root. This explains the marked drop in the imaging speed in 2015. The image quality however is good leading to better segmented images and more reliable features traits.

The problems of the setup system in 2015 were fixed in 2016. We now have an opening at the top rear part of the setup box used for replacing the roots. Also, this time the roots were clamped at equal heights which enabled us to crop the images to remove the pipe, used for clamping the root, before segmenting the images. Since, no external light is allowed inside the images were very good leading to excellent segmentation outputs.

Finally, comparing the imaging speed to that of the REST system, our system runs faster taking into account the synchronous operation of multiple cameras and downloading the images after images were taken for every root.

The Table 6.2 shows the segmentation time taken by our phenotyping system by

Table 6.2: Average time taken for segmentation procedure

Segmentation Method	**Average segmentation time (seconds)**
RVM implemenation in MATLAB	90
EM implementation in MATLAB	50
EM implementation in C++ with CPU acceleration	25
EM implementation in C++ with GPU acceleration	10
Otsu's thresholding with trait extraction in REST system	6
DIRT imlementation of Otsu's thresholding	22

various algorithms implemented. The purpose of comparing these times is to select the best segmentation procedure that takes least amount of time for the system to achieve high-throughput plant root phenotyping. We observe that the RVM implementation takes large amount of time due to the fact that the input images need to be preprocessed before segmenting them using the RVM algorithm. Training of the algorithm also takes larger time due to the presence of large amounts of image database. EM implementation in MATLAB is significantly better as we remove unnecessary preprocessing. Unlike RVM, in this case the algorithm is iterative and hence a significant portion of the runtime is taken for maximizing log likelihood compared to initialization of the algorithm based on histograms. The segmentation and feature extraction for the multi-camera system is performed on PC with Intel Xeon E3-1271 v3 processor having 4 cores and 16GB of RAM. The PC has NVIDIA Quadro K600 GPU with 192 CUDA cores having compute capability 3.0. Optimization is achieved further with the usage of harware acceleration techniques for CPU and GPU, which makes this program suitable for online segmentation of images as we image the plant roots in the field and check the image quality with the segmented outputs. As discussed in the chapter 4, Otsu' thresholding, although is faster, may not always give

good segmentation results.

The average time taken by our feature extraction program, which was implemented in MATLAB, was 26.19 seconds. This average was taken by considering the processing time for extracting traits from the complete 2016 image dataset containing 7530 images from all the 5 cameras. The DIRT system takes an average of 860.84 seconds for extracting features from the 2016 image dataset. The DIRT system was run in multi-threaded mode on PC running Ubuntu linux with Intel Core i5-3440 processor having 4 cores.

6.2 Correlation with the manually extracted feature traits

For 2014 and 2015 image sets, we computed 32 features in total, whereas in 2016 we also added the PCA reduced dimensions of radius and orientation histograms. Additionally we also added computational time required to extract the features as one of the traits. With a total of 39 feature traits, the correlation analysis is performed between image traits and the manually extracted traits. When planting the soybean plants in the field by the people from plant science division, the plants were divided into plots. Each plot is a replication of a genotype. Hence, for a specific genotype, multiple plots were planted in the field. Each plot typically contained 5 or 10 plants of same genotype. In the 2014, each plot consisted of 10 plants. All the 10 plants were imaged, whereas only 3 plants per plot were selected for manual feature extraction. In 2015 and 2016, each plot consisted of 5 plants and all the 5 plants were selected for both image and manual feature extraction. When collecting the data, two teams

worked in parallel, one team was imaging the plant roots, other team worked on plant root digging and manual feature extraction. In the years 2014 and 2015, all the images of plants in each plot were imaged and traits extracted manually, but did not keep track of which set of manual features correspond to which image in the image database. The plots were identified by the plot number, but the order of manually extracting/imaging changed between teams. As a result, we have all the image and manual traits of all the plants in a plot, which was not useful for feature comparison of individual plant roots. Hence, for the years of 2014 and 2015, we computed the mean of each image and manual feature for every plant in the plot, and used these values in correlation analysis. However, use of feature means across plot is advantageous in that, it removes the effects of outliers. For example, if one plant root in the whole plot may be very large whereas other plant roots are small, taking mean across the plot reduces the effect of the large root and thus helps in improving the correlation with manual features. In case 2016 data, we kept a track of the manual features corresponding to each image being photographed. Hence, for the 2016 data, we did correlation analysis using both the individual features and the feature mean across each plot. In this section, when performing correlation analysis between features that were extracted from the images in 2015 and 2016, we also show scatter plots of 6 best and 6 least feature combinations displaying both the corresponding Pearson correlation and its P-value. Throughout these scatter plots, the P-values corresponding to the best correlations are very small, indicating that there is a strong evidence that the feature combinations are correlated.

Due to lower quality of images taken in 2014, only the images from camera 5 (the camera front facing towards the background) were processed and the correlation

analysis was performed. We observe that 3 image based traits (Network area, Solidity and maximum radius) better correlate with the overall complexity. we also observe later that many features extracted from images correlate with the overall complexity. In the 2014 image data, the highest correlation is seen with the lower root area and the stem diameter followed by correlation between network area and stem diameter. Since, the images were taken from the cameras at a distance 1 meter from the plant root, and due to lack of quality in the images, most of the lateral roots may not be identified. This may lead to the segmentation containing smaller number of pixels, where most pixels are located at the center of the root, which in turn leads to smaller values of lower root area and network area. As a result, we may find that these image features correlate with the stem diameter. The Table 6.3 shows the correlations of the image traits extracted from the images of front facing camera and the manually extracted features.

In the 2015 image data features were extracted from all the upper 5 cameras. The Table 6.4 show the correlations obtained with every image trait extracted with every manual trait, with all trait values averaged over the plot. In this dataset, we observe many parameters such as median number of roots , network area, perimeter, number of holes strongly correlate with overall complexity. The maximum correlation obtained was between median number of roots and the overall complexity with a correlation value of 0.723. This is logical as the plant root has more number of roots, the complexity is also increased. These correlation values suggest complexity can also be estimated from traits such as perimeter, network area and number of holes. As we hypothesized earlier, more the number of holes that separate the background into several connected components, more will be the overall complexity. This may not be

always true. For example, a very complex plant root may not have holes in the image at all. Most the holes are covered by either some of its lateral roots or shadows. Care has been taken not to create shadows of the plant roots while imaging. This may be one of the reason why the correlation of the overall complexity versus the number of holes did not exceed 0.7. Another set of strong correlations can be observed with number of lower roots and lateral root density lower manual feature traits. Since, most of the root topology is present in the lower roots, many of the image traits agree with these manual features. Specifically, we observe that the median number of roots correlates with number of lower roots with the Pearson correlation of 0.691. Similarly, the network area predominantly comes from the lower roots and hence has a correlation of 0.58. Our phenotyping program sometimes finds a large segmented blob of pixels in the lower root portion of the image and determines the minimum distance of the nearest background pixel from the center of the blob. This distance will be taken as maximum radius. Although such a radius value may not exist in the actual plant root, from the segmented image we cannot distinguish the nearby roots. Hence, the maximum radius correlates with lateral root density lower and not the number of lower roots. We also observe that some of the bins in radius histogram correlate negatively on lateral root density lower trait. This tells us that if the root has wider and more thick lateral roots, then their count is smaller. Also overall complexity weakly correlates with the first bin of the radius tells us that complex roots usually have tinier roots. The Figure 6.1 and Figure 6.2 shows the scatter plot of the traits between best and worst correlated trait combinations respectively. We observe that some of the feature trait combinations are uncorrelated, which logically correct. For example, the mean lower angle of all the lower roots of a plant root is

not related to the volume occupied by the root.

We then performed correlation analysis on a simple merge of the features from all the cameras for the 2015 image dataset. The traits merged were the plot averages in all the cameras. The merging operation is determined as the mean across all the cameras. For example, a set of 5 plant roots belonging to a plot were imaged. These images were segmented and features extracted. Then we compute the mean of these features for that plot for each camera separately followed by merging of the features. The merging involves taking the mean of these plot averages from all the cameras. Hence, if we image 100 plots of plant data, we get 100 samples of trait feature vectors after merging the features. Using these merged features, we perform the correlation analysis with the plot averages of the manually extracted features for 2015 image dataset. The results of the correlation analysis is given in the Table 6.5. The values marked in red indicate the correlation was greater than any correlation done using features from single cameras. The correlation between the median number of roots and the overall complexity for the camera number 6 (located at the right end of the wooden plank in the experimental setup box) is 0.736. when the correlation is performed on the merged features, this correlation value decreased slightly to 0.729. On the other hand, several other correlation values with various feature combinations improved. The Figure 6.3 and Figure 6.4 shows the scatter plot of the traits between best and worst correlated trait combinations for merged features respectively.

Table 6.3: Pearson correlation values between the automatically extracted features and the manually extracted features for 2014 data. The feature values averaged for each plot from front facing camera, are used in the correlation analysis.

Feature Names	SD	OC	NS	NUR	MDUA	MEUA	NLR	MDLA	MELA
Median no. of roots	0.41	0.33	0.36	0.02	0.03	0.03	0.21	-0.01	-0.03
Maximum no. of roots	0.35	0.30	0.36	0.04	-0.01	-0.02	0.20	-0.09	-0.11
Total root length	0.46	0.38	0.37	0.02	0.06	0.05	0.22	-0.03	-0.05
Depth	0.29	0.18	0.19	0.10	0.07	0.09	0.13	0.00	0.00
Maximum width	0.36	0.15	0.11	-0.01	0.02	0.02	0.15	-0.10	-0.10
Width-to-depth ratio	0.25	0.07	0.00	-0.08	-0.02	-0.03	0.09	-0.12	-0.13
Network area	0.50	0.47	0.33	-0.03	0.08	0.07	0.27	0.00	-0.01
Convex area	0.41	0.21	0.17	0.02	0.06	0.06	0.18	-0.05	-0.05
Solidity	0.25	0.49	0.30	-0.05	0.06	0.04	0.20	0.08	0.06
Perimeter	0.44	0.34	0.35	0.04	0.04	0.04	0.22	-0.04	-0.05
Average radius	0.15	0.27	-0.01	-0.08	0.05	0.04	0.09	0.08	0.08
Volume	-0.01	0.04	-0.01	0.04	0.02	0.03	0.00	0.00	0.01
Surface area	0.39	0.40	0.27	0.00	0.08	0.07	0.21	0.01	0.00
Maximum radius	0.40	0.47	0.25	0.01	0.03	0.03	0.21	0.07	0.07
Lower root area	0.51	0.41	0.33	-0.03	0.08	0.07	0.24	0.02	0.00
radhist1	-0.28	-0.19	-0.02	0.11	-0.04	-0.03	-0.06	-0.06	-0.05
radhist2	0.27	0.18	0.02	-0.11	0.04	0.03	0.06	0.06	0.06
radhist3	0.34	0.34	0.15	-0.11	0.07	0.05	0.11	0.07	0.06
radhist4	0.27	0.39	0.15	-0.10	0.06	0.05	0.13	0.08	0.06
radhist5	0.13	0.32	0.11	-0.06	0.05	0.04	0.10	0.07	0.06
radhist6	-0.02	0.23	0.04	0.00	0.01	0.01	0.04	0.06	0.04
radhist7	-0.10	0.14	0.01	0.04	-0.01	-0.01	-0.01	0.04	0.03
radhist8	-0.04	0.11	0.02	0.02	-0.03	-0.02	-0.02	0.04	0.03
radhist9	0.11	0.13	0.09	0.00	-0.04	-0.03	-0.01	0.04	0.04
radhist10	0.28	0.19	0.12	-0.01	0.01	0.01	0.04	0.04	0.03
orihist1	0.08	0.25	0.29	0.16	-0.01	0.01	0.08	0.07	0.07
orihist2	0.08	0.13	0.14	0.07	-0.01	0.00	0.11	0.04	0.01
orihist3	-0.15	-0.26	-0.32	-0.08	0.02	0.02	-0.12	-0.11	-0.11
orihist4	-0.07	-0.18	-0.25	-0.13	-0.03	-0.05	-0.08	-0.07	-0.06
orihist5	0.13	0.22	0.25	0.01	0.03	0.02	0.07	0.08	0.08
orihist6	0.08	0.27	0.31	0.15	-0.01	0.01	0.09	0.04	0.04
Number of Holes	0.31	0.25	0.32	0.03	0.00	-0.01	0.11	-0.08	-0.10

Table 6.4: Pearson correlation values between the automatically extracted features of 2015 trait data and the manually extracted features. The feature values from front facing camera, averaged over plots, are used in the correlation analysis.

Feature Names	SD	TR	OC	NS	ND	NUR	LRDU	MDUA	MEUA	NLR	LRDL	MDLA	MELA
Median no. of roots	0.07	-0.09	0.72	0.36	0.54	0.34	0.40	0.15	0.18	0.69	0.49	0.07	0.11
Max. no. of roots	0.05	-0.03	0.63	0.39	0.55	0.28	0.48	0.06	0.09	0.55	0.62	-0.08	-0.04
Total root length	0.08	-0.06	0.63	0.31	0.49	0.33	0.47	0.10	0.14	0.57	0.57	0.00	0.03
Depth	-0.01	-0.25	0.43	0.22	0.33	0.24	0.46	0.12	0.13	0.41	0.39	0.01	0.04
Max. width	-0.01	-0.03	0.33	0.25	0.28	0.20	0.40	0.02	0.04	0.37	0.54	-0.15	-0.12
Width-to-depth ratio	0.01	0.12	0.06	0.16	0.09	0.06	0.15	-0.07	-0.05	0.19	0.41	-0.21	-0.20
Network area	0.09	-0.04	0.66	0.32	0.48	0.34	0.46	0.14	0.18	0.61	0.59	-0.01	0.02
Convex area	-0.02	-0.09	0.43	0.23	0.32	0.24	0.47	0.07	0.10	0.43	0.55	-0.07	-0.04
Solidity	0.14	0.27	0.04	-0.14	0.00	-0.01	-0.24	0.06	0.06	0.02	-0.07	0.10	0.10
Perimeter	0.05	-0.09	0.70	0.34	0.54	0.34	0.48	0.13	0.18	0.66	0.56	0.01	0.05
Average radius	0.05	0.27	-0.57	-0.38	-0.47	-0.27	-0.44	-0.08	-0.11	-0.46	-0.21	-0.03	-0.06
Volume	0.09	0.05	0.41	0.22	0.32	0.24	0.35	0.08	0.10	0.38	0.56	-0.02	0.00
Surface area	0.10	-0.01	0.56	0.29	0.43	0.31	0.43	0.10	0.13	0.50	0.59	-0.02	0.01
Maximum radius	0.09	0.08	0.35	0.27	0.40	0.14	0.28	0.03	0.04	0.39	0.64	-0.02	0.00
Lower root area	0.04	-0.11	0.63	0.28	0.41	0.33	0.44	0.14	0.18	0.61	0.54	0.03	0.07
radhist1	0.05	-0.09	0.47	0.35	0.42	0.26	0.32	0.07	0.10	0.45	0.22	0.01	0.04
radhist2	0.02	0.08	-0.37	-0.18	-0.32	-0.20	-0.18	-0.05	-0.07	-0.17	0.22	-0.08	-0.09
radhist3	-0.09	-0.08	-0.31	-0.15	-0.24	-0.13	-0.23	0.00	-0.02	-0.33	-0.25	0.02	0.01
radhist4	-0.11	-0.04	-0.35	-0.19	-0.25	-0.13	-0.34	0.00	-0.02	-0.41	-0.53	0.07	0.04
radhist5	-0.11	-0.03	-0.39	-0.26	-0.30	-0.18	-0.40	-0.02	-0.05	-0.45	-0.56	0.08	0.05
radhist6	-0.09	0.00	-0.41	-0.30	-0.33	-0.25	-0.40	-0.06	-0.09	-0.45	-0.58	0.03	0.00
radhist7	-0.07	0.05	-0.44	-0.34	-0.33	-0.30	-0.38	-0.07	-0.11	-0.41	-0.52	0.00	-0.03
radhist8	-0.02	0.13	-0.43	-0.39	-0.37	-0.27	-0.43	-0.08	-0.11	-0.38	-0.38	-0.05	-0.08
radhist9	0.05	0.31	-0.44	-0.38	-0.34	-0.20	-0.39	-0.04	-0.07	-0.29	-0.07	-0.07	-0.09
radhist10	0.07	0.27	-0.43	-0.32	-0.29	-0.21	-0.33	-0.10	-0.12	-0.20	0.17	-0.14	-0.15
orihist1	-0.07	-0.16	0.18	-0.06	0.14	-0.01	0.10	0.14	0.15	-0.12	-0.31	0.32	0.30
orihist2	0.00	-0.12	0.37	0.19	0.30	0.18	0.30	0.11	0.11	0.25	0.23	0.19	0.20
orihist3	-0.03	0.05	-0.39	-0.04	-0.28	-0.13	-0.19	-0.08	-0.09	-0.15	0.07	-0.35	-0.36
orihist4	0.05	0.21	-0.31	-0.20	-0.22	-0.12	-0.31	-0.13	-0.14	-0.06	0.04	-0.26	-0.25
orihist5	0.05	-0.08	0.50	0.19	0.38	0.20	0.32	0.10	0.14	0.30	0.12	0.26	0.30
orihist6	-0.05	-0.15	0.14	-0.05	0.11	-0.04	0.17	0.05	0.06	-0.15	-0.30	0.29	0.28
holes	0.10	-0.03	0.66	0.31	0.54	0.30	0.43	0.08	0.12	0.58	0.52	0.02	0.05

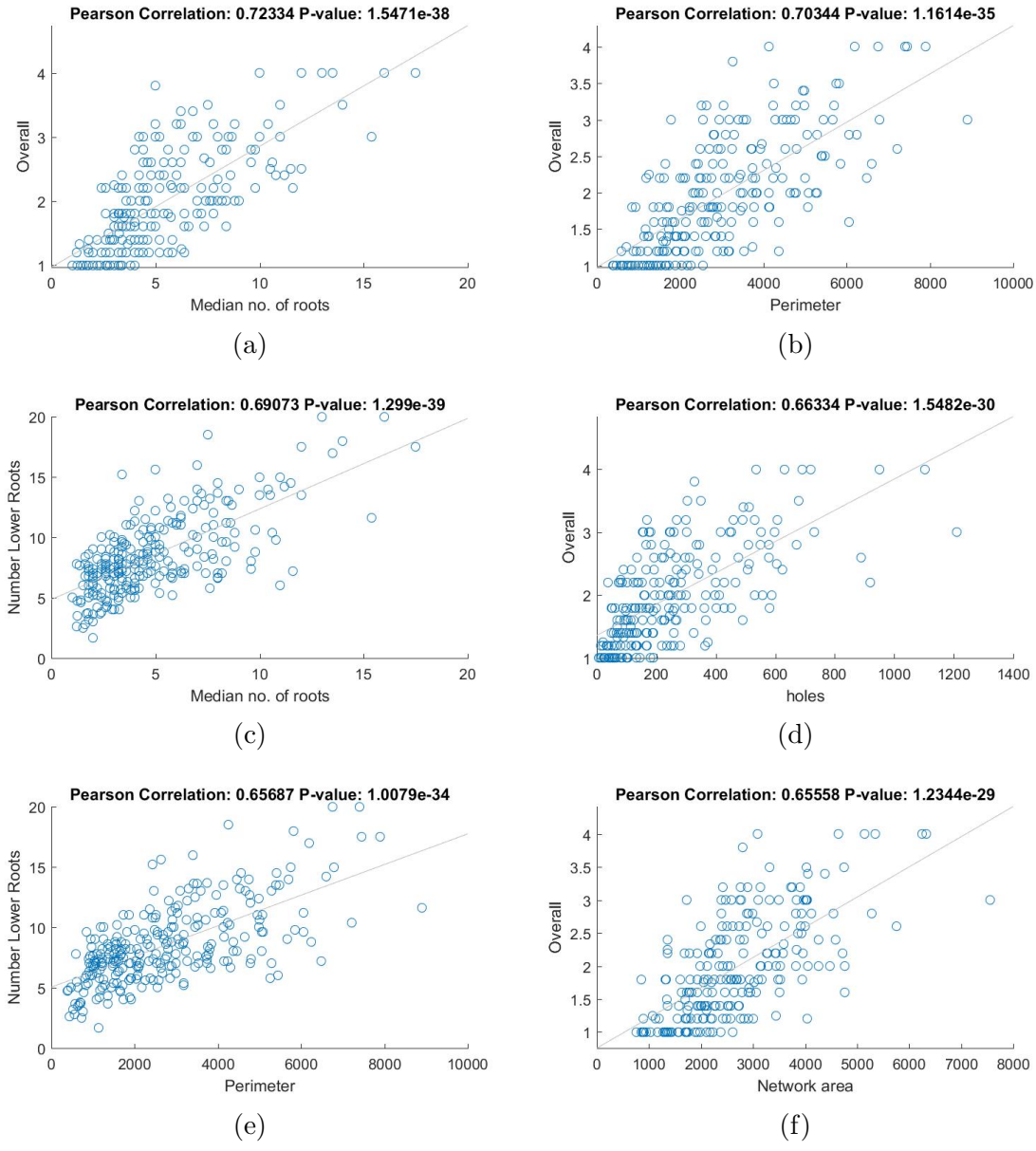

Figure 6.1: Best Pearson correlation values obtained between front facing camera features and the manual features for 2015 image dataset. The traits were averaged over plots before correlation analysis.

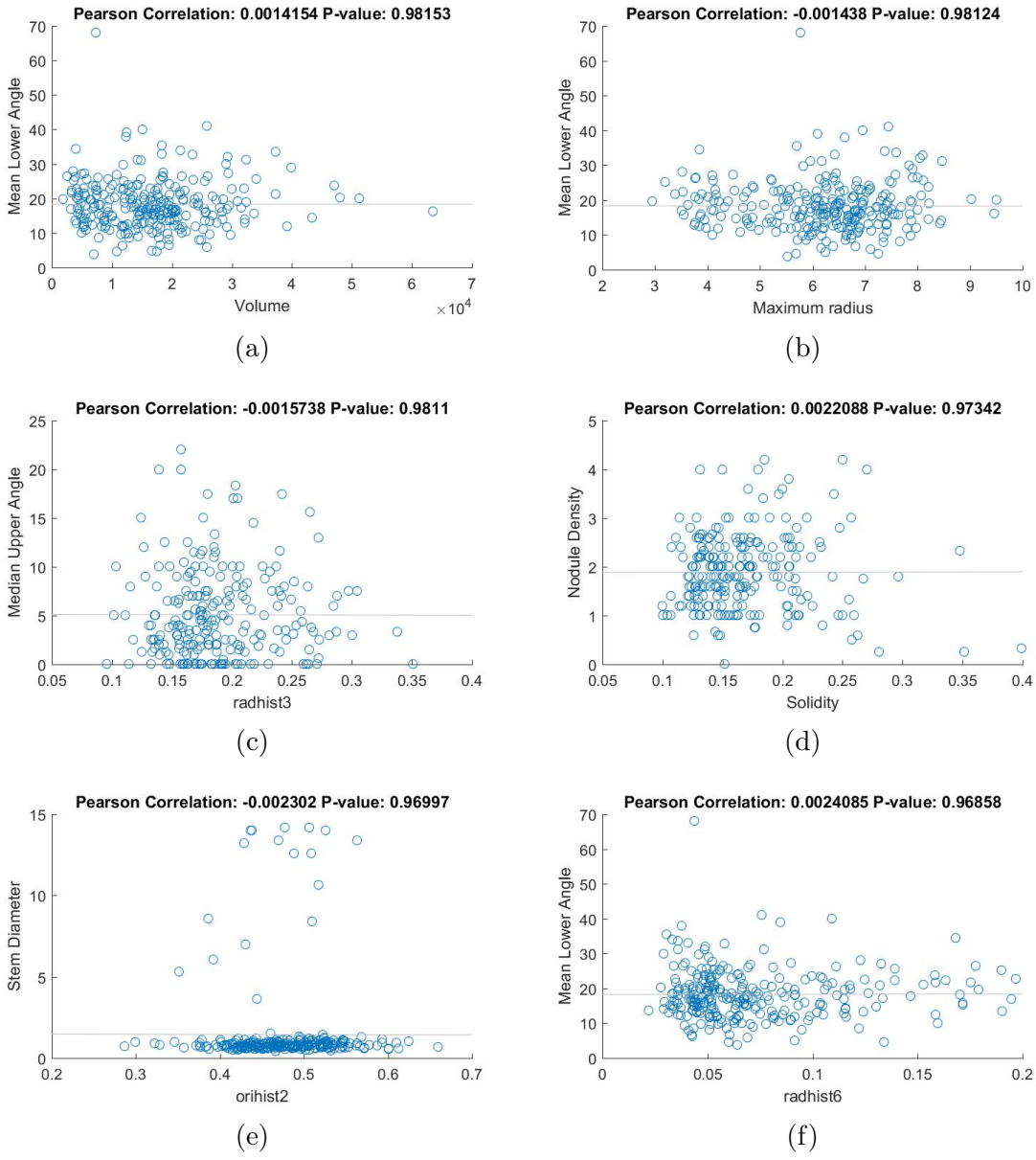

Figure 6.2: Trait combinations with least correlation between front facing camera features and the manual features for 2015 image dataset. The traits were averaged over plots before correlation analysis.

Table 6.5: Pearson correlation values between the automatically extracted features of 2015 trait data and the manually extracted features. The mean values across all cameras of the automatically extracted features, averaged over the plots, are used in the correlation analysis.

Feature Names	SD	TR	OC	NS	ND	NUR	LRDU	MDUA	MEUA	NLR	LRDL	MDLA	MELA
Median no. of roots	0.08	-0.09	0.73	0.36	0.56	0.35	0.40	0.14	0.18	0.69	0.49	0.07	0.10
Max. no. of roots	0.05	-0.05	0.64	0.41	0.57	0.30	0.50	0.06	0.10	0.55	0.62	-0.07	-0.05
Total root length	0.07	-0.06	0.65	0.32	0.51	0.33	0.48	0.10	0.14	0.58	0.57	0.01	0.04
Depth	0.02	-0.22	0.42	0.21	0.32	0.24	0.47	0.10	0.12	0.40	0.41	-0.00	0.03
Max. width	0.01	-0.02	0.35	0.25	0.29	0.20	0.43	0.01	0.04	0.39	0.57	-0.13	-0.10
Width-to-depth ratio	0.02	0.12	0.10	0.17	0.12	0.07	0.19	-0.07	-0.05	0.22	0.45	-0.20	-0.19
Network area	0.10	-0.04	0.66	0.32	0.49	0.34	0.46	0.14	0.18	0.61	0.59	0.01	0.04
Convex area	0.01	-0.08	0.44	0.22	0.32	0.25	0.49	0.07	0.10	0.44	0.57	-0.06	-0.03
Solidity	0.12	0.27	0.04	-0.14	-0.01	-0.01	-0.27	0.07	0.06	0.02	-0.06	0.10	0.10
Perimeter	0.07	-0.09	0.71	0.34	0.55	0.35	0.48	0.13	0.18	0.66	0.56	0.02	0.05
Average radius	0.05	0.29	-0.58	-0.38	-0.48	-0.29	-0.45	-0.08	-0.11	-0.46	-0.19	-0.05	-0.07
Volume	0.08	0.06	0.40	0.22	0.32	0.22	0.35	0.07	0.09	0.38	0.56	-0.02	-0.01
Surface area	0.09	-0.01	0.56	0.29	0.44	0.31	0.44	0.10	0.13	0.51	0.59	-0.01	0.02
Maximum radius	0.11	0.12	0.34	0.25	0.39	0.13	0.26	0.03	0.05	0.37	0.64	-0.02	-0.01
LowerRootArea	0.04	-0.10	0.64	0.28	0.43	0.33	0.43	0.16	0.19	0.61	0.53	0.05	0.09
radhist1	0.06	-0.13	0.53	0.38	0.47	0.29	0.34	0.06	0.10	0.47	0.19	-0.02	0.00
radhist2	0.02	0.12	-0.45	-0.23	-0.39	-0.25	-0.18	-0.05	-0.08	-0.17	0.27	-0.03	-0.04
radhist3	-0.07	-0.04	-0.38	-0.20	-0.32	-0.16	-0.26	-0.00	-0.03	-0.34	-0.18	0.04	0.02
radhist4	-0.12	-0.03	-0.40	-0.21	-0.30	-0.16	-0.35	0.00	-0.02	-0.45	-0.49	0.07	0.05
radhist5	-0.12	-0.03	-0.45	-0.26	-0.32	-0.22	-0.40	-0.02	-0.05	-0.48	-0.55	0.09	0.07
radhist6	-0.11	0.01	-0.45	-0.29	-0.34	-0.26	-0.42	-0.07	-0.10	-0.48	-0.58	0.03	0.00
radhist7	-0.09	0.04	-0.47	-0.32	-0.36	-0.30	-0.41	-0.08	-0.11	-0.46	-0.56	-0.02	-0.04
radhist8	-0.05	0.12	-0.46	-0.36	-0.37	-0.30	-0.43	-0.09	-0.12	-0.42	-0.42	-0.07	-0.10
radhist9	0.03	0.28	-0.51	-0.36	-0.38	-0.27	-0.44	-0.09	-0.13	-0.36	-0.15	-0.12	-0.15
radhist10	0.06	0.34	-0.50	-0.38	-0.37	-0.26	-0.41	-0.12	-0.16	-0.28	0.06	-0.14	-0.15
orihist1	-0.07	-0.15	0.13	-0.13	0.09	-0.03	0.06	0.12	0.14	-0.19	-0.38	0.28	0.27
orihist2	-0.01	-0.15	0.45	0.25	0.36	0.21	0.34	0.15	0.16	0.30	0.28	0.23	0.24
orihist3	-0.06	0.04	-0.38	-0.06	-0.28	-0.14	-0.21	-0.06	-0.08	-0.12	0.07	-0.35	-0.36
orihist4	0.05	0.19	-0.39	-0.21	-0.27	-0.15	-0.31	-0.15	-0.17	-0.09	0.05	-0.30	-0.30
orihist5	0.09	-0.02	0.50	0.20	0.40	0.21	0.31	0.09	0.12	0.30	0.15	0.28	0.31
orihist6	-0.07	-0.14	0.14	-0.09	0.11	-0.01	0.12	0.07	0.09	-0.20	-0.39	0.24	0.24
holes	0.06	-0.06	0.67	0.33	0.56	0.31	0.43	0.09	0.13	0.60	0.50	0.04	0.06

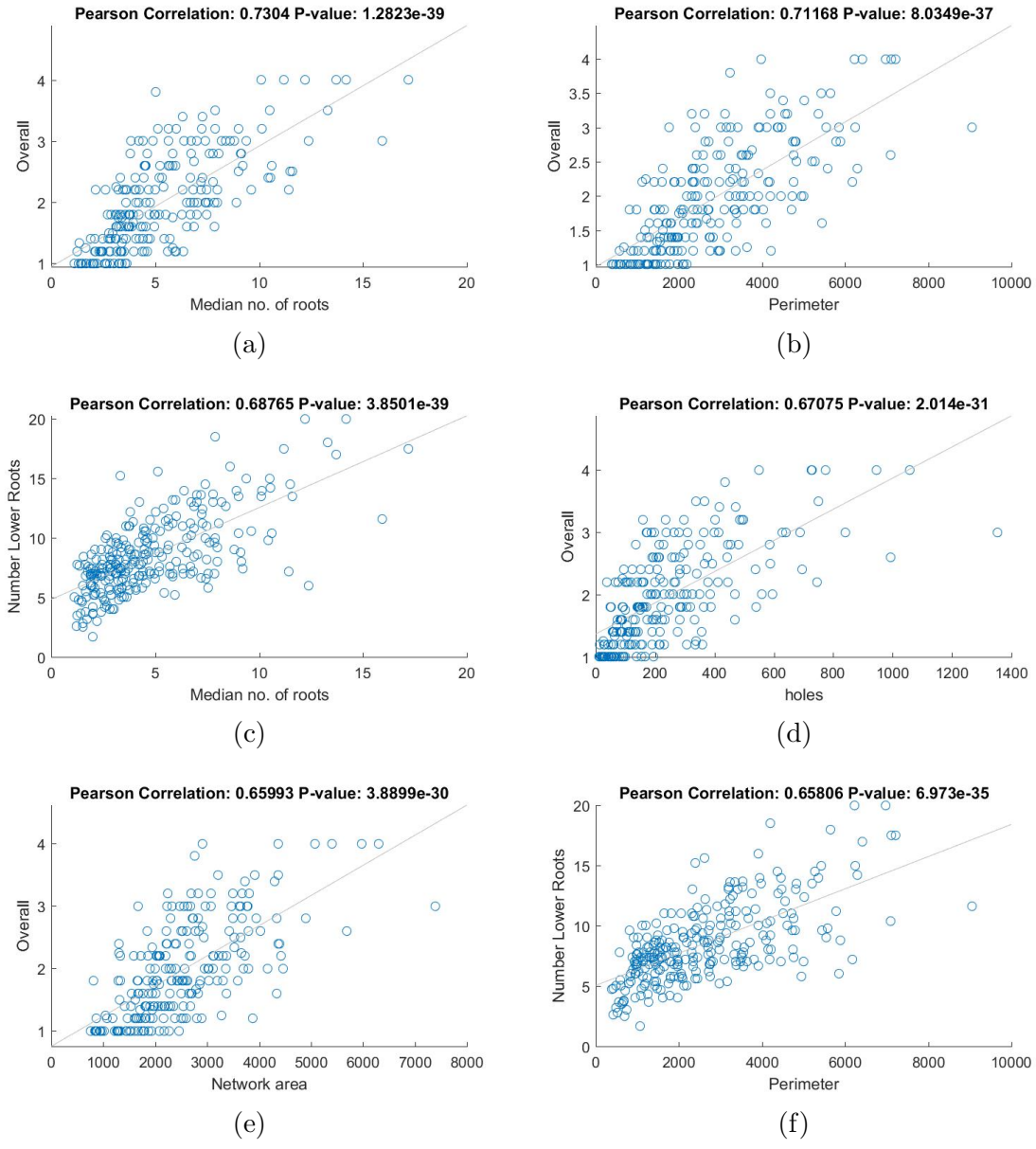

Figure 6.3: Best Pearson correlation values obtained between combined mean features from all the cameras and the manual features for 2015 image dataset. The traits were averaged over plots before correlation analysis.

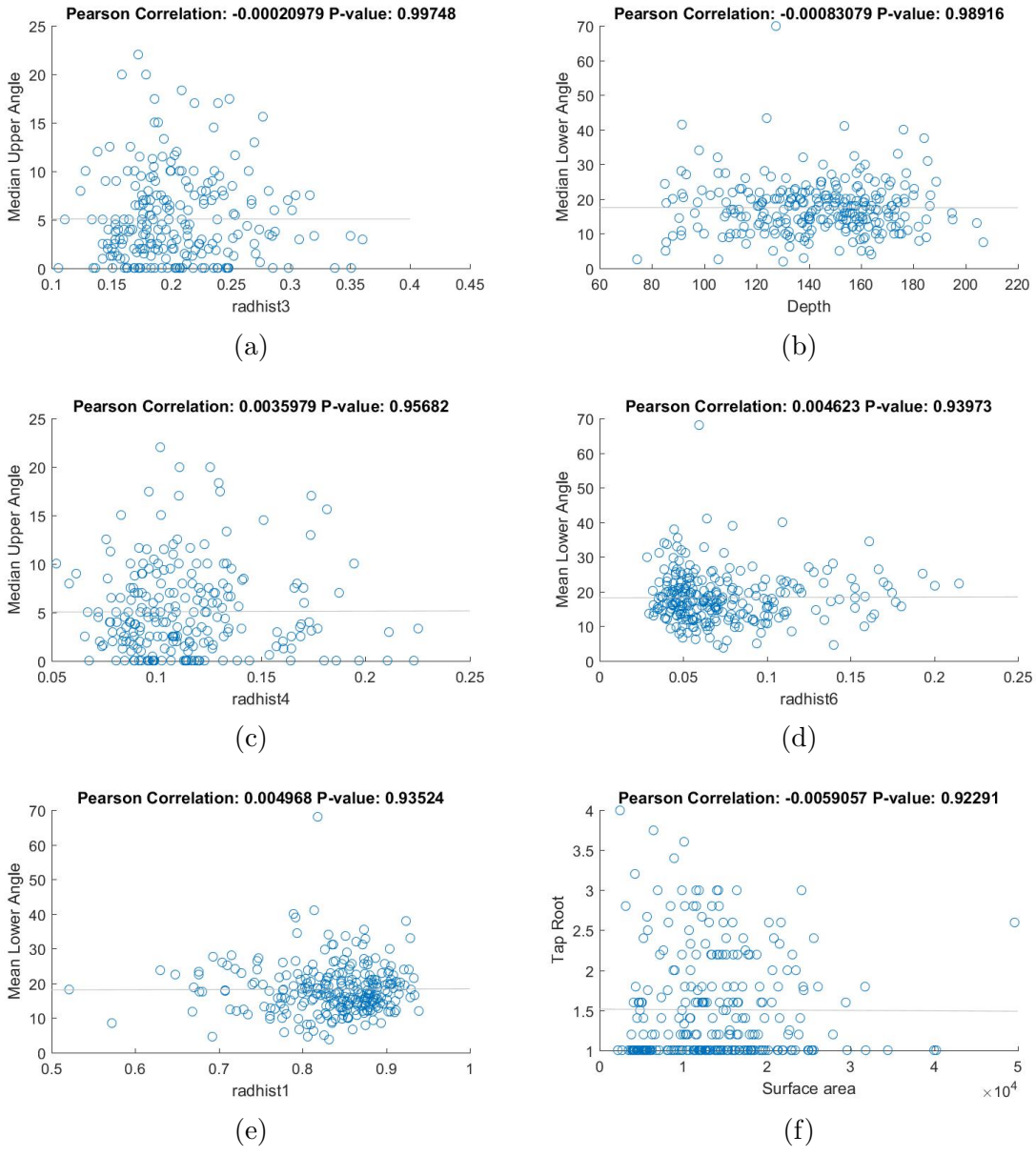

Figure 6.4: Trait combinations with least correlation between combined mean features from all the cameras and the manual features for 2015 image dataset. The traits were averaged over plots before correlation analysis.

The DIRT phenotyping program is run on the 2015 image dataset, which extracted 53 features in total from each image. These features are then compared to the manually extracted features. The Table 6.6 and the Table 6.7 contain the correlation values obtained with the manually extracted features for the features from the front facing camera and the merge of the features from all the cameras. Using only the features from the front facing camera, the highest correlation is obtained between skeleton vertices DIRT feature and the overall complexity with the Pearson correlation of 0.68. When the features were combined, this correlation value is then 0.69. we also observe a marked improvement in the correlation values over a number of feature combinations as shown in the Table 6.7. The values marked in red indicate that the correlation was greater with merged features than with features from any single camera. The Figure 6.5 and Figure 6.6 shows the scatter plot of the traits between best and worst correlated trait combinations respectively for the DIRT features from the front facing camera. The Figure 6.7 and Figure 6.8 shows the scatter plot of the traits between best and worst correlated trait combinations respectively for the DIRT features that are obtained by merging the features from all cameras.

Table 6.6: Pearson correlation values between the automatically extracted DIRT features of 2015 trait data and the manually extracted features. The feature values from the front facing camera, averaged over plots, are used in the correlation analysis.

Feature Names	SD	TR	OC	NS	ND	NUR	LRDU	MDUA	MEUA	NLR	LRDL	MDLA	MELA
Skeleton Vertices	0.07	-0.08	0.68	0.33	0.51	0.33	0.47	0.14	0.18	0.64	0.56	0.02	0.05
stemDia	-0.02	0.00	-0.02	0.00	0.01	-0.01	0.05	0.02	0.04	0.12	0.27	-0.02	-0.02
avg. Root Density	-0.03	0.09	-0.02	0.00	0.06	-0.04	-0.03	0.05	0.07	-0.05	0.03	-0.04	-0.07
STA range	-0.03	-0.15	0.41	0.22	0.37	0.22	0.41	0.07	0.08	0.38	0.34	0.06	0.08
STA dom. angle 1	-0.03	-0.15	-0.02	0.05	0.03	-0.14	-0.10	-0.08	-0.08	-0.06	-0.12	0.08	0.08
STA dom. angle 2	-0.01	-0.05	-0.09	0.03	-0.01	-0.22	-0.06	-0.09	-0.09	-0.15	-0.06	0.07	0.06
STA 25% 1	0.03	0.00	0.15	0.02	0.11	0.13	0.03	0.16	0.14	0.10	0.02	0.04	0.03
STA 25% 2	-0.02	0.01	0.04	-0.06	-0.05	0.05	-0.14	0.11	0.09	0.02	-0.14	-0.05	-0.05
STA 50% 1	0.04	0.09	0.03	-0.06	-0.03	-0.03	0.04	0.15	0.14	-0.01	0.04	-0.12	-0.13
STA 50% 2	0.02	0.14	-0.15	-0.10	-0.14	-0.11	-0.13	0.04	0.02	-0.23	-0.11	-0.05	-0.09
STA 75% 1	0.09	0.08	-0.12	-0.08	-0.12	-0.11	-0.03	-0.03	-0.05	-0.12	0.05	-0.05	-0.03
STA 75% 2	-0.03	0.14	-0.19	-0.13	-0.13	-0.14	-0.12	-0.03	-0.03	-0.24	-0.14	0.14	0.12
STA 90% 1	0.11	0.06	-0.19	-0.12	-0.15	-0.11	-0.03	-0.09	-0.09	-0.20	-0.10	0.03	0.03
STA 90% 2	-0.03	0.06	-0.22	-0.21	-0.23	-0.09	-0.10	0.00	-0.01	-0.24	-0.24	0.16	0.16
RTA dom. angle 1	0.02	0.06	-0.21	-0.25	-0.19	0.02	-0.07	-0.00	0.00	-0.21	-0.13	-0.03	-0.03
RTA dom. angle 2	-0.03	0.03	-0.15	-0.28	-0.15	0.01	-0.19	0.07	0.08	-0.24	-0.30	0.09	0.09
STA min.	0.05	0.15	-0.41	-0.20	-0.35	-0.24	-0.40	-0.10	-0.11	-0.37	-0.33	-0.07	-0.08
STA max.	0.06	-0.05	0.20	0.17	0.20	0.06	0.19	-0.06	-0.06	0.20	0.17	-0.00	0.02
STA median	-0.01	-0.04	-0.16	-0.16	-0.21	-0.08	-0.17	0.04	0.03	-0.16	-0.19	-0.05	-0.01
RTA range	-0.02	-0.07	0.32	-0.02	0.12	0.08	0.07	0.23	0.24	0.17	-0.14	0.45	0.45
RTA min.	-0.06	0.01	-0.25	-0.16	-0.16	-0.17	-0.19	-0.04	-0.02	-0.27	-0.38	0.06	0.05
RTA max.	0.11	0.11	0.43	0.25	0.38	0.22	0.29	0.05	0.07	0.36	0.41	-0.02	-0.00
RTA median	0.11	0.11	0.44	0.26	0.39	0.23	0.30	0.05	0.07	0.37	0.43	-0.03	-0.01
Nr. of RTPs	0.09	-0.06	0.53	0.25	0.39	0.30	0.45	0.07	0.11	0.50	0.54	-0.01	0.02
TD median	-0.03	0.06	-0.03	-0.05	0.04	-0.07	-0.01	-0.02	-0.00	-0.04	0.07	-0.04	-0.06
TD mean	0.03	0.15	-0.16	-0.14	-0.09	-0.15	-0.21	-0.05	-0.05	-0.11	-0.10	0.03	-0.01
DD90 max.	0.08	0.02	0.35	0.18	0.30	0.17	0.22	0.11	0.11	0.45	0.43	0.08	0.12
median Width	0.05	0.06	0.38	0.21	0.31	0.19	0.33	0.05	0.09	0.35	0.44	-0.04	-0.03
max. Width	-0.02	-0.01	0.36	0.25	0.33	0.20	0.42	0.02	0.05	0.37	0.55	-0.12	-0.10
D10	-0.04	-0.07	0.29	0.11	0.22	0.12	0.13	0.11	0.11	0.09	-0.15	0.12	0.15
D20	-0.01	-0.02	0.26	0.04	0.17	0.12	0.08	0.11	0.12	0.03	-0.21	0.13	0.15
D30	-0.01	-0.00	0.29	0.03	0.15	0.17	0.07	0.14	0.14	0.05	-0.21	0.13	0.16

D40	-0.00	0.03	0.32	0.04	0.14	0.19	0.07	0.15	0.16	0.08	-0.20	0.13	0.16
D50	-0.00	0.05	0.35	0.04	0.14	0.21	0.06	0.17	0.19	0.11	-0.18	0.14	0.17
D60	0.00	0.05	0.36	0.04	0.15	0.21	0.07	0.16	0.18	0.13	-0.15	0.14	0.16
D70	0.02	0.05	0.37	0.05	0.16	0.20	0.08	0.16	0.18	0.15	-0.11	0.13	0.15
D80	0.02	0.05	0.40	0.07	0.19	0.21	0.09	0.18	0.20	0.20	-0.07	0.11	0.12
D90	0.02	0.01	0.45	0.10	0.24	0.23	0.11	0.21	0.24	0.27	-0.00	0.13	0.14
DS10	-0.04	-0.08	-0.14	0.11	-0.10	-0.10	0.02	-0.10	-0.11	0.02	0.20	-0.15	-0.16
DS20	-0.07	-0.11	-0.24	0.01	-0.09	-0.21	0.01	-0.13	-0.14	-0.12	0.06	-0.06	-0.08
DS30	-0.06	-0.12	-0.32	-0.07	-0.10	-0.25	-0.04	-0.13	-0.15	-0.22	-0.01	-0.09	-0.09
DS40	-0.06	-0.12	-0.32	-0.09	-0.12	-0.22	-0.04	-0.16	-0.18	-0.26	-0.05	-0.10	-0.10
DS50	-0.07	-0.04	-0.33	-0.08	-0.15	-0.22	-0.06	-0.13	-0.16	-0.26	-0.14	-0.04	-0.04
DS60	-0.11	-0.03	-0.34	-0.12	-0.19	-0.18	-0.08	-0.10	-0.12	-0.28	-0.22	0.01	0.01
DS70	-0.11	-0.01	-0.37	-0.13	-0.24	-0.17	-0.13	-0.12	-0.15	-0.31	-0.27	0.05	0.06
DS80	-0.06	0.01	-0.39	-0.15	-0.29	-0.20	-0.18	-0.16	-0.19	-0.35	-0.29	0.00	0.00
DS90	-0.06	0.05	-0.26	-0.12	-0.19	-0.14	-0.13	-0.13	-0.15	-0.32	-0.26	-0.14	-0.14
spatial root distr. X	0.10	-0.02	-0.04	-0.04	-0.04	-0.02	-0.11	-0.04	-0.03	-0.04	-0.17	0.07	0.05
spatial root ditr. Y	-0.03	0.20	-0.53	-0.21	-0.36	-0.27	-0.38	-0.18	-0.20	-0.44	-0.26	-0.04	-0.07
CPD 25	0.12	0.09	-0.04	0.02	0.03	-0.02	0.10	-0.09	-0.06	-0.07	0.21	-0.02	-0.03
CPD 50	0.09	0.14	-0.06	0.05	0.03	-0.07	-0.04	-0.07	-0.06	-0.05	0.17	-0.06	-0.08
CPD 75	0.04	0.14	-0.11	0.00	-0.04	-0.08	-0.11	-0.06	-0.04	-0.11	0.10	-0.08	-0.11
CPD 90	-0.01	0.10	-0.26	-0.15	-0.22	-0.15	-0.06	-0.09	-0.10	-0.25	0.02	-0.06	-0.09

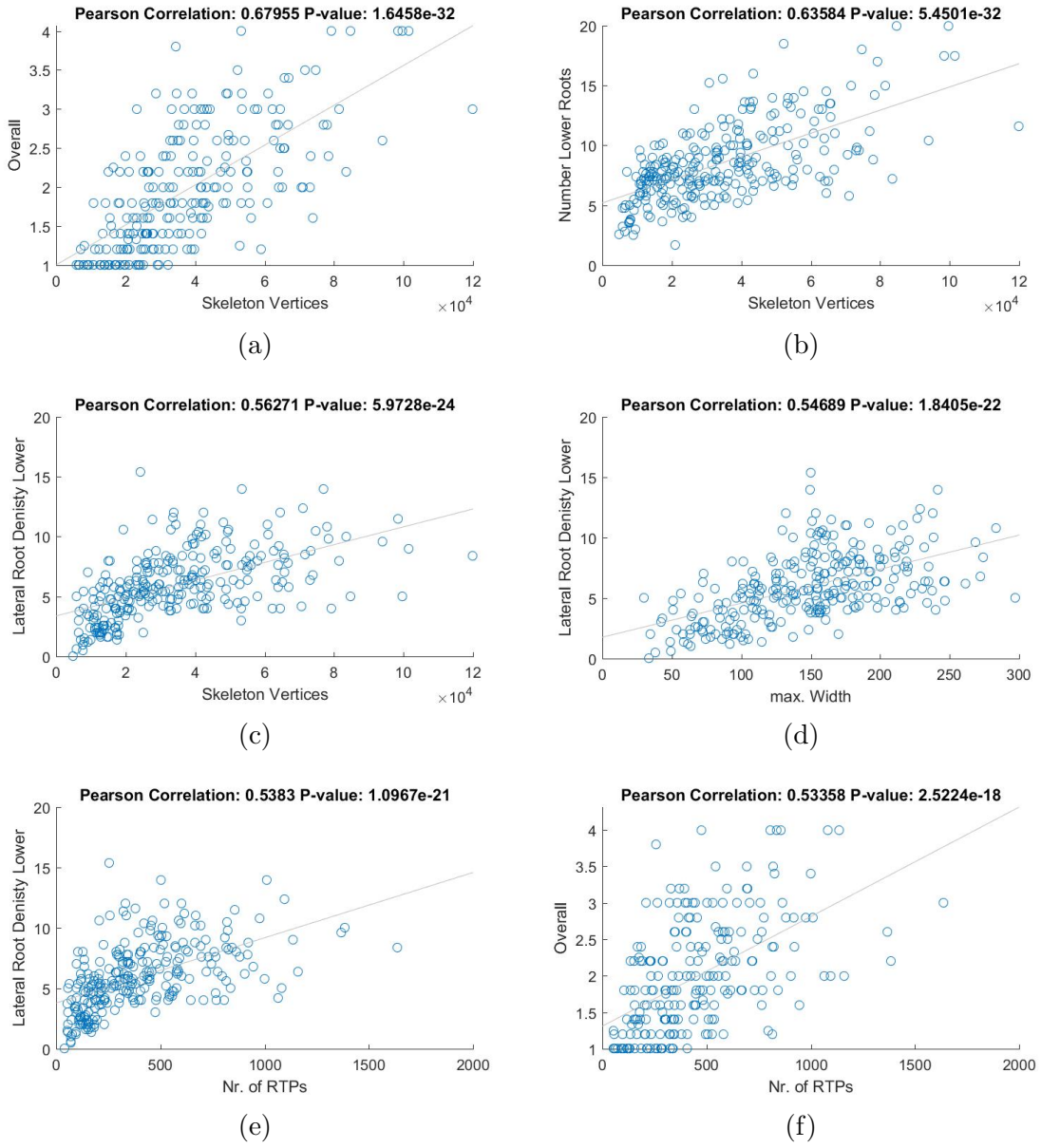

Figure 6.5: Best Pearson correlation values obtained between DIRT features from the front facing camera and the manual features for 2015 image dataset. The traits were averaged over plots before correlation analysis.

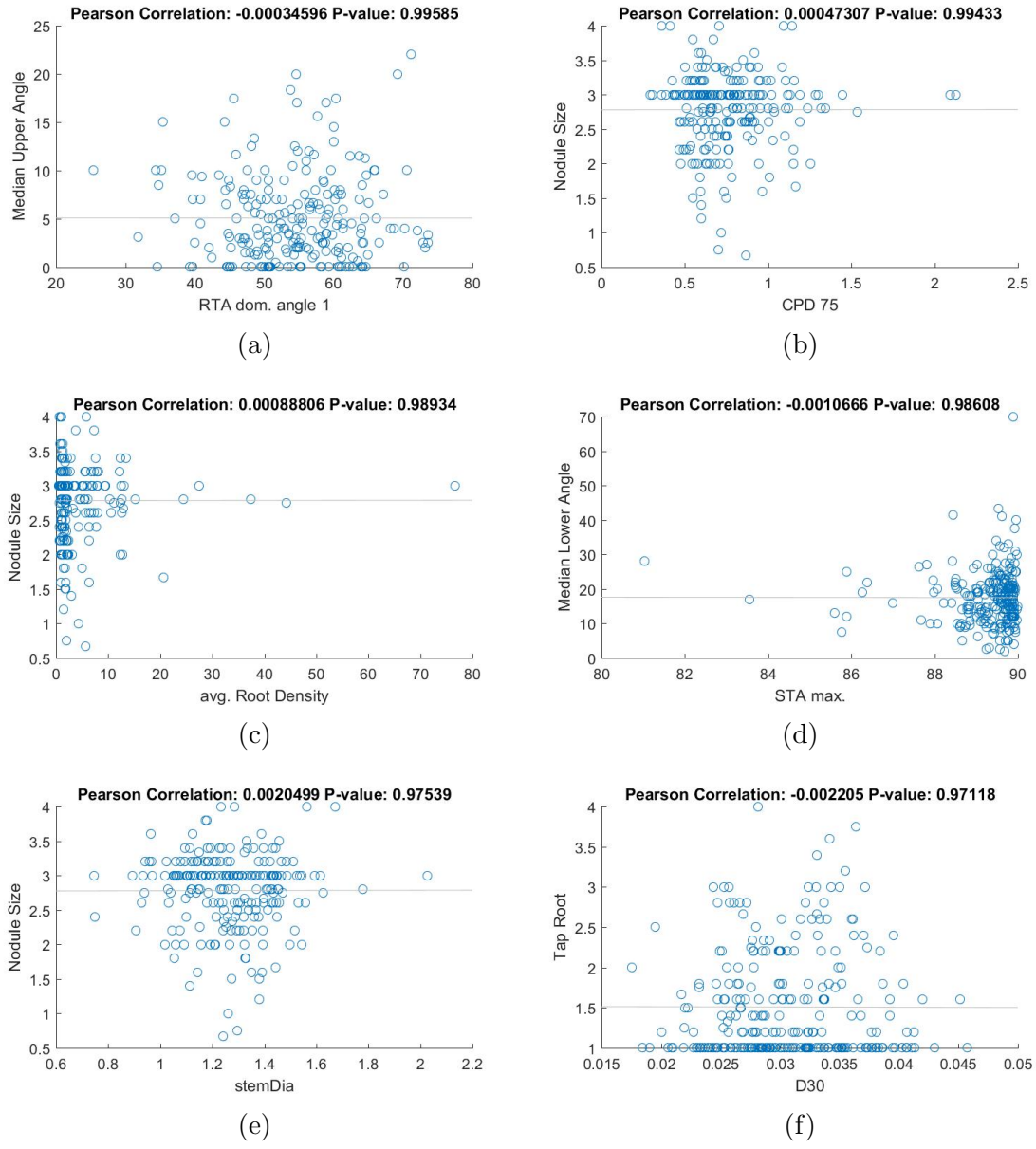

Figure 6.6: Trait combinations with least correlation between DIRT features from the front facing camera and the manual features for 2015 image dataset. The traits were averaged over plots before correlation analysis.

Table 6.7: Pearson correlation values between the automatically extracted DIRT features of 2015 trait data and the manually extracted features. The mean feature values from all the cameras, averaged over plots, are used in the correlation analysis.

Feature Names	SD	TR	OC	NS	ND	NUR	LRDU	MDUA	MEUA	NLR	LRDL	MDLA	MELA
Skeleton Vertices	0.07	-0.08	0.69	0.34	0.53	0.35	0.47	0.13	0.17	0.64	0.57	0.03	0.06
stemDia	-0.07	0.00	-0.05	-0.04	0.01	-0.03	0.03	0.06	0.07	0.13	0.28	0.00	-0.00
avg. Root Density	-0.05	0.12	-0.09	-0.06	0.02	-0.07	-0.05	0.04	0.06	-0.09	0.02	-0.06	-0.08
STA range	0.04	-0.16	0.48	0.43	0.45	0.29	0.44	0.05	0.06	0.47	0.45	-0.00	0.02
STA dom. angle 1	-0.02	-0.02	-0.14	0.03	-0.09	-0.05	-0.15	-0.11	-0.10	-0.22	-0.20	-0.18	-0.19
STA dom. angle 2	-0.04	0.01	-0.23	-0.09	-0.18	-0.21	-0.18	-0.14	-0.16	-0.26	-0.24	-0.07	-0.10
STA 25% 1	0.01	0.01	0.06	0.02	0.06	0.06	0.08	0.04	0.01	-0.01	0.07	-0.12	-0.10
STA 25% 2	-0.07	0.10	-0.24	-0.14	-0.22	-0.13	-0.23	0.03	-0.00	-0.33	-0.36	-0.05	-0.02
STA 50% 1	-0.01	0.09	-0.13	-0.10	-0.13	-0.06	0.04	0.00	-0.01	-0.15	0.03	-0.20	-0.23
STA 50% 2	-0.03	0.08	-0.21	-0.16	-0.18	-0.11	-0.21	-0.00	0.02	-0.33	-0.28	-0.09	-0.14
STA 75% 1	0.01	0.12	-0.24	-0.09	-0.18	-0.10	-0.02	-0.05	-0.06	-0.24	0.03	-0.15	-0.16
STA 75% 2	-0.05	0.10	-0.33	-0.19	-0.28	-0.20	-0.22	-0.11	-0.10	-0.36	-0.30	0.04	0.01
STA 90% 1	-0.09	0.00	-0.40	-0.13	-0.30	-0.20	-0.01	-0.09	-0.12	-0.32	-0.11	-0.05	-0.07
STA 90% 2	-0.07	0.09	-0.36	-0.29	-0.36	-0.23	-0.19	-0.02	-0.04	-0.37	-0.36	0.13	0.11
RTA dom. angle 1	-0.04	0.01	-0.50	-0.22	-0.43	-0.20	-0.14	-0.04	-0.07	-0.43	-0.24	-0.10	-0.13
RTA dom. angle 2	-0.06	0.06	-0.44	-0.32	-0.45	-0.21	-0.30	0.03	0.03	-0.45	-0.51	0.03	0.01
STA min.	-0.02	0.16	-0.47	-0.42	-0.45	-0.29	-0.44	-0.07	-0.07	-0.46	-0.44	0.03	0.00
STA max.	0.08	-0.10	0.36	0.32	0.31	0.22	0.31	-0.01	0.00	0.34	0.34	0.09	0.12
STA median	-0.00	-0.05	-0.23	-0.14	-0.27	-0.11	-0.23	-0.03	-0.04	-0.25	-0.28	0.12	0.15
RTA range	-0.00	-0.05	0.33	0.01	0.10	0.09	0.09	0.20	0.19	0.15	-0.17	0.45	0.45
RTA min.	-0.11	0.06	-0.23	-0.25	-0.20	-0.22	-0.23	0.03	0.03	-0.31	-0.46	0.01	-0.02
RTA max.	0.13	0.06	0.47	0.29	0.42	0.27	0.36	0.13	0.15	0.39	0.47	-0.01	0.02
RTA median	0.13	0.06	0.47	0.30	0.42	0.27	0.37	0.12	0.15	0.40	0.48	-0.01	0.02
Nr. of RTPs	0.08	-0.05	0.57	0.28	0.44	0.31	0.47	0.07	0.10	0.52	0.56	-0.00	0.03
TD median	-0.04	0.15	-0.12	-0.19	-0.05	-0.11	-0.11	0.01	0.02	-0.08	-0.01	-0.05	-0.07
TD mean	0.02	0.17	-0.23	-0.27	-0.18	-0.17	-0.29	-0.00	-0.00	-0.17	-0.23	0.03	0.01
DD90 max.	0.13	-0.00	0.44	0.22	0.35	0.23	0.24	0.16	0.19	0.48	0.49	0.07	0.10
median Width	0.06	0.06	0.45	0.21	0.35	0.23	0.38	0.07	0.11	0.41	0.50	-0.05	-0.03
max. Width	0.01	-0.01	0.38	0.25	0.35	0.21	0.46	0.02	0.05	0.40	0.58	-0.11	-0.08
D10	-0.02	-0.04	0.32	0.18	0.23	0.10	0.14	0.07	0.07	0.08	-0.14	0.10	0.13
D20	-0.01	-0.00	0.28	0.10	0.18	0.10	0.09	0.08	0.09	0.02	-0.21	0.12	0.14
D30	0.01	0.02	0.30	0.08	0.16	0.13	0.07	0.10	0.10	0.02	-0.22	0.13	0.15

D40	0.02	0.04	0.32	0.07	0.14	0.16	0.06	0.12	0.13	0.05	-0.21	0.14	0.16
D50	0.02	0.06	0.35	0.06	0.14	0.18	0.06	0.14	0.16	0.08	-0.19	0.15	0.17
D60	0.02	0.08	0.37	0.05	0.15	0.19	0.07	0.15	0.17	0.11	-0.16	0.15	0.17
D70	0.03	0.09	0.38	0.07	0.16	0.19	0.08	0.15	0.17	0.14	-0.11	0.13	0.15
D80	0.04	0.09	0.42	0.08	0.19	0.20	0.09	0.17	0.19	0.20	-0.06	0.13	0.14
D90	0.03	0.05	0.45	0.10	0.22	0.22	0.11	0.21	0.23	0.27	-0.00	0.13	0.15
DS10	-0.01	-0.08	-0.17	0.07	-0.13	-0.11	0.03	-0.10	-0.12	0.03	0.25	-0.15	-0.15
DS20	-0.10	-0.13	-0.27	0.03	-0.11	-0.22	-0.01	-0.12	-0.13	-0.12	0.07	-0.07	-0.09
DS30	-0.10	-0.14	-0.34	-0.03	-0.13	-0.27	-0.03	-0.15	-0.16	-0.24	-0.03	-0.06	-0.07
DS40	-0.10	-0.14	-0.36	-0.07	-0.14	-0.26	-0.04	-0.16	-0.18	-0.29	-0.08	-0.07	-0.07
DS50	-0.10	-0.10	-0.38	-0.07	-0.17	-0.24	-0.06	-0.14	-0.17	-0.31	-0.17	-0.03	-0.04
DS60	-0.10	-0.07	-0.40	-0.11	-0.21	-0.22	-0.10	-0.13	-0.16	-0.33	-0.26	0.01	0.01
DS70	-0.10	-0.03	-0.42	-0.14	-0.25	-0.19	-0.14	-0.14	-0.17	-0.36	-0.31	0.02	0.01
DS80	-0.06	0.01	-0.42	-0.14	-0.28	-0.20	-0.20	-0.17	-0.19	-0.38	-0.34	-0.02	-0.02
DS90	-0.06	0.05	-0.29	-0.11	-0.21	-0.18	-0.14	-0.16	-0.18	-0.34	-0.29	-0.06	-0.07
spatial root distr. X	0.14	-0.02	0.02	-0.03	-0.02	0.05	-0.09	-0.04	-0.03	0.01	-0.15	0.09	0.09
spatial root ditr. Y	-0.07	0.18	-0.52	-0.21	-0.35	-0.27	-0.40	-0.14	-0.16	-0.43	-0.29	-0.04	-0.07
CPD 25	0.04	0.16	-0.07	0.05	0.07	-0.03	0.04	-0.04	-0.02	-0.06	0.20	-0.05	-0.06
CPD 50	0.04	0.18	-0.09	0.05	0.06	-0.09	-0.06	-0.06	-0.05	-0.05	0.19	-0.09	-0.10
CPD 75	0.01	0.20	-0.17	-0.02	-0.02	-0.15	-0.11	-0.04	-0.04	-0.11	0.15	-0.10	-0.12
CPD 90	-0.01	0.07	-0.27	-0.14	-0.12	-0.15	-0.08	0.01	0.01	-0.19	0.05	-0.02	-0.05

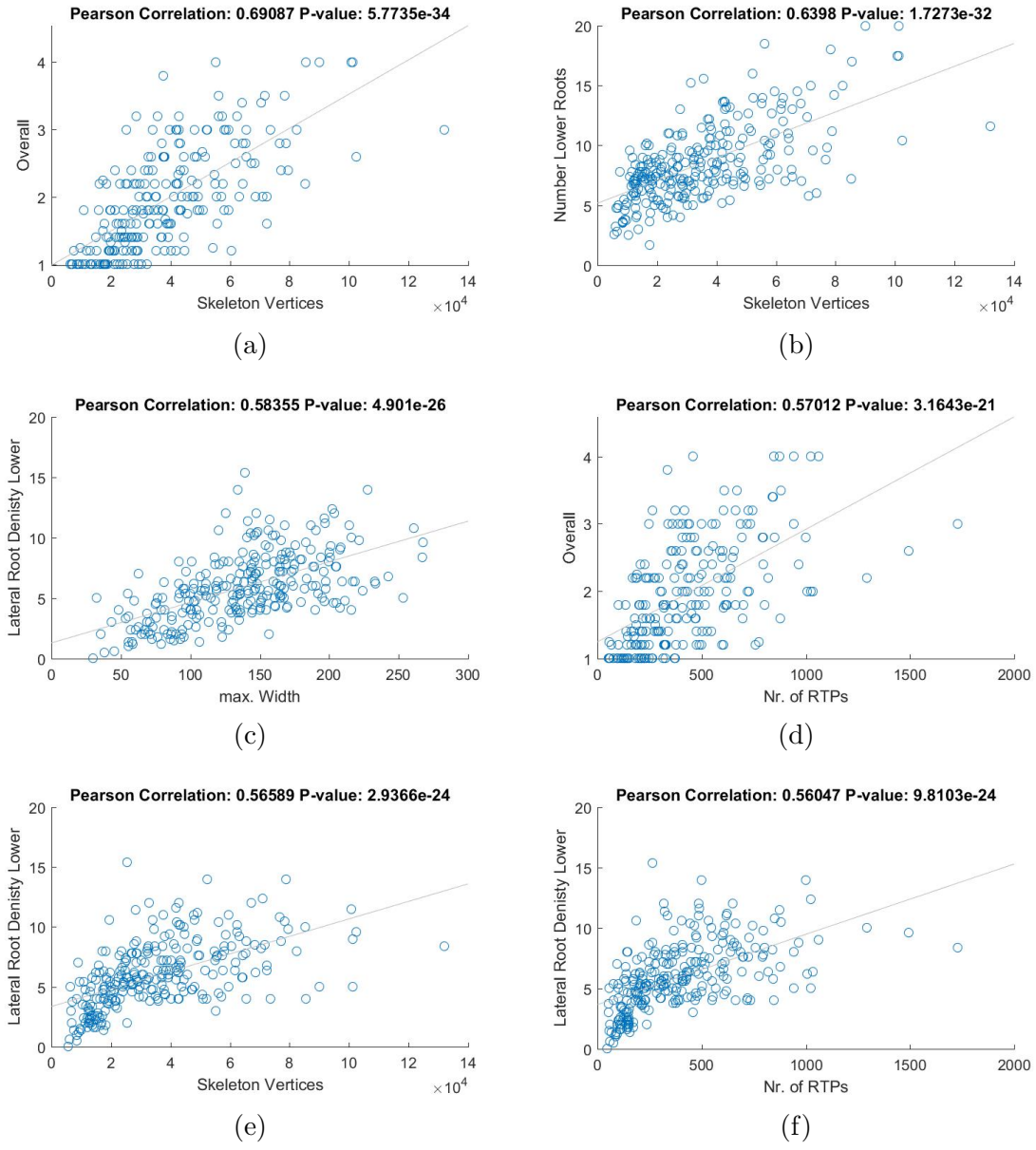

Figure 6.7: Best Pearson correlation values obtained between DIRT features from the combined mean features from all the cameras and the manual features for 2015 image dataset. The traits were averaged over plots before correlation analysis.

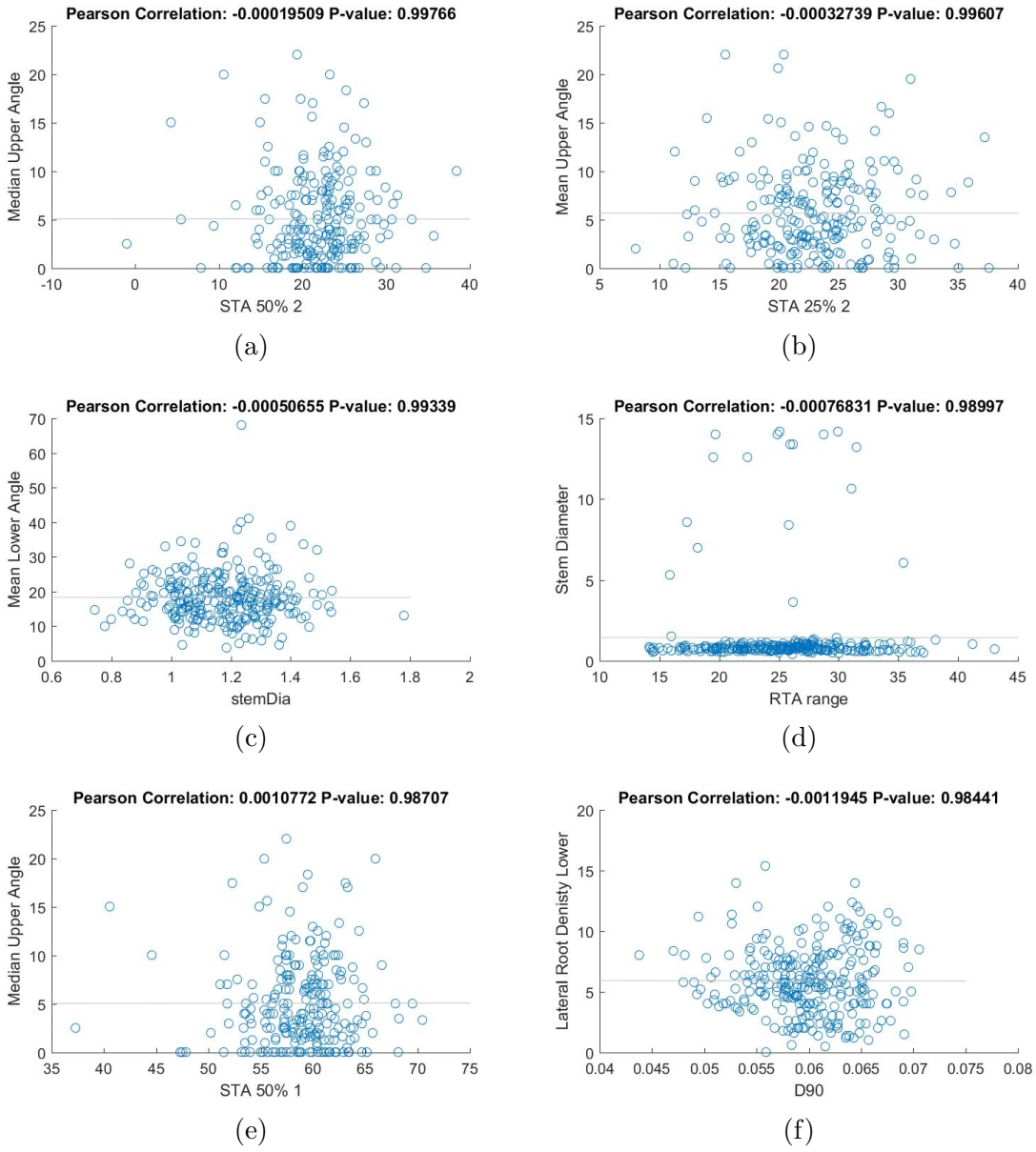

Figure 6.8: Trait combinations with least correlation between DIRT features from the combined mean features from all the cameras and the manual features for 2015 image dataset. The traits were averaged over plots before correlation analysis.

For the 2016 image dataset, we extracted few more features such as the PCA reduced radius and orientation histograms as well a the computational time needed to extract trait features from each of the images. Here again, we observe that from the Table 6.8 and the Table 6.9, when individual features were used without taking plot means, we observe lesser correlation values with the image based features and overall complexity. For example the correlation between network area and the overall complexity is 0.57 when individual features were used and the same correlation increases to 0.59 when mean of plots were used. Similarly, the Table 6.10 and the Table 6.11 shows that the correlation between network area and the overall complexity is increased further as taking the mean of the features across the cameras and across plots of the same genotype decreases the outlier effect. Especially, when the plant root is seen from one perspective, it width may be smaller, leading us to think that it is an outlier. Taking the mean of width across many perspectives helps us extract the features of better reliability.

In the Table 6.9, we see many red marked values which shows that merging features across all the cameras using the individual features from the cameras, increases the correlation in large number of feature combinations. Whereas when we look at the number of better correlations in the Table 6.11 we find that only a few feature correlations got better. This is because the outlier effect was smoothed out at two stages: 1) when taking mean of the features across each plot and 2) when taking mean of the features across cameras from multiple perspectives.

The scatter plots containing best correlations of the samples for individual features (of front facing camera), individual merged features, plot averaged features (of front facing camera) and plot averaged and merged features are shown in the Figures 6.9,

6.11, 6.13 and 6.15 respectively. The scatter plots containing worst correlations of the samples for individual features (of front facing camera), individual merged features, plot averaged features (of front facing camera) and plot averaged and merged features are shown in the Figures 6.10, 6.12, 6.14 and 6.16 respectively. In all of these scatter plots, we observe that the data points are distributed uniformly, which tells us that the scatter data plotted is indeed valid and our phenotyping system generates reliable trait values.

Table 6.8: Pearson correlation values between the automatically extracted features of 2016 trait data and the manually extracted features. The feature values from the front facing camera are used in the correlation analysis.

Feature Names	SD	TR	OC	NS	ND	NUR	LRDU	MDUA	MEUA	NLR	LRDL	MDLA	MELA
Median no. of roots	0.15	0.18	0.48	0.19	0.28	0.00	0.04	0.01	0.02	0.36	0.12	0.04	0.03
Maximum no. of roots	0.16	0.12	0.45	0.23	0.28	0.00	0.05	0.03	0.04	0.29	0.12	-0.07	-0.08
Total root length	0.27	0.21	0.56	0.23	0.35	0.04	0.10	0.01	0.04	0.38	0.14	-0.01	-0.02
Depth	0.17	0.07	0.14	0.03	0.11	0.12	0.11	-0.05	-0.03	0.07	-0.01	-0.03	-0.02
Maximum width	0.34	0.19	0.31	0.22	0.20	0.15	0.15	-0.08	-0.06	0.09	0.01	-0.10	-0.11
Width-to-depth ratio	0.26	0.16	0.24	0.20	0.15	0.09	0.09	-0.06	-0.05	0.06	0.00	-0.08	-0.09
Network area	0.44	0.27	0.57	0.25	0.36	0.11	0.16	0.00	0.03	0.33	0.14	-0.03	-0.03
Convex area	0.38	0.22	0.36	0.20	0.24	0.17	0.17	-0.07	-0.05	0.15	0.04	-0.09	-0.10
Solidity	0.11	0.06	0.34	0.09	0.19	-0.05	0.02	0.09	0.09	0.28	0.15	0.07	0.08
Perimeter	0.22	0.18	0.55	0.22	0.33	0.04	0.07	-0.01	0.01	0.38	0.12	-0.02	-0.03
Average radius	0.39	0.27	-0.16	-0.04	-0.11	-0.02	-0.03	0.11	0.12	-0.14	0.03	-0.02	-0.01
Volume	0.55	0.40	0.37	0.21	0.26	0.01	0.05	0.10	0.12	0.25	0.12	-0.01	0.00
Surface area	0.49	0.35	0.51	0.24	0.33	0.05	0.11	0.06	0.09	0.33	0.15	-0.02	-0.02
Maximum radius	0.36	0.24	0.37	0.24	0.32	-0.03	-0.01	0.03	0.05	0.28	0.15	-0.06	-0.05
Lower Root Area	0.41	0.28	0.50	0.20	0.30	0.09	0.13	0.05	0.07	0.33	0.15	0.01	0.01
radhist1	-0.29	-0.14	0.10	0.01	0.09	-0.05	0.00	-0.05	-0.07	0.24	0.02	-0.02	-0.04
radhist2	0.26	0.08	0.01	0.04	0.01	0.13	0.09	-0.01	0.01	-0.19	-0.01	0.01	0.03
radhist3	0.33	0.17	-0.06	0.04	-0.03	0.07	-0.01	0.06	0.09	-0.22	0.00	0.02	0.03
radhist4	0.30	0.19	-0.11	0.00	-0.06	-0.05	-0.06	0.09	0.11	-0.18	0.03	0.00	0.01
radhist5	0.18	0.18	-0.18	-0.05	-0.11	-0.13	-0.12	0.13	0.14	-0.14	0.03	-0.01	0.00
radhist6	0.07	0.14	-0.23	-0.10	-0.15	-0.16	-0.13	0.15	0.16	-0.12	0.03	-0.03	-0.02
radhist7	-0.02	0.11	-0.29	-0.13	-0.19	-0.17	-0.16	0.13	0.13	-0.12	0.03	-0.03	-0.03
radhist8	-0.08	0.07	-0.33	-0.16	-0.23	-0.17	-0.17	0.12	0.12	-0.14	0.00	-0.02	-0.03
radhist9	-0.05	0.07	-0.33	-0.16	-0.23	-0.15	-0.15	0.14	0.14	-0.15	0.00	-0.02	-0.02
radhist10	0.02	0.11	-0.30	-0.13	-0.23	-0.11	-0.13	0.12	0.11	-0.14	-0.03	-0.01	-0.02
orihist1	-0.05	-0.03	0.06	-0.03	0.05	-0.04	-0.02	0.09	0.08	-0.01	0.07	0.08	0.09
orihist2	-0.07	-0.07	0.13	0.02	0.10	-0.03	0.00	0.08	0.08	0.05	0.01	0.07	0.07
orihist3	0.09	0.08	-0.13	0.00	-0.09	-0.01	0.02	-0.02	-0.02	-0.06	-0.03	-0.15	-0.17
orihist4	0.10	0.09	-0.14	0.01	-0.08	0.03	0.01	-0.07	-0.08	-0.07	-0.01	-0.11	-0.12
orihist5	-0.05	-0.05	0.12	-0.01	0.06	0.01	0.00	-0.02	-0.02	0.07	0.03	0.10	0.12
orihist6	-0.03	-0.02	0.08	-0.02	0.05	-0.04	-0.01	0.07	0.06	0.01	0.08	0.06	0.06
holes	0.10	0.09	0.52	0.21	0.34	0.01	0.10	0.00	0.02	0.36	0.13	0.00	-0.01
radpca1	0.32	0.16	-0.08	0.01	-0.06	0.06	0.01	0.05	0.08	-0.24	0.00	0.01	0.03
radpca2	0.02	-0.10	0.22	0.09	0.14	0.19	0.17	-0.13	-0.12	0.03	-0.03	0.02	0.03
radpca3	0.17	0.04	0.19	0.14	0.15	0.10	0.04	-0.04	-0.02	0.04	0.01	0.03	0.02
oripca1	-0.06	-0.06	0.11	-0.01	0.06	0.01	-0.01	0.00	-0.01	0.06	0.03	0.12	0.13
oripca2	-0.10	-0.09	0.15	0.00	0.10	-0.03	-0.01	0.09	0.09	0.06	0.02	0.11	0.11
oripca3	-0.01	-0.01	0.00	0.03	0.04	0.02	-0.01	0.00	0.00	-0.01	0.02	0.03	0.02
Computation	0.27	0.20	0.51	0.20	0.31	0.02	0.07	0.00	0.02	0.35	0.14	-0.01	-0.02

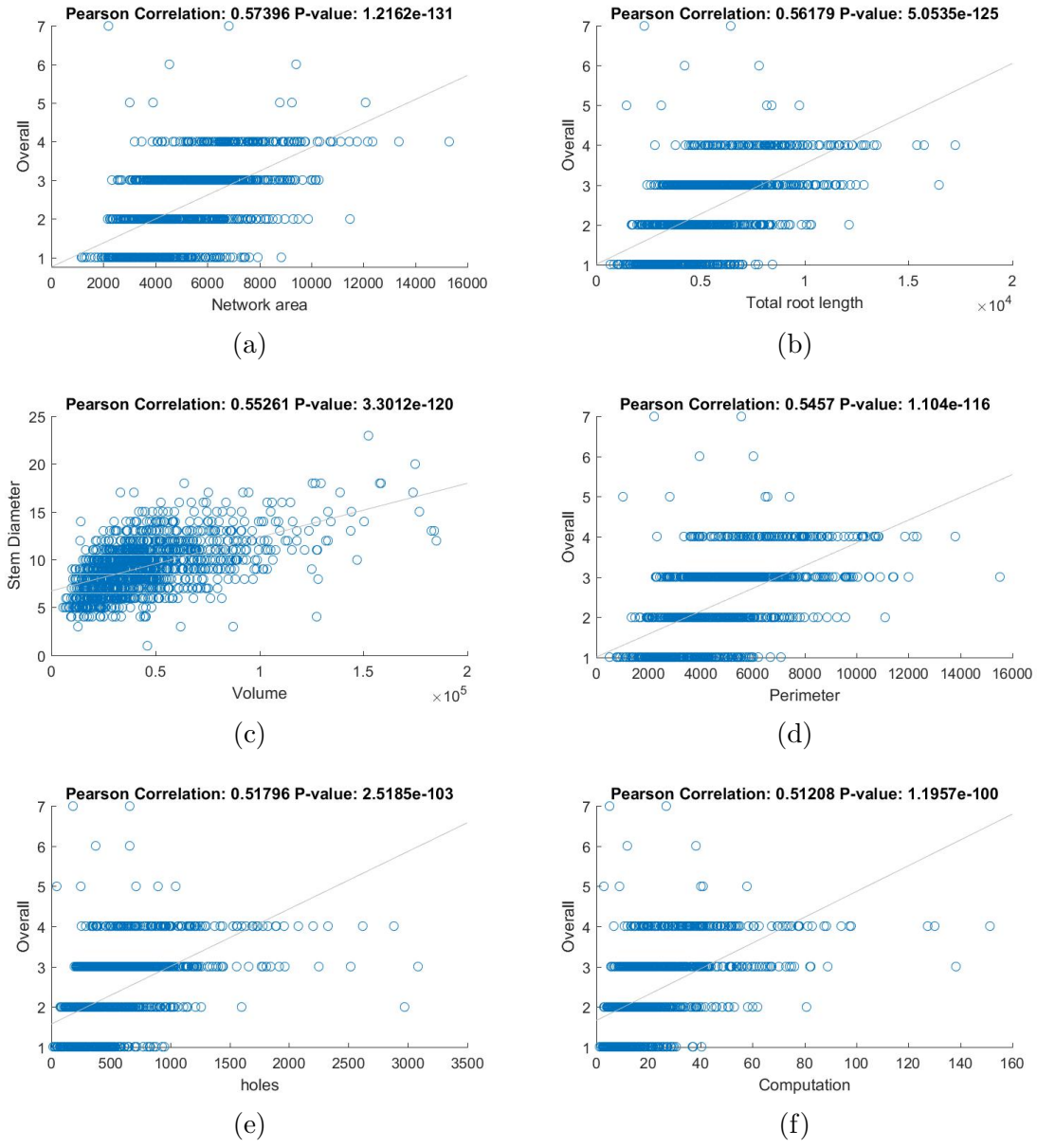

Figure 6.9: Best Pearson correlation values obtained between front facing camera features and the manual features for 2016 image dataset.

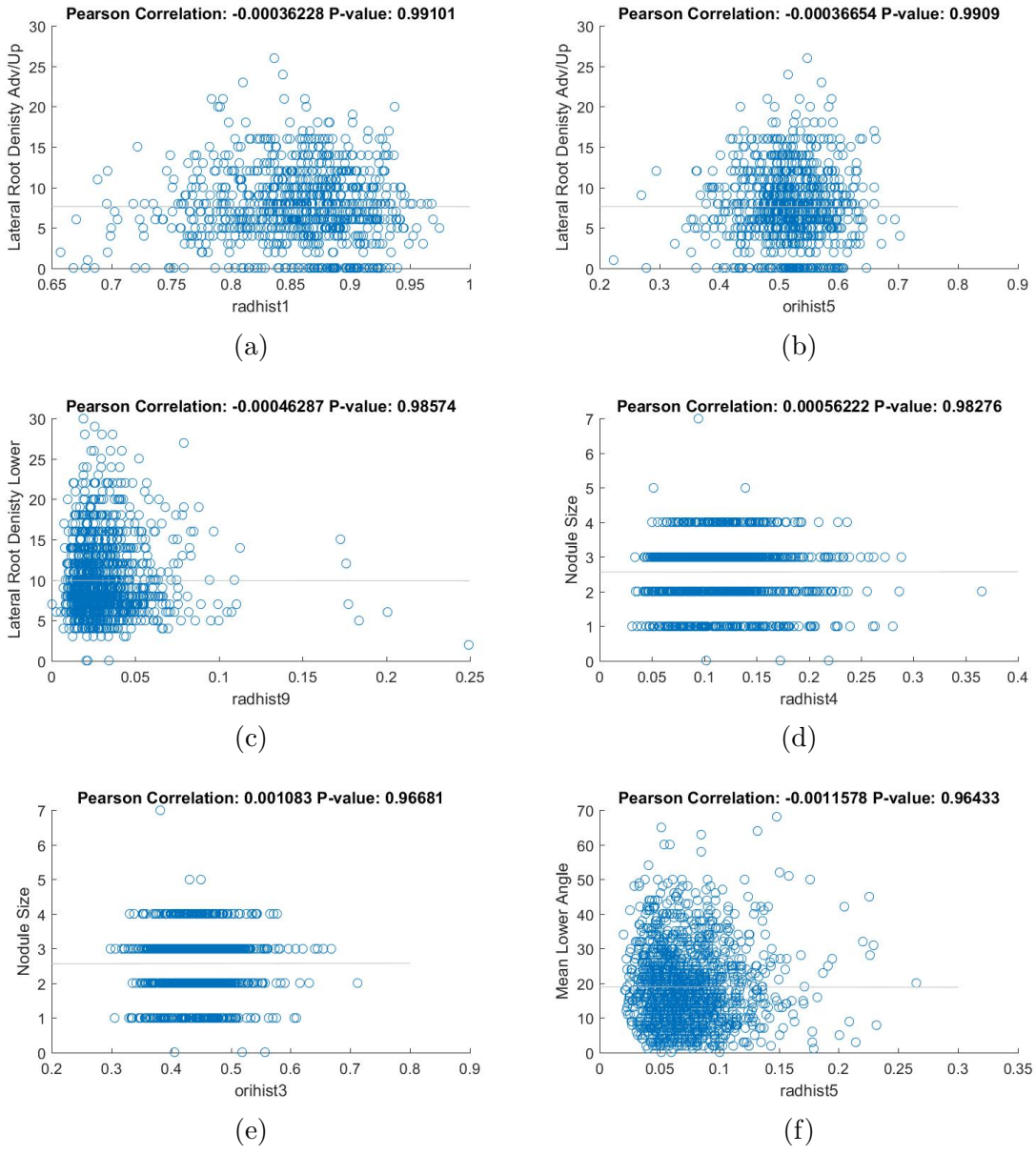

Figure 6.10: Trait combinations with least correlation obtained between front facing camera features and the manual features for 2016 image dataset.

Table 6.9: Pearson correlation values between the automatically extracted features of 2016 trait data and the manually extracted features. The mean feature values from all the cameras are used in the correlation analysis.

Feature Names	SD	TR	OC	NS	ND	NUR	LRDU	MDUA	MEUA	NLR	LRDL	MDLA	MELA
Median no. of roots	0.14	0.17	0.46	0.21	0.31	-0.00	0.09	-0.00	0.01	0.36	0.16	0.03	0.02
Max. no. of roots	0.18	0.17	0.49	0.26	0.34	-0.04	0.09	0.05	0.06	0.33	0.20	-0.08	-0.09
Total root length	0.29	0.25	0.57	0.25	0.37	0.00	0.13	0.04	0.06	0.40	0.22	-0.02	-0.03
Depth	0.21	0.18	0.16	0.03	0.08	0.05	0.08	0.00	0.01	0.12	0.06	-0.02	-0.01
Max. width	0.38	0.22	0.36	0.25	0.23	0.16	0.16	-0.06	-0.04	0.12	0.02	-0.11	-0.11
Width-to-depth ratio	0.26	0.12	0.25	0.22	0.17	0.12	0.11	-0.07	-0.05	0.05	-0.02	-0.09	-0.10
Network area	0.44	0.30	0.59	0.26	0.37	0.10	0.16	0.01	0.04	0.35	0.16	-0.02	-0.03
Convex area	0.41	0.28	0.39	0.21	0.25	0.14	0.16	-0.04	-0.01	0.19	0.06	-0.09	-0.09
Solidity	0.11	0.05	0.37	0.11	0.23	-0.04	0.04	0.08	0.08	0.28	0.16	0.08	0.08
Perimeter	0.24	0.22	0.54	0.24	0.35	0.00	0.09	0.01	0.03	0.40	0.18	-0.03	-0.04
Average radius	0.41	0.27	-0.16	-0.05	-0.12	0.02	-0.06	0.09	0.10	-0.16	-0.04	-0.02	-0.00
Volume	0.57	0.42	0.36	0.20	0.25	0.01	0.05	0.10	0.13	0.24	0.13	-0.01	-0.00
Surface area	0.51	0.38	0.51	0.24	0.33	0.04	0.12	0.07	0.10	0.32	0.18	-0.02	-0.02
Maximum radius	0.37	0.26	0.39	0.25	0.33	-0.02	-0.02	0.03	0.05	0.28	0.14	-0.06	-0.05
Lower Root Area	0.42	0.30	0.53	0.21	0.32	0.08	0.15	0.06	0.08	0.34	0.16	0.01	0.01
radhist1	-0.30	-0.14	0.12	0.04	0.10	-0.07	-0.00	-0.04	-0.06	0.26	0.04	-0.02	-0.03
radhist2	0.26	0.09	-0.00	0.02	-0.01	0.15	0.10	-0.02	0.00	-0.20	-0.03	0.01	0.03
radhist3	0.35	0.17	-0.06	0.02	-0.04	0.08	-0.01	0.05	0.07	-0.23	-0.02	0.02	0.04
radhist4	0.32	0.19	-0.11	-0.02	-0.07	-0.02	-0.06	0.10	0.12	-0.19	0.02	-0.01	-0.00
radhist5	0.21	0.19	-0.18	-0.06	-0.11	-0.12	-0.11	0.12	0.13	-0.16	0.04	-0.03	-0.02
radhist6	0.11	0.16	-0.26	-0.11	-0.16	-0.16	-0.13	0.14	0.14	-0.15	0.04	-0.04	-0.03
radhist7	-0.00	0.12	-0.32	-0.14	-0.20	-0.19	-0.16	0.14	0.14	-0.14	0.05	-0.05	-0.04
radhist8	-0.07	0.07	-0.36	-0.17	-0.24	-0.19	-0.17	0.14	0.13	-0.15	0.02	-0.04	-0.04
radhist9	-0.07	0.06	-0.37	-0.19	-0.26	-0.16	-0.17	0.15	0.14	-0.17	-0.00	-0.03	-0.04
radhist10	-0.01	0.10	-0.36	-0.17	-0.25	-0.12	-0.15	0.13	0.13	-0.17	-0.02	-0.02	-0.02
orihist1	-0.06	-0.06	0.05	-0.03	0.05	-0.07	-0.02	0.12	0.11	-0.01	0.07	0.06	0.07
orihist2	-0.09	-0.09	0.14	0.01	0.10	-0.04	0.01	0.08	0.08	0.07	0.03	0.07	0.08
orihist3	0.10	0.09	-0.16	0.01	-0.11	-0.01	-0.01	-0.04	-0.03	-0.08	-0.04	-0.18	-0.19
orihist4	0.11	0.10	-0.16	-0.00	-0.09	0.04	-0.00	-0.08	-0.08	-0.08	-0.02	-0.13	-0.14
orihist5	-0.03	-0.03	0.14	0.02	0.09	0.03	0.02	-0.01	-0.02	0.08	0.03	0.13	0.14
orihist6	-0.05	-0.05	0.04	-0.04	0.03	-0.06	-0.02	0.07	0.06	-0.01	0.06	0.07	0.08
holes	0.12	0.16	0.42	0.23	0.33	-0.05	0.17	0.04	0.07	0.32	0.28	-0.04	-0.04
radpca1	0.33	0.17	-0.10	-0.01	-0.07	0.07	0.01	0.05	0.07	-0.25	-0.02	0.01	0.03
radpca2	0.01	-0.10	0.22	0.10	0.13	0.21	0.18	-0.13	-0.13	0.04	-0.05	0.03	0.04
radpca3	0.19	0.03	0.26	0.15	0.18	0.11	0.04	-0.04	-0.02	0.07	0.00	0.05	0.04
oripca1	-0.05	-0.04	0.09	0.00	0.07	0.03	-0.00	-0.01	-0.02	0.05	0.02	0.12	0.12
oripca2	0.08	0.08	-0.12	-0.00	-0.07	0.01	-0.04	-0.03	-0.02	-0.08	-0.05	-0.14	-0.14
oripca3	0.03	0.00	0.05	-0.02	0.02	0.01	-0.00	0.04	0.04	0.01	-0.02	0.02	0.01
Computation	0.28	0.25	0.51	0.22	0.33	-0.01	0.11	0.02	0.04	0.36	0.22	-0.03	-0.04

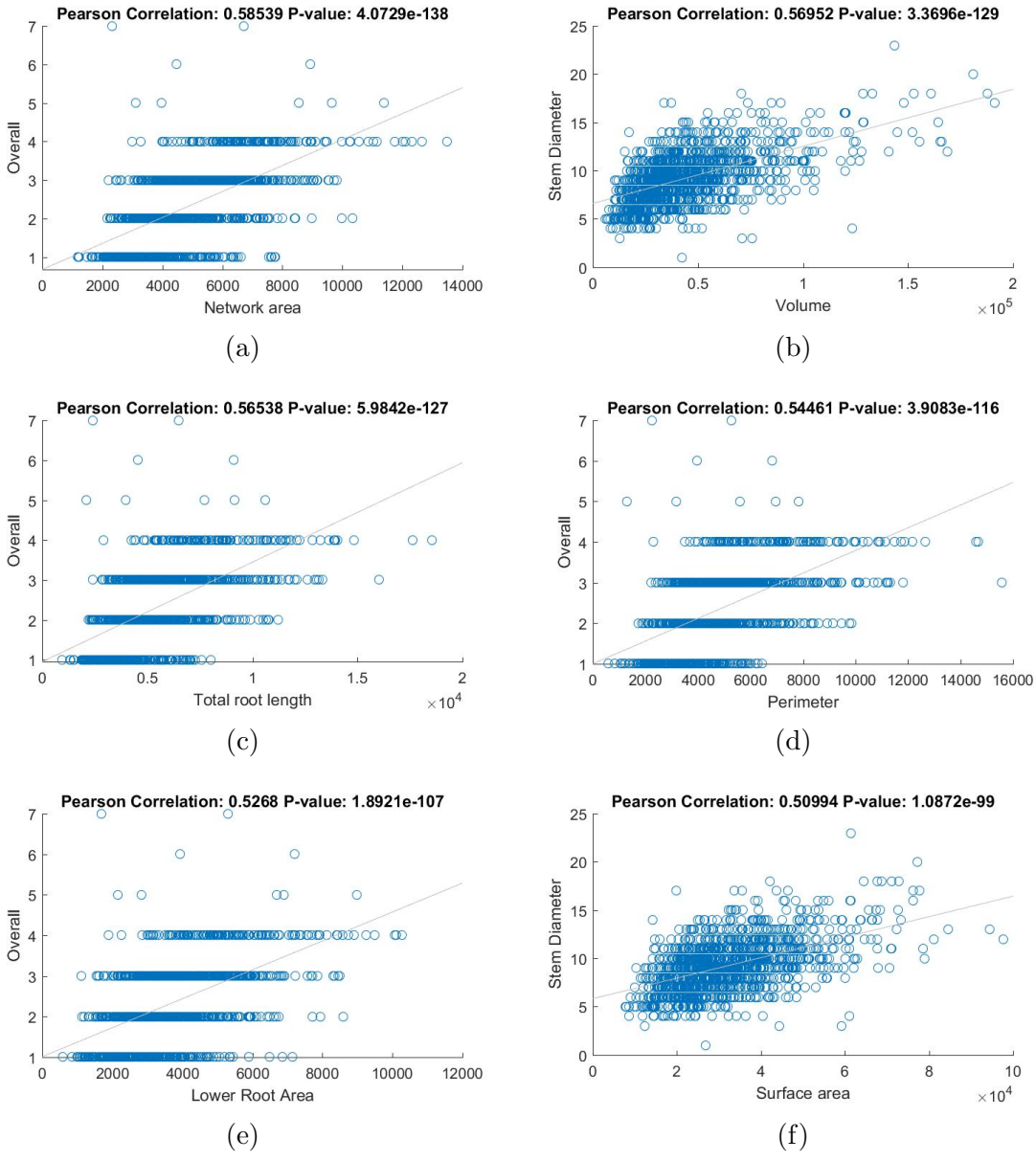

Figure 6.11: Best Pearson correlation values obtained for 2016 dataset between combined features from all cameras and the manual features

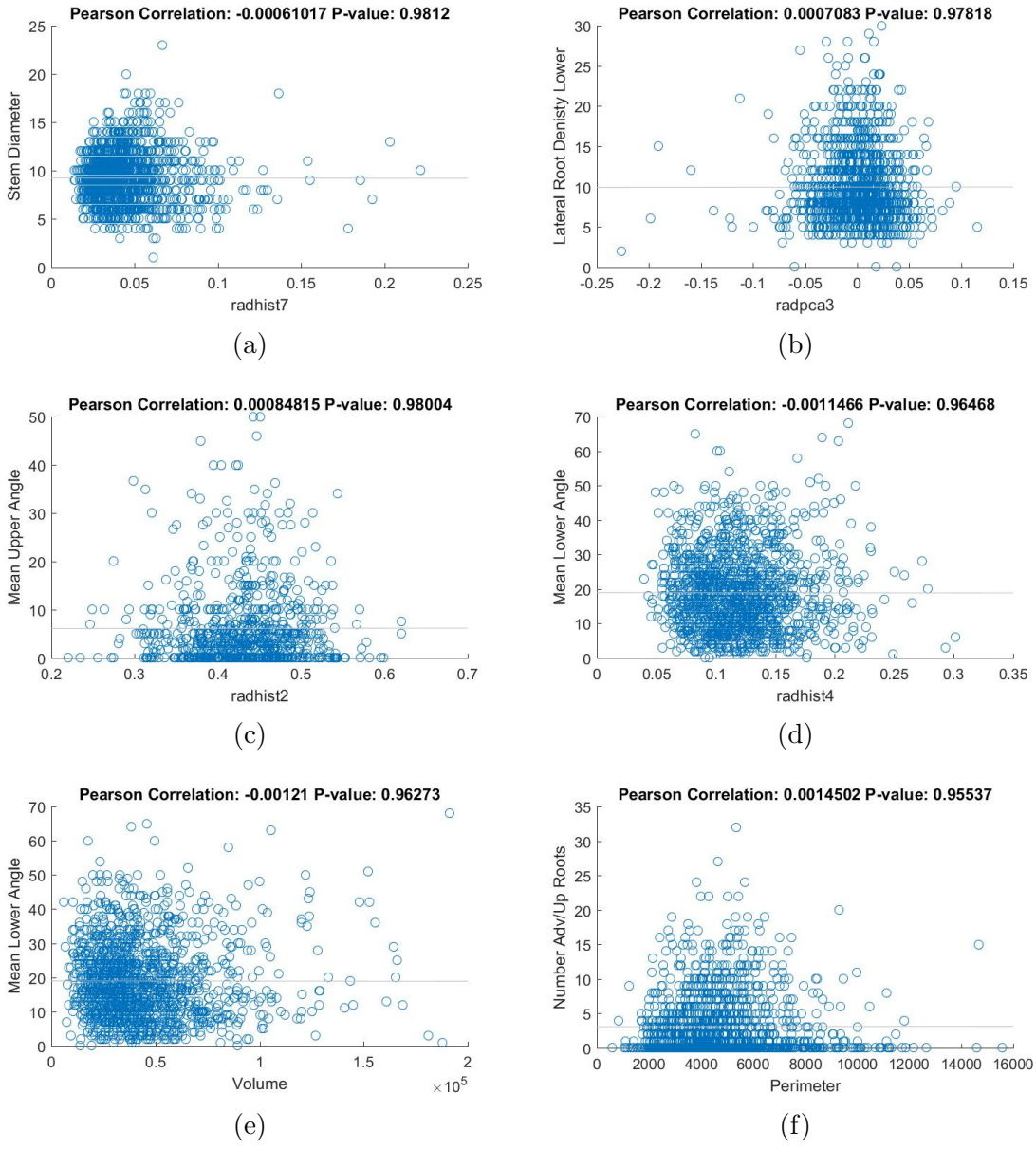

Figure 6.12: Trait combinations with least correlation obtained for 2016 dataset between combined features from all cameras and the manual features.

Table 6.10: Pearson correlation values between the automatically extracted features of 2016 trait data and the manually extracted features. The feature values from the front facing camera, averaged over plots, are used in the correlation analysis.

Feature Names	SD	TR	OC	NS	ND	NUR	LRDU	MDUA	MEUA	NLR	LRDL	MDLA	MELA
Median no. of roots	0.11	0.19	0.53	0.13	0.27	-0.08	-0.03	0.03	0.04	0.44	0.09	0.04	0.02
Maximum no. of roots	0.11	0.09	0.50	0.18	0.29	-0.05	0.02	0.06	0.07	0.39	0.10	-0.09	-0.11
Total root length	0.21	0.17	0.59	0.15	0.31	-0.03	0.02	0.02	0.04	0.45	0.10	-0.03	-0.05
Depth	0.20	0.01	0.24	0.05	0.19	0.26	0.07	-0.09	-0.07	0.12	-0.02	-0.07	-0.09
Maximum width	0.38	0.13	0.39	0.23	0.25	0.23	0.01	-0.15	-0.14	0.12	-0.09	-0.15	-0.17
Width-to-depth ratio	0.30	0.12	0.28	0.21	0.16	0.13	-0.03	-0.13	-0.12	0.05	-0.11	-0.12	-0.13
Network area	0.40	0.20	0.63	0.17	0.33	0.10	0.06	-0.02	0.01	0.38	0.11	-0.06	-0.06
Convex area	0.42	0.17	0.45	0.20	0.28	0.25	0.04	-0.10	-0.09	0.20	-0.02	-0.13	-0.16
Solidity	0.07	0.05	0.34	0.00	0.14	-0.17	0.05	0.11	0.12	0.31	0.20	0.07	0.09
Perimeter	0.16	0.14	0.58	0.15	0.31	-0.02	-0.02	0.00	0.01	0.44	0.07	-0.04	-0.06
Average radius	0.39	0.26	-0.24	-0.10	-0.16	-0.04	-0.02	0.09	0.12	-0.18	0.11	-0.05	-0.03
Volume	0.52	0.39	0.36	0.13	0.22	-0.07	-0.03	0.11	0.14	0.27	0.13	-0.05	-0.04
Surface area	0.45	0.31	0.52	0.15	0.28	-0.02	0.02	0.07	0.09	0.37	0.14	-0.05	-0.05
Maximum radius	0.34	0.23	0.37	0.17	0.30	-0.06	-0.04	0.05	0.07	0.31	0.18	-0.15	-0.13
Lower Root Area	0.39	0.23	0.56	0.11	0.26	0.08	0.07	0.05	0.07	0.38	0.13	-0.02	-0.02
radhist1	-0.27	-0.08	0.22	0.12	0.23	-0.04	0.03	-0.06	-0.10	0.30	-0.03	-0.04	-0.07
radhist2	0.21	-0.03	-0.08	-0.04	-0.11	0.17	0.02	-0.03	0.01	-0.26	-0.01	0.04	0.07
radhist3	0.34	0.14	-0.17	-0.06	-0.17	0.04	-0.06	0.09	0.13	-0.27	0.03	0.03	0.05
radhist4	0.31	0.22	-0.22	-0.10	-0.19	-0.14	-0.08	0.15	0.17	-0.20	0.10	0.00	0.02
radhist5	0.19	0.26	-0.28	-0.12	-0.22	-0.24	-0.09	0.17	0.18	-0.15	0.12	-0.02	0.00
radhist6	0.08	0.24	-0.28	-0.14	-0.21	-0.29	-0.08	0.18	0.19	-0.09	0.12	-0.05	-0.03
radhist7	-0.02	0.19	-0.35	-0.15	-0.24	-0.31	-0.05	0.18	0.18	-0.09	0.15	-0.06	-0.05
radhist8	-0.08	0.15	-0.40	-0.18	-0.28	-0.30	-0.06	0.17	0.18	-0.12	0.10	-0.04	-0.04
radhist9	-0.02	0.15	-0.42	-0.19	-0.28	-0.26	-0.06	0.15	0.15	-0.15	0.09	-0.04	-0.05
radhist10	0.05	0.20	-0.39	-0.18	-0.27	-0.21	-0.07	0.12	0.13	-0.14	0.04	-0.02	-0.03
orihist1	-0.05	-0.04	0.12	-0.09	0.01	-0.08	0.03	0.04	0.03	0.03	0.10	0.14	0.15
orihist2	-0.15	0.00	0.18	-0.09	0.08	-0.10	-0.05	0.02	-0.01	0.12	0.00	0.17	0.17
orihist3	0.13	0.15	-0.19	0.06	-0.08	0.00	-0.02	-0.04	-0.03	-0.04	-0.01	-0.23	-0.25
orihist4	0.16	0.08	-0.21	0.10	-0.05	0.07	0.05	0.02	0.05	-0.11	0.02	-0.23	-0.24
orihist5	-0.06	-0.16	0.18	-0.02	0.06	0.04	0.02	0.01	0.00	0.05	0.00	0.17	0.19
orihist6	-0.02	-0.06	0.11	-0.06	0.04	-0.09	0.07	0.00	-0.01	0.00	0.12	0.10	0.12
holes	0.07	0.06	0.56	0.16	0.33	-0.04	0.07	0.01	0.02	0.43	0.10	0.01	-0.02
radpca1	0.29	0.11	-0.21	-0.09	-0.20	0.03	-0.04	0.07	0.12	-0.29	0.04	0.03	0.06
radpca2	-0.03	-0.23	0.25	0.11	0.16	0.32	0.09	-0.18	-0.17	0.00	-0.12	0.05	0.05
radpca3	0.26	0.02	0.28	0.15	0.18	0.19	-0.03	-0.03	-0.02	0.04	-0.05	0.04	0.04
oripca1	-0.08	-0.16	0.18	-0.03	0.06	0.03	0.03	0.02	0.01	0.03	0.01	0.19	0.21
oripca2	-0.16	-0.05	0.20	-0.10	0.07	-0.09	-0.04	0.01	-0.02	0.12	0.00	0.22	0.23
oripca3	-0.03	0.01	-0.02	0.00	0.06	0.00	0.03	0.08	0.09	-0.03	0.03	0.02	0.03
Computation	0.22	0.17	0.56	0.12	0.27	-0.05	0.02	0.02	0.04	0.42	0.11	-0.02	-0.04

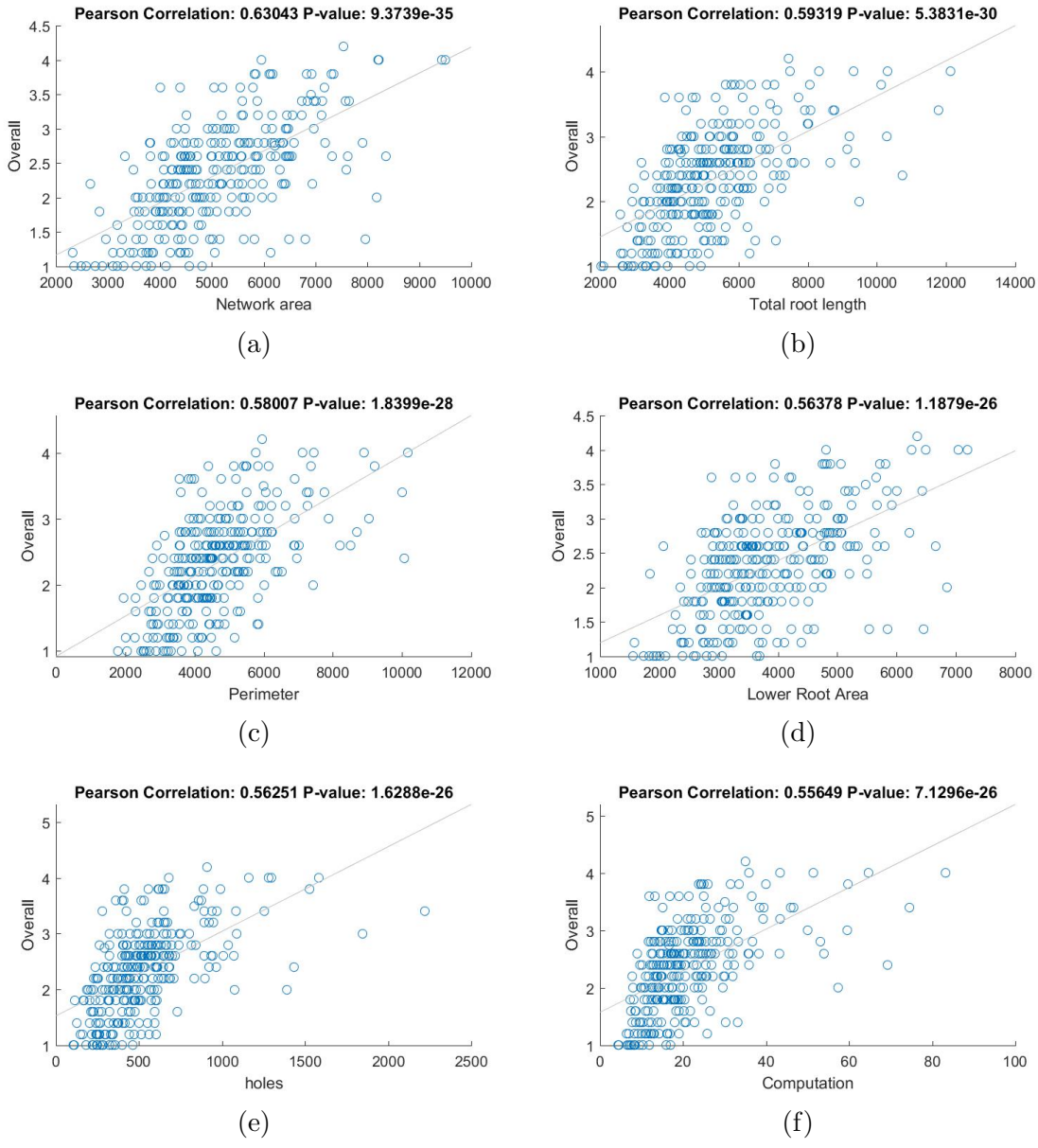

Figure 6.13: Best Pearson correlation values obtained for 2016 dataset between plot means of features from the front facing camera and the plot means of manual features.

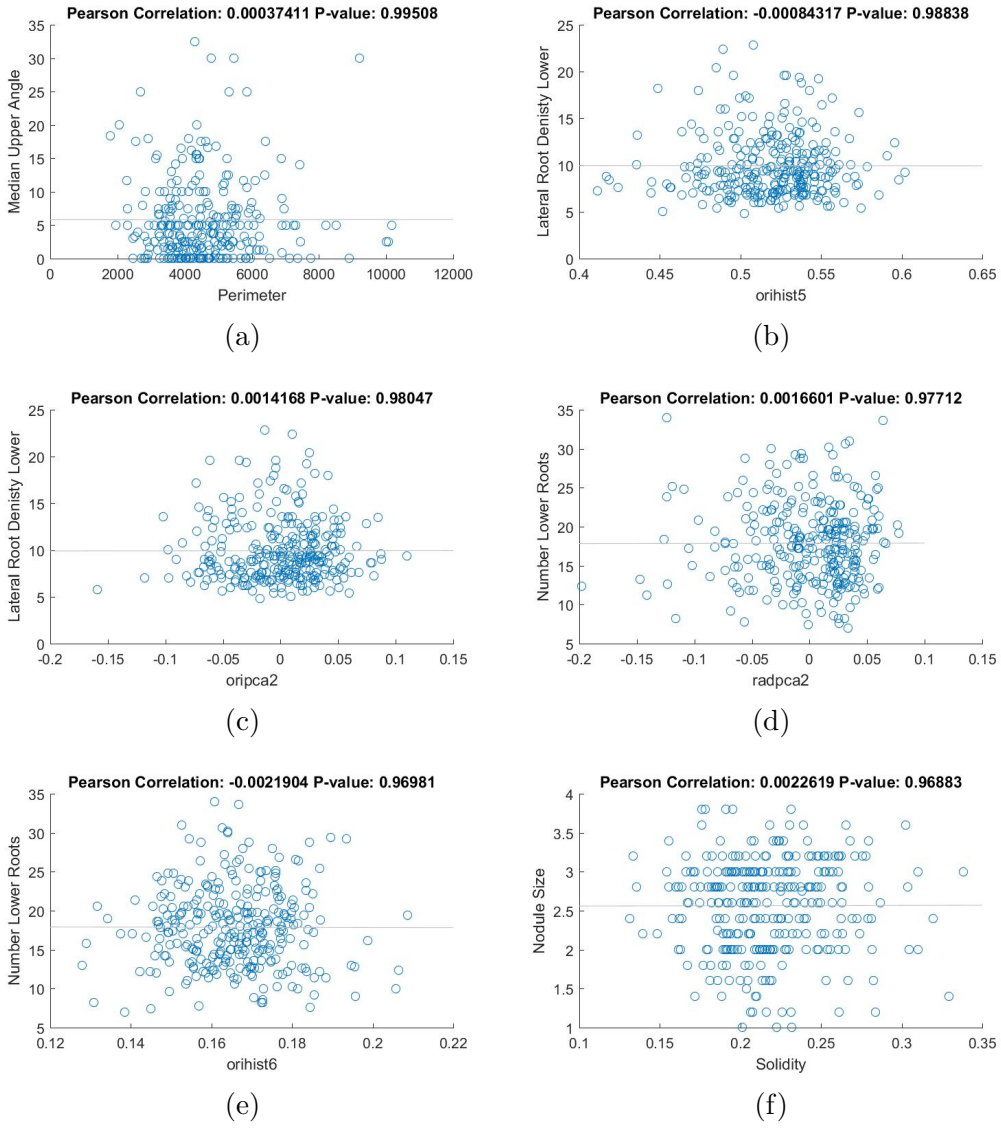

Figure 6.14: Trait combinations with least correlation for 2016 dataset between plot means of features from the front facing camera and the plot means of manual features.

Table 6.11: Pearson correlation values between the automatically extracted features of 2016 trait data and the manually extracted features. The mean feature values averaged over plot from all the cameras are used in the correlation analysis.

Feature Names	SD	TR	OC	NS	ND	NUR	LRDU	MDUA	MEUA	NLR	LRDL	MDLA	MELA
Median no. of roots	0.13	0.20	0.52	0.17	0.32	-0.10	0.03	0.05	0.06	0.43	0.15	0.01	-0.01
Max. no. of roots	0.12	0.16	0.51	0.22	0.34	-0.14	0.08	0.07	0.09	0.39	0.23	-0.11	-0.12
Total root length	0.24	0.24	0.58	0.17	0.33	-0.10	0.08	0.06	0.08	0.45	0.23	-0.06	-0.07
Depth	0.24	0.23	0.24	-0.01	0.10	0.07	0.06	-0.02	-0.00	0.21	0.13	-0.05	-0.06
Max. width	0.40	0.15	0.43	0.24	0.26	0.23	0.02	-0.13	-0.11	0.14	-0.08	-0.14	-0.16
Width-to-depth ratio	0.28	0.04	0.29	0.23	0.20	0.19	-0.01	-0.12	-0.11	0.02	-0.15	-0.12	-0.13
Network area	0.41	0.24	0.64	0.17	0.33	0.07	0.07	-0.01	0.02	0.39	0.14	-0.05	-0.06
Convex area	0.45	0.25	0.47	0.18	0.25	0.18	0.03	-0.08	-0.06	0.25	0.03	-0.12	-0.14
Solidity	0.06	0.02	0.38	0.04	0.21	-0.15	0.07	0.11	0.12	0.31	0.22	0.06	0.09
Perimeter	0.19	0.22	0.56	0.18	0.32	-0.09	0.03	0.04	0.05	0.45	0.17	-0.06	-0.08
Average radius	0.39	0.22	-0.24	-0.12	-0.19	0.03	-0.07	0.06	0.08	-0.21	-0.01	-0.03	-0.01
Volume	0.54	0.41	0.33	0.11	0.19	-0.08	-0.02	0.13	0.15	0.25	0.14	-0.05	-0.04
Surface area	0.47	0.36	0.51	0.14	0.27	-0.05	0.04	0.08	0.11	0.36	0.18	-0.05	-0.06
Maximum radius	0.34	0.25	0.37	0.18	0.29	-0.06	-0.06	0.03	0.04	0.30	0.16	-0.15	-0.13
Lower Root Area	0.40	0.26	0.57	0.11	0.26	0.05	0.07	0.06	0.08	0.38	0.15	-0.00	-0.01
radhist1	-0.27	-0.09	0.23	0.14	0.25	-0.07	0.03	-0.05	-0.09	0.30	0.00	-0.03	-0.06
radhist2	0.20	-0.01	-0.09	-0.06	-0.12	0.22	0.03	-0.02	0.02	-0.26	-0.04	0.04	0.07
radhist3	0.34	0.13	-0.17	-0.09	-0.20	0.06	-0.07	0.07	0.11	-0.28	0.00	0.03	0.06
radhist4	0.31	0.20	-0.23	-0.13	-0.22	-0.10	-0.07	0.12	0.15	-0.22	0.09	-0.01	0.00
radhist5	0.20	0.25	-0.28	-0.13	-0.22	-0.23	-0.07	0.15	0.17	-0.16	0.13	-0.04	-0.03
radhist6	0.11	0.23	-0.31	-0.15	-0.23	-0.28	-0.06	0.18	0.19	-0.13	0.14	-0.06	-0.04
radhist7	0.01	0.19	-0.36	-0.16	-0.25	-0.31	-0.04	0.18	0.19	-0.10	0.16	-0.07	-0.06
radhist8	-0.06	0.15	-0.41	-0.18	-0.29	-0.30	-0.05	0.18	0.18	-0.13	0.12	-0.05	-0.05
radhist9	-0.05	0.14	-0.45	-0.21	-0.31	-0.28	-0.06	0.17	0.17	-0.15	0.09	-0.05	-0.06
radhist10	0.01	0.16	-0.44	-0.19	-0.29	-0.22	-0.07	0.14	0.15	-0.17	0.06	-0.04	-0.05
orihist1	-0.05	-0.03	0.10	-0.05	0.02	-0.09	0.06	0.04	0.03	0.03	0.11	0.14	0.16
orihist2	-0.17	-0.03	0.24	-0.05	0.14	-0.10	-0.04	0.02	-0.00	0.17	0.01	0.17	0.17
orihist3	0.09	0.12	-0.23	0.03	-0.14	-0.01	-0.04	-0.05	-0.03	-0.07	-0.02	-0.26	-0.27
orihist4	0.16	0.08	-0.24	0.04	-0.11	0.07	0.04	0.01	0.04	-0.14	0.01	-0.25	-0.25
orihist5	-0.03	-0.10	0.21	0.03	0.13	0.06	0.04	0.02	0.01	0.05	0.02	0.19	0.21
orihist6	-0.04	-0.07	0.07	-0.07	0.01	-0.09	0.06	0.01	-0.01	-0.01	0.09	0.14	0.15
holes	0.11	0.20	0.40	0.21	0.33	-0.14	0.20	0.09	0.12	0.34	0.35	-0.07	-0.09
radpca1	0.29	0.11	-0.21	-0.12	-0.23	0.06	-0.04	0.07	0.11	-0.30	0.01	0.02	0.05
radpca2	-0.03	-0.21	0.25	0.11	0.16	0.34	0.09	-0.17	-0.16	0.01	-0.14	0.06	0.06
radpca3	0.26	-0.01	0.32	0.15	0.19	0.17	-0.06	-0.07	-0.07	0.06	-0.08	0.06	0.06
oripca1	-0.03	-0.12	0.16	0.00	0.08	0.05	0.03	0.01	0.00	0.03	-0.00	0.18	0.19
oripca2	0.06	0.15	-0.26	-0.08	-0.19	0.00	-0.07	-0.04	-0.02	-0.10	-0.05	-0.20	-0.20
oripca3	0.03	0.00	0.07	-0.07	0.04	-0.02	-0.03	0.08	0.06	0.02	-0.10	0.05	0.04
Computation	0.26	0.26	0.53	0.15	0.29	-0.12	0.08	0.06	0.08	0.41	0.24	-0.05	-0.07

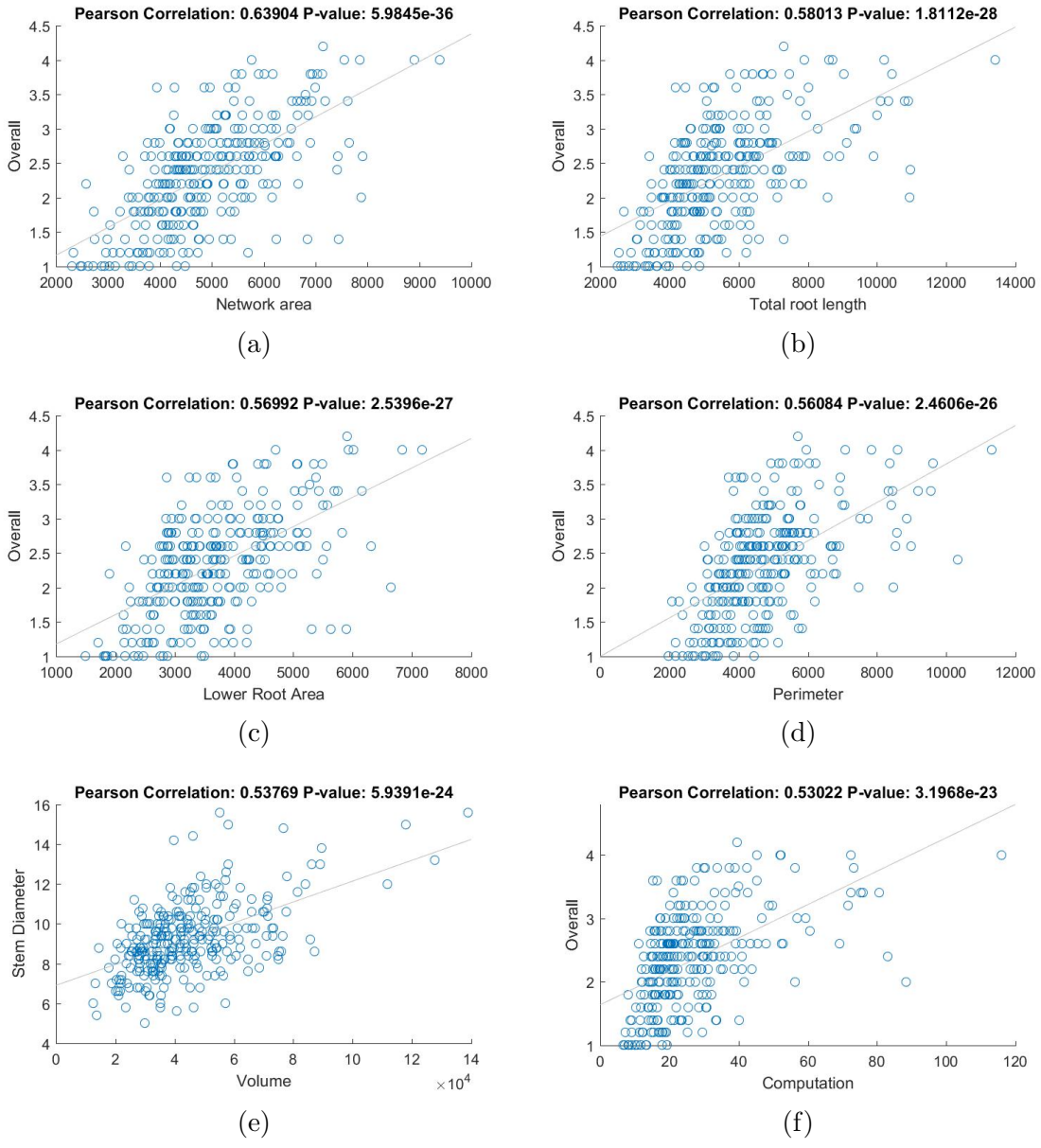

Figure 6.15: Best Pearson correlation values obtained for 2016 dataset between plot means of combined features of all cameras and the plot means of manual features.

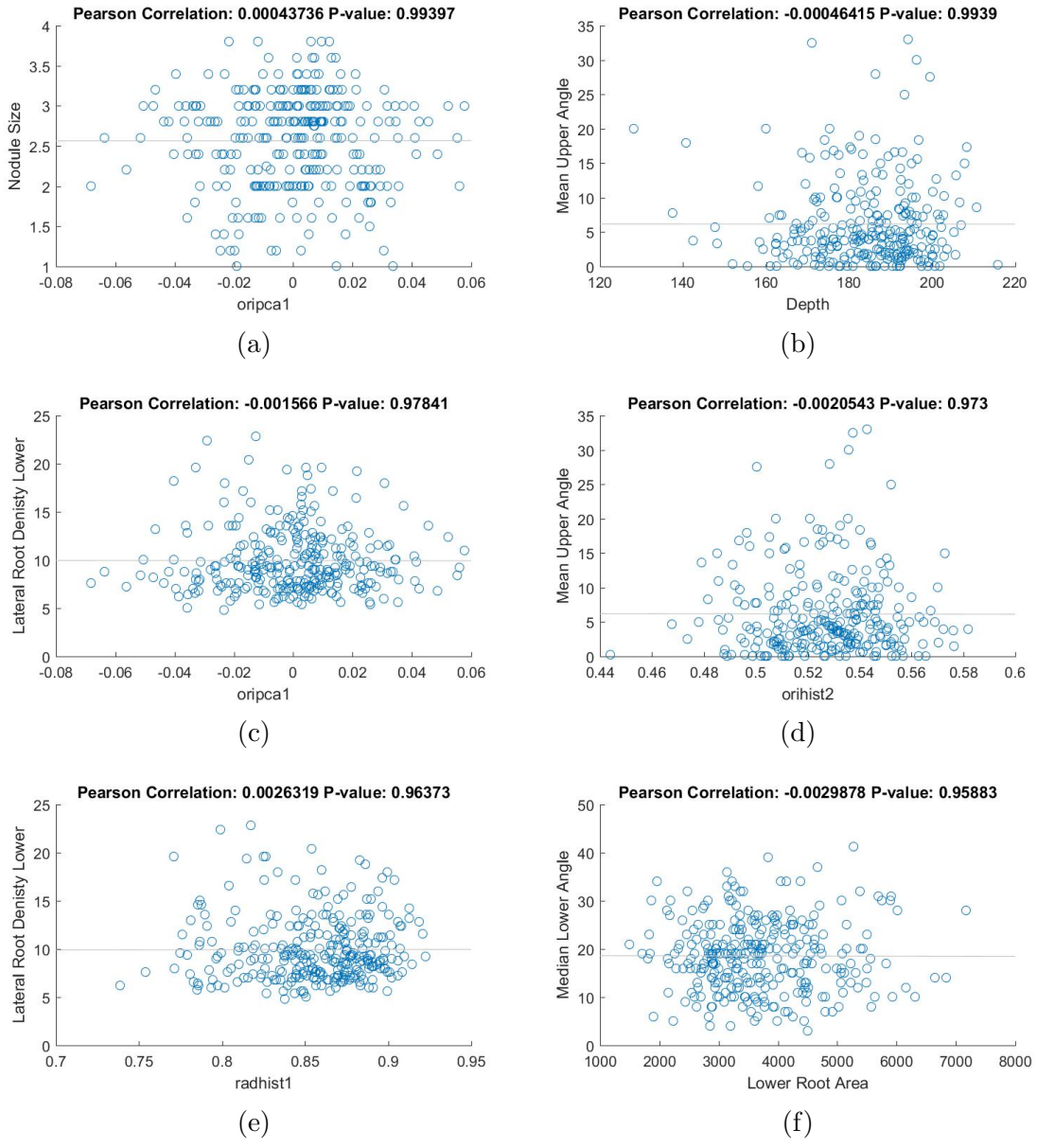

Figure 6.16: Trait combinations with least correlation for 2016 dataset between plot means of combined features of all cameras and the plot means of manual features.

The Tables 6.12, 6.13, 6.14 and 6.15 show the correlations between the features extracted by the DIRT system and the manually extracted features. The Table 6.12 shows the correlations between DIRT features extracted from the images of the front facing camera in the setup box. The Table 6.13 shows the correlations between DIRT features that were merged from the images of all the cameras. The Table 6.14 shows the correlations between DIRT features, that were averaged over the plot, from the images of the front facing camera in the setup box. The Table 6.15 shows the correlations between DIRT features that were averaged over plot, from the images of all the cameras in the setup box. For the DIRT features, merging is done by taking mean of the features from all the cameras as the difference in magnification between Canon G1X and Canon S110 is very small (Section 5.15). For each of these correlation tables, six highly correlated and least correlated feature combinations were plotted in the Figures 6.17, 6.18, 6.19, 6.20, 6.21, 6.22, 6.23, 6.24. The correlations between the features extracted using our multi-camera high-throughput phenotyping system is consistently better than the correlations between the DIRT features and the manually extracted features. We also observe that merging features from multiple cameras not only improved the correlation between the features extracted by our system and the manual features, but also improved the correlations between the DIRT features and the manual features. For example, the correlation between the DIRT features from the front facing camera, Skeleton vertices and Overall complexity is 0.56309 (Figure 6.17). This correlation improved to 0.57695 when the features from all the cameras were merged (Figure 6.19). This correlation further improved to 0.6017 when the features were averaged over plots (Figure 6.23). This is due to smoothing the outlier data that was present in individual camera data and the plant data in each plot.

Table 6.12: Pearson correlation values between the automatically extracted DIRT features of 2016 trait data and the manually extracted features. The feature values from the front facing camera, are used in the correlation analysis.

Feature Names	SD	TR	OC	NS	ND	NUR	LRDU	MDUA	MEUA	NLR	LRDL	MDLA	MELA
Skeleton Vertices	0.27	0.20	0.56	0.23	0.35	0.05	0.08	0.02	0.04	0.38	0.14	-0.00	-0.01
stemDia	0.43	0.30	0.05	0.08	0.04	0.03	-0.02	0.08	0.08	0.01	0.01	0.03	0.03
avg. Root Density	0.02	0.04	-0.02	-0.00	-0.01	-0.03	-0.05	0.03	0.02	0.02	-0.03	0.00	0.01
STA range	0.03	0.05	0.08	0.05	0.04	0.02	-0.04	0.04	0.04	0.08	0.05	-0.02	-0.03
STA dom. angle 1	-0.03	-0.01	-0.05	-0.02	-0.00	-0.02	-0.01	-0.00	0.01	-0.00	0.01	-0.03	-0.04
STA dom. angle 2	-0.02	-0.02	-0.05	-0.01	-0.00	0.01	0.00	0.05	0.07	-0.01	-0.00	0.01	0.00
STA 25% 1	0.06	0.10	0.01	0.02	0.02	0.02	0.04	-0.05	-0.06	0.03	0.03	-0.03	-0.03
STA 25% 2	-0.00	0.03	-0.02	-0.06	-0.03	-0.02	0.01	-0.02	-0.03	-0.01	0.03	0.03	0.02
STA 50% 1	-0.03	-0.02	0.02	0.03	0.00	0.02	0.05	-0.03	-0.03	0.02	0.05	0.01	0.03
STA 50% 2	-0.03	-0.05	0.02	-0.02	-0.00	-0.00	0.07	-0.01	-0.02	-0.01	0.05	0.12	0.12
STA 75% 1	0.06	0.04	0.03	0.02	0.01	0.02	0.08	-0.02	-0.02	0.02	0.04	-0.02	-0.02
STA 75% 2	0.04	-0.04	0.07	0.04	0.04	-0.01	0.07	0.02	0.02	-0.01	0.04	0.08	0.08
STA 90% 1	0.02	-0.02	0.01	-0.06	-0.04	-0.00	0.02	-0.07	-0.07	-0.02	-0.00	-0.00	-0.00
STA 90% 2	-0.02	-0.08	0.03	-0.05	-0.02	0.00	0.02	0.03	0.03	-0.06	0.02	0.10	0.10
RTA dom. angle 1	-0.00	-0.01	0.02	-0.02	-0.04	0.03	0.06	-0.07	-0.06	-0.03	-0.02	0.04	0.05
RTA dom. angle 2	-0.03	-0.07	0.01	-0.04	-0.04	0.01	0.03	-0.01	-0.01	-0.06	-0.02	0.11	0.12
STA min.	-0.03	-0.05	-0.07	-0.05	-0.03	-0.02	0.05	-0.04	-0.04	-0.08	-0.04	0.03	0.03
STA max.	-0.01	0.01	0.07	0.05	0.06	0.05	0.05	0.02	0.03	0.05	0.07	0.04	0.05
STA median	-0.05	-0.10	-0.06	-0.05	-0.04	-0.01	0.00	0.01	0.00	-0.04	-0.04	0.03	0.03
RTA range	-0.11	-0.12	0.07	-0.05	0.03	-0.04	0.02	0.13	0.12	-0.00	0.04	0.30	0.31
RTA min.	-0.01	-0.01	-0.02	0.01	0.02	-0.02	0.06	-0.02	-0.03	-0.02	-0.00	0.03	0.04
RTA max.	0.01	-0.03	0.15	0.10	0.10	0.06	0.04	0.04	0.04	0.04	0.03	-0.00	0.00
RTA median	0.01	-0.03	0.15	0.10	0.09	0.06	0.02	0.04	0.05	0.04	0.03	-0.01	-0.01
Nr. of RTPs	0.24	0.19	0.50	0.22	0.32	0.05	0.09	0.02	0.03	0.36	0.13	-0.01	-0.03
TD median	0.03	0.03	-0.00	0.03	-0.01	-0.03	-0.04	-0.01	-0.01	-0.00	-0.03	-0.02	-0.02
TD mean	0.05	-0.05	-0.13	-0.08	-0.11	0.13	0.03	-0.08	-0.08	-0.16	-0.07	0.03	0.04
DD90 max.	0.12	0.05	0.10	0.01	0.05	0.12	0.05	-0.07	-0.06	-0.00	-0.01	0.03	0.03
median Width	0.27	0.21	0.39	0.20	0.25	0.08	0.09	-0.00	0.01	0.21	0.07	-0.05	-0.05
max. Width	0.33	0.18	0.35	0.21	0.21	0.13	0.14	-0.02	-0.01	0.13	0.03	-0.10	-0.10
D10	-0.03	-0.06	0.07	0.07	0.05	0.00	0.05	0.11	0.10	0.01	-0.02	0.05	0.06
D20	0.00	-0.02	0.06	0.07	0.04	0.02	0.06	0.11	0.10	-0.01	-0.03	0.09	0.10
D30	0.02	0.01	0.06	0.06	0.04	0.03	0.06	0.11	0.11	-0.00	-0.04	0.12	0.13

D40	0.04	0.04	0.06	0.05	0.04	0.05	0.06	0.11	0.11	0.01	-0.04	0.13	0.14
D50	0.05	0.07	0.06	0.06	0.04	0.06	0.06	0.10	0.10	0.01	-0.03	0.13	0.14
D60	0.06	0.09	0.07	0.07	0.05	0.06	0.06	0.09	0.09	0.02	-0.02	0.13	0.14
D70	0.07	0.11	0.09	0.07	0.07	0.05	0.06	0.08	0.08	0.03	-0.01	0.13	0.13
D80	0.07	0.12	0.09	0.06	0.07	0.04	0.06	0.08	0.08	0.05	0.01	0.10	0.11
D90	0.07	0.13	0.10	0.07	0.07	0.03	0.06	0.06	0.06	0.08	0.03	0.08	0.09
DS10	-0.07	-0.05	-0.06	-0.01	-0.01	-0.02	-0.02	-0.07	-0.07	-0.04	0.03	-0.13	-0.13
DS20	-0.09	-0.11	-0.07	-0.01	-0.04	-0.04	-0.04	-0.03	-0.03	-0.06	0.02	-0.14	-0.15
DS30	-0.11	-0.14	-0.09	-0.02	-0.07	-0.05	-0.03	-0.01	-0.01	-0.08	-0.01	-0.12	-0.11
DS40	-0.10	-0.15	-0.09	-0.06	-0.09	-0.06	-0.03	-0.00	-0.01	-0.10	-0.05	-0.06	-0.05
DS50	-0.08	-0.13	-0.11	-0.07	-0.10	-0.04	-0.04	0.01	0.01	-0.09	-0.07	-0.05	-0.05
DS60	-0.07	-0.11	-0.15	-0.07	-0.12	0.00	-0.01	-0.00	-0.00	-0.11	-0.06	-0.01	-0.01
DS70	-0.05	-0.09	-0.14	-0.03	-0.10	0.04	-0.01	0.00	0.00	-0.12	-0.07	0.05	0.04
DS80	-0.03	-0.07	-0.13	-0.07	-0.09	0.01	-0.02	0.02	0.02	-0.13	-0.09	0.07	0.06
DS90	-0.00	-0.03	-0.13	-0.04	-0.06	0.04	-0.00	0.06	0.05	-0.14	-0.10	0.06	0.06
spatial root distr. X	-0.03	-0.01	0.01	-0.01	0.05	0.03	-0.01	0.01	0.01	-0.01	-0.01	-0.01	-0.01
spatial root ditr. Y	-0.20	-0.09	-0.12	-0.05	-0.08	-0.17	-0.10	0.00	-0.00	-0.04	0.07	-0.05	-0.05
CPD 25	0.09	0.03	0.22	0.18	0.22	0.03	0.05	0.03	0.03	0.12	0.07	-0.02	-0.02
CPD 50	0.10	0.05	0.22	0.16	0.20	0.02	0.03	-0.04	-0.03	0.14	0.07	-0.05	-0.05
CPD 75	0.07	0.06	0.16	0.13	0.14	0.01	0.02	-0.08	-0.07	0.11	0.05	-0.10	-0.09
CPD 90	0.03	0.01	0.02	0.04	-0.00	0.01	0.01	-0.10	-0.08	-0.00	0.03	-0.08	-0.08
computation time	0.30	0.21	0.50	0.22	0.31	0.07	0.13	0.01	0.04	0.31	0.14	-0.02	-0.03

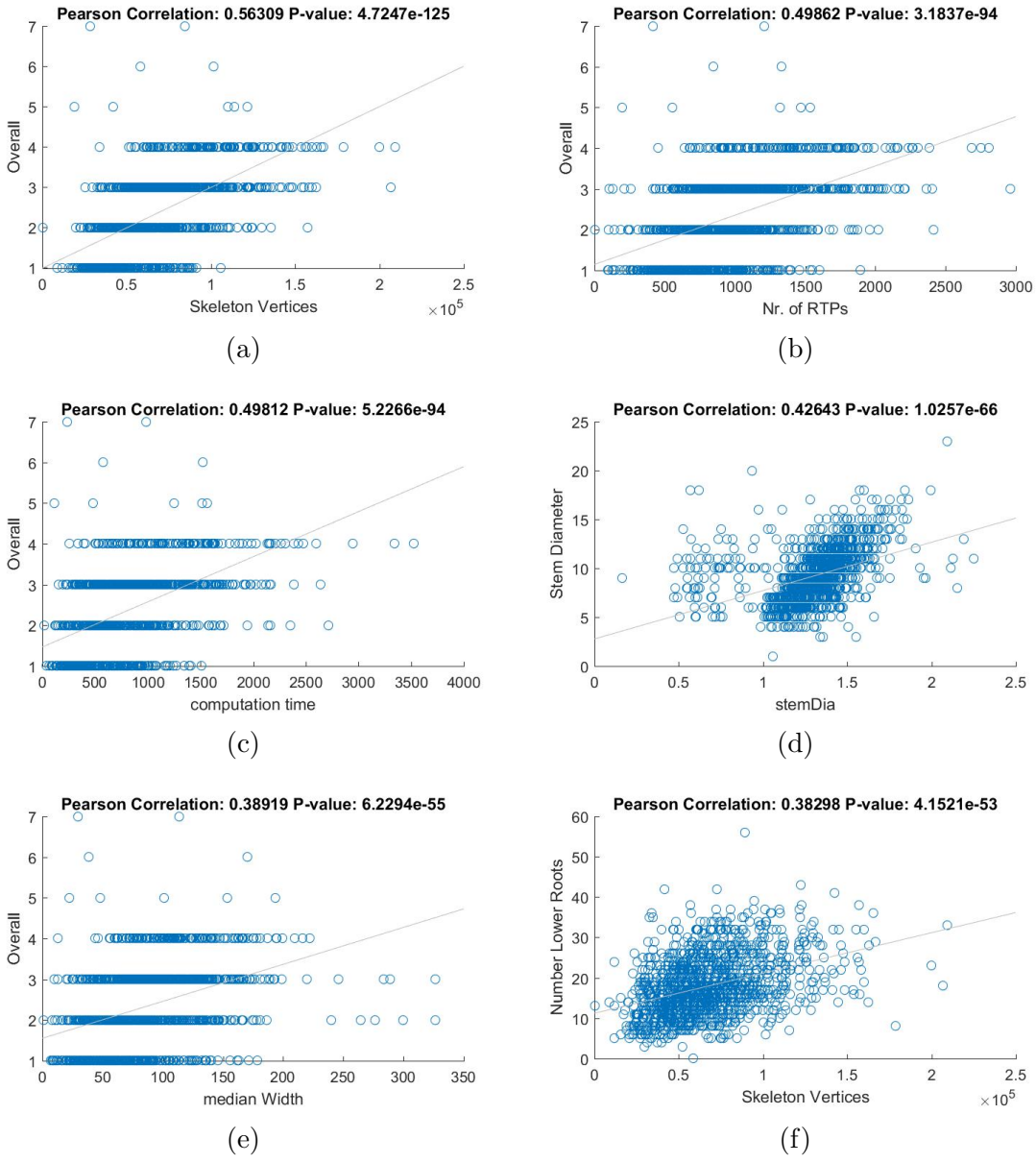

Figure 6.17: Best Pearson correlation values obtained between DIRT features from the front facing camera and the manual features for 2016 image dataset.

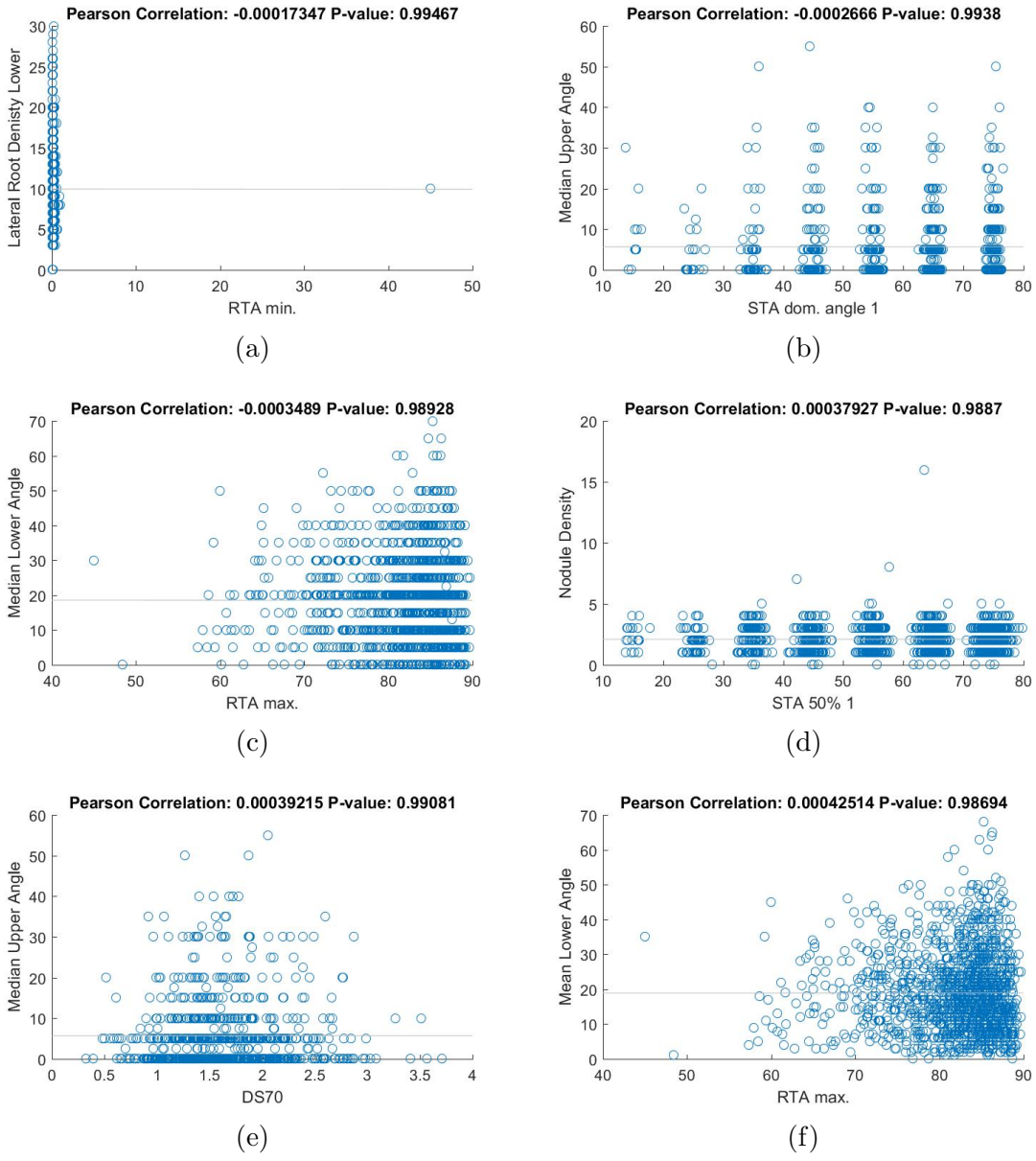

Figure 6.18: Trait combinations with least correlation between DIRT features from the front facing camera and the manual features for 2016 image dataset.

Table 6.13: Pearson correlation values between the automatically extracted DIRT features of 2016 trait data and the manually extracted features. The mean feature values from all the cameras, are used in the correlation analysis.

Feature Names	SD	TR	OC	NS	ND	NUR	LRDU	MDUA	MEUA	NLR	LRDL	MDLA	MELA
Skeleton Vertices	0.28	0.24	0.58	0.24	0.36	0.01	0.10	0.03	0.05	0.40	0.19	-0.01	-0.02
stemDia	0.53	0.38	0.07	0.09	0.04	0.03	-0.01	0.11	0.12	0.03	0.02	0.04	0.05
avg. Root Density	0.03	0.03	-0.06	-0.03	-0.05	-0.08	-0.08	0.08	0.07	-0.03	-0.04	0.03	0.04
STA range	0.02	0.02	0.10	0.05	0.05	0.02	0.02	0.04	0.05	0.11	0.06	0.02	0.02
STA dom. angle 1	0.03	0.03	-0.03	0.01	0.02	0.01	0.00	-0.00	-0.01	-0.02	0.01	-0.06	-0.07
STA dom. angle 2	0.01	-0.02	-0.06	0.02	0.03	0.02	-0.01	0.04	0.04	-0.02	-0.02	-0.01	-0.02
STA 25% 1	0.04	0.05	0.01	0.02	0.01	0.01	0.07	-0.02	-0.03	0.01	0.04	-0.03	-0.02
STA 25% 2	-0.01	-0.00	-0.01	-0.04	-0.04	-0.00	0.04	-0.00	-0.00	-0.05	0.02	0.04	0.04
STA 50% 1	0.01	0.00	0.04	0.08	0.04	0.01	0.05	-0.03	-0.04	0.01	0.00	-0.01	-0.00
STA 50% 2	-0.00	-0.02	0.02	0.04	0.01	0.01	0.05	0.00	0.01	-0.04	0.04	0.16	0.17
STA 75% 1	0.02	-0.02	0.03	0.03	0.01	0.01	0.04	-0.04	-0.04	-0.01	0.00	-0.03	-0.02
STA 75% 2	-0.04	-0.10	0.06	0.02	0.04	-0.00	0.03	0.01	0.02	-0.04	-0.01	0.10	0.11
STA 90% 1	-0.01	-0.04	-0.00	-0.02	-0.02	0.01	0.03	-0.05	-0.05	-0.02	-0.04	0.00	0.02
STA 90% 2	-0.06	-0.10	0.01	-0.04	-0.01	-0.01	0.00	0.04	0.04	-0.05	-0.03	0.15	0.17
RTA dom. angle 1	-0.02	-0.07	-0.01	-0.02	-0.04	-0.00	0.03	-0.06	-0.06	-0.06	-0.02	0.02	0.03
RTA dom. angle 2	-0.07	-0.11	0.01	-0.01	0.00	-0.02	0.02	-0.03	-0.02	-0.05	-0.00	0.14	0.15
STA min.	-0.04	-0.05	-0.14	-0.07	-0.08	-0.02	-0.01	-0.06	-0.06	-0.14	-0.05	0.00	0.00
STA max.	-0.02	-0.03	0.01	0.01	-0.02	0.00	0.01	-0.00	0.01	0.01	0.04	0.03	0.03
STA median	-0.04	-0.07	-0.09	-0.04	-0.04	-0.02	-0.01	-0.00	-0.00	-0.08	-0.00	0.04	0.04
RTA range	-0.13	-0.14	0.10	-0.05	0.04	-0.04	0.04	0.14	0.13	0.02	0.04	0.32	0.33
RTA min.	-0.04	-0.02	-0.02	-0.03	-0.03	-0.03	0.05	-0.03	-0.03	-0.04	-0.02	0.02	0.03
RTA max.	0.00	-0.08	0.20	0.10	0.12	0.07	0.05	0.01	0.01	0.01	-0.00	0.05	0.06
RTA median	0.01	-0.07	0.20	0.11	0.12	0.07	0.05	0.02	0.01	0.02	-0.00	0.05	0.05
Nr. of RTPs	0.25	0.23	0.52	0.23	0.34	0.01	0.11	0.02	0.04	0.38	0.19	-0.02	-0.03
TD median	0.06	0.02	-0.03	-0.01	-0.04	-0.02	-0.07	-0.05	-0.04	-0.05	-0.07	-0.02	-0.02
TD mean	0.08	-0.07	-0.12	-0.07	-0.12	0.20	0.03	-0.10	-0.10	-0.19	-0.16	0.05	0.06
DD90 max.	0.19	0.06	0.13	0.06	0.08	0.20	0.05	-0.09	-0.08	-0.02	-0.07	0.03	0.04
median Width	0.28	0.20	0.43	0.23	0.29	0.10	0.12	-0.02	-0.00	0.22	0.06	-0.04	-0.04
max. Width	0.37	0.20	0.40	0.24	0.24	0.13	0.16	-0.02	-0.01	0.16	0.04	-0.10	-0.11
D10	-0.06	-0.11	0.07	0.08	0.07	0.02	0.07	0.09	0.08	-0.01	-0.03	0.06	0.06
D20	-0.02	-0.08	0.06	0.08	0.05	0.04	0.08	0.10	0.09	-0.03	-0.05	0.10	0.11
D30	-0.00	-0.05	0.06	0.07	0.05	0.06	0.08	0.09	0.09	-0.03	-0.07	0.14	0.14

D40	0.01	-0.03	0.05	0.06	0.05	0.08	0.09	0.09	0.09	-0.03	-0.08	0.15	0.15
D50	0.02	-0.01	0.05	0.06	0.05	0.09	0.09	0.08	0.08	-0.02	-0.08	0.15	0.15
D60	0.03	0.01	0.05	0.06	0.06	0.10	0.09	0.07	0.07	-0.02	-0.07	0.15	0.15
D70	0.03	0.03	0.06	0.06	0.06	0.09	0.09	0.07	0.06	-0.01	-0.06	0.14	0.14
D80	0.03	0.05	0.07	0.06	0.07	0.08	0.08	0.06	0.06	0.01	-0.05	0.12	0.12
D90	0.03	0.06	0.09	0.07	0.07	0.06	0.07	0.06	0.05	0.05	-0.02	0.10	0.10
DS10	-0.06	-0.03	-0.07	-0.02	-0.02	-0.05	-0.03	-0.09	-0.09	-0.02	0.07	-0.16	-0.16
DS20	-0.09	-0.09	-0.07	-0.02	-0.05	-0.08	-0.05	-0.04	-0.05	-0.04	0.04	-0.17	-0.17
DS30	-0.10	-0.11	-0.08	-0.02	-0.06	-0.09	-0.04	-0.01	-0.01	-0.07	0.03	-0.13	-0.13
DS40	-0.08	-0.11	-0.09	-0.05	-0.09	-0.09	-0.05	0.01	0.00	-0.08	0.00	-0.07	-0.06
DS50	-0.07	-0.11	-0.11	-0.07	-0.11	-0.07	-0.05	0.03	0.03	-0.09	-0.03	-0.04	-0.04
DS60	-0.06	-0.11	-0.14	-0.07	-0.13	-0.01	-0.02	0.02	0.02	-0.11	-0.05	-0.01	-0.01
DS70	-0.04	-0.09	-0.14	-0.04	-0.11	0.03	0.00	0.00	-0.00	-0.11	-0.06	0.04	0.04
DS80	-0.02	-0.08	-0.16	-0.07	-0.10	0.02	0.01	0.02	0.02	-0.15	-0.10	0.07	0.06
DS90	-0.00	-0.04	-0.17	-0.05	-0.09	0.05	0.02	0.05	0.05	-0.18	-0.13	0.09	0.08
spatial root distr. X	-0.01	-0.01	0.01	-0.02	0.02	0.03	0.00	-0.00	0.01	0.00	0.02	-0.00	-0.01
spatial root ditr. Y	-0.23	-0.15	-0.15	-0.05	-0.08	-0.13	-0.11	-0.03	-0.04	-0.07	0.02	-0.06	-0.07
CPD 25	0.16	0.08	0.29	0.20	0.28	0.02	0.04	0.00	0.02	0.17	0.13	-0.04	-0.03
CPD 50	0.12	0.06	0.29	0.21	0.30	0.04	0.04	-0.02	-0.00	0.18	0.12	-0.08	-0.08
CPD 75	0.11	0.07	0.21	0.17	0.23	0.06	0.06	-0.06	-0.04	0.12	0.08	-0.11	-0.11
CPD 90	0.10	0.06	0.09	0.09	0.07	0.07	0.08	-0.11	-0.08	0.01	0.03	-0.09	-0.09
computation time	0.32	0.24	0.52	0.23	0.33	0.03	0.13	0.03	0.05	0.32	0.18	-0.02	-0.03

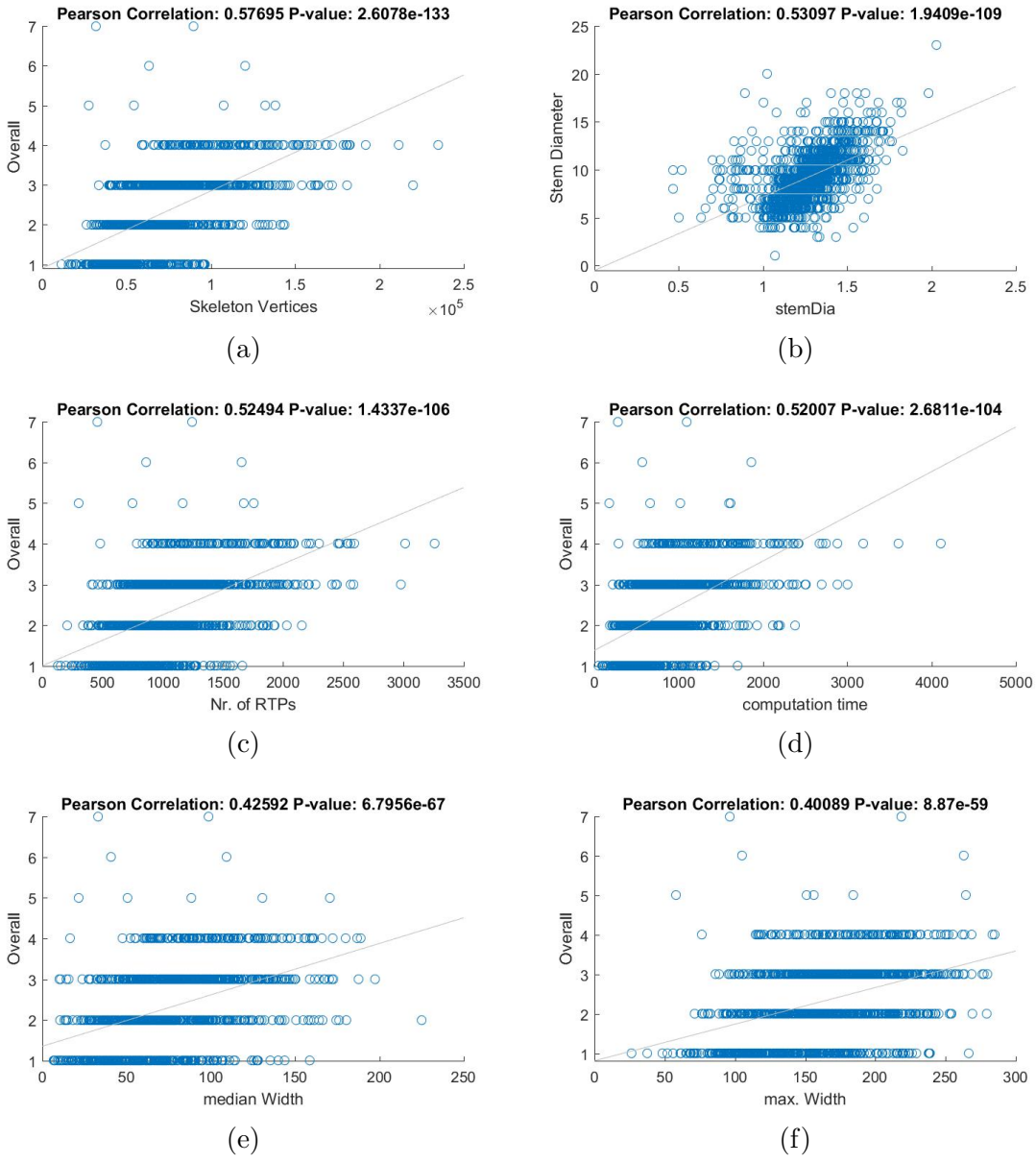

Figure 6.19: Best Pearson correlation values obtained between DIRT features from the combined mean features from all the cameras and the manual features for 2016 image dataset.

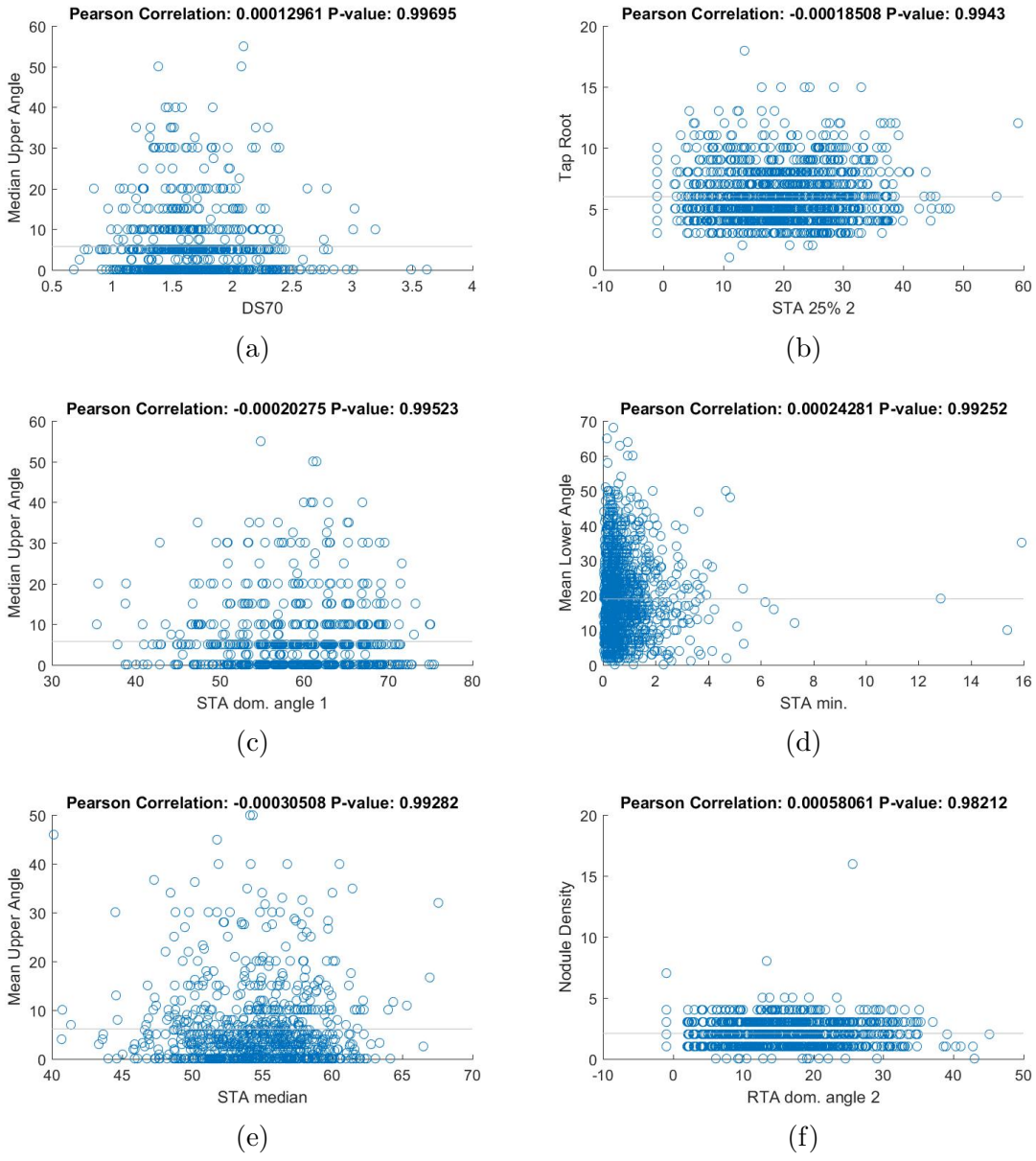

Figure 6.20: Trait combinations with least correlation between DIRT features from the combined mean features from all the cameras and the manual features for 2016 image dataset.

Table 6.14: Pearson correlation values between the automatically extracted DIRT features of 2016 trait data and the manually extracted features. The feature values from the front facing camera, averaged over plots, are used in the correlation analysis.

Feature Names	SD	TR	OC	NS	ND	NUR	LRDU	MDUA	MEUA	NLR	LRDL	MDLA	MELA
Skeleton Vertices	0.20	0.16	0.60	0.14	0.31	-0.02	-0.01	0.02	0.04	0.45	0.09	-0.02	-0.04
stemDia	0.51	0.35	-0.03	0.03	-0.01	0.01	-0.08	0.12	0.12	-0.06	-0.01	0.02	0.01
avg. Root Density	0.04	0.10	-0.04	-0.03	-0.06	-0.08	-0.08	0.07	0.06	0.03	-0.06	-0.00	0.00
STA range	0.06	0.10	0.07	0.04	0.04	0.01	-0.01	-0.02	-0.01	0.17	0.04	-0.00	-0.01
STA dom. angle 1	-0.05	-0.00	-0.10	-0.03	-0.05	-0.03	-0.03	-0.05	-0.05	-0.02	0.00	-0.08	-0.10
STA dom. angle 2	-0.02	-0.04	-0.07	-0.02	-0.06	-0.02	-0.04	0.04	0.05	0.08	-0.00	-0.07	-0.10
STA 25% 1	0.11	0.18	0.06	0.14	0.12	0.00	0.13	-0.04	-0.04	0.09	0.10	-0.06	-0.07
STA 25% 2	0.08	0.11	0.02	0.03	0.05	0.03	0.14	-0.03	-0.04	0.08	0.09	0.02	0.01
STA 50% 1	-0.01	0.07	0.00	0.06	0.05	0.04	0.06	-0.01	-0.02	0.03	-0.01	-0.03	-0.02
STA 50% 2	-0.03	0.02	-0.04	-0.03	-0.05	-0.03	0.11	0.04	0.02	-0.02	0.02	0.14	0.15
STA 75% 1	0.10	0.08	0.04	0.02	-0.01	0.01	0.00	-0.04	-0.04	0.04	0.07	-0.09	-0.09
STA 75% 2	0.11	-0.06	0.12	0.04	0.03	-0.08	0.10	0.00	0.02	0.00	0.10	0.10	0.11
STA 90% 1	0.05	-0.01	-0.00	-0.03	-0.08	-0.01	-0.03	-0.10	-0.09	-0.02	-0.01	-0.04	-0.04
STA 90% 2	0.05	-0.09	0.04	-0.05	-0.04	0.03	0.04	-0.05	-0.03	-0.13	0.07	0.16	0.15
RTA dom. angle 1	0.06	0.01	0.04	0.06	-0.03	0.02	0.00	-0.13	-0.12	-0.03	-0.02	0.03	0.04
RTA dom. angle 2	0.04	-0.07	0.06	0.04	-0.01	0.01	-0.00	-0.09	-0.08	-0.10	-0.02	0.15	0.15
STA min.	-0.06	-0.11	-0.06	-0.03	-0.02	0.00	0.02	0.02	0.01	-0.16	-0.03	0.00	0.01
STA max.	-0.03	-0.04	0.11	0.10	0.16	0.06	0.06	-0.00	0.01	0.09	0.12	-0.02	-0.02
STA median	-0.21	-0.21	-0.10	-0.15	-0.05	-0.02	0.02	0.04	0.05	-0.11	-0.01	0.03	0.03
RTA range	-0.06	-0.09	0.10	-0.15	-0.04	-0.05	0.02	0.11	0.09	-0.04	0.01	0.37	0.39
RTA min.	-0.02	-0.02	0.01	0.06	0.02	-0.04	0.01	0.01	0.00	-0.05	0.04	0.03	0.05
RTA max.	0.02	-0.08	0.21	0.16	0.16	0.15	-0.01	-0.01	-0.01	0.05	-0.06	-0.04	-0.03
RTA median	0.02	-0.08	0.21	0.14	0.15	0.15	-0.01	-0.01	-0.01	0.06	-0.06	-0.04	-0.03
Nr. of RTPs	0.20	0.18	0.53	0.16	0.31	-0.02	0.02	0.03	0.05	0.43	0.10	-0.04	-0.06
TD median	0.09	-0.11	-0.13	-0.07	-0.11	0.27	0.05	-0.08	-0.08	-0.22	-0.07	0.02	0.05
TD mean	0.09	-0.11	-0.13	-0.07	-0.11	0.27	0.05	-0.08	-0.08	-0.22	-0.07	0.02	0.05
DD90 max.	0.20	0.04	0.15	0.05	0.08	0.23	0.04	-0.14	-0.14	-0.08	-0.06	-0.00	0.01
median Width	0.34	0.24	0.50	0.16	0.27	0.12	0.00	-0.04	-0.04	0.27	0.02	-0.07	-0.08
max. Width	0.37	0.14	0.45	0.22	0.26	0.21	0.01	-0.08	-0.06	0.17	-0.06	-0.13	-0.15
D10	-0.03	-0.09	0.11	0.12	0.09	-0.03	0.06	0.03	0.04	0.05	-0.04	0.10	0.12
D20	0.00	-0.05	0.10	0.12	0.07	0.01	0.04	0.03	0.03	0.01	-0.09	0.16	0.18
D30	0.04	0.01	0.12	0.12	0.08	0.05	0.03	0.02	0.03	-0.00	-0.12	0.20	0.22

D40	0.07	0.07	0.13	0.12	0.09	0.06	0.02	0.03	0.03	0.01	-0.12	0.20	0.21
D50	0.10	0.11	0.14	0.13	0.10	0.05	0.00	0.03	0.04	0.03	-0.11	0.19	0.21
D60	0.13	0.15	0.17	0.13	0.11	0.04	-0.01	0.04	0.04	0.06	-0.09	0.20	0.21
D70	0.15	0.18	0.18	0.11	0.10	0.02	-0.02	0.05	0.04	0.09	-0.06	0.19	0.21
D80	0.15	0.21	0.17	0.09	0.07	-0.03	-0.02	0.06	0.06	0.12	-0.02	0.17	0.19
D90	0.14	0.23	0.18	0.10	0.06	-0.07	-0.01	0.07	0.07	0.19	0.03	0.13	0.15
DS10	-0.11	-0.11	-0.12	-0.03	-0.04	-0.08	0.08	-0.07	-0.06	-0.02	0.13	-0.22	-0.22
DS20	-0.13	-0.18	-0.17	-0.02	-0.08	-0.15	0.06	-0.01	0.01	-0.03	0.14	-0.22	-0.22
DS30	-0.20	-0.25	-0.22	-0.07	-0.15	-0.11	0.02	-0.01	0.01	-0.06	0.09	-0.13	-0.12
DS40	-0.19	-0.26	-0.22	-0.12	-0.15	-0.06	0.01	-0.02	-0.02	-0.16	-0.02	-0.01	-0.00
DS50	-0.20	-0.25	-0.25	-0.11	-0.15	0.02	0.02	-0.04	-0.03	-0.22	-0.09	-0.01	-0.01
DS60	-0.18	-0.23	-0.26	-0.08	-0.14	0.08	0.03	-0.04	-0.02	-0.24	-0.12	-0.01	-0.03
DS70	-0.07	-0.17	-0.18	0.01	-0.05	0.14	0.00	-0.02	-0.01	-0.24	-0.16	0.05	0.03
DS80	-0.04	-0.15	-0.15	-0.07	-0.08	0.11	-0.08	-0.03	-0.02	-0.28	-0.22	0.11	0.10
DS90	0.02	-0.09	-0.16	-0.05	-0.07	0.17	-0.09	-0.02	-0.02	-0.28	-0.23	0.17	0.17
spatial root distr. X	-0.05	-0.07	0.11	0.05	0.15	-0.01	0.01	0.01	-0.02	0.05	0.03	-0.02	-0.01
spatial root ditr. Y	-0.28	-0.03	-0.26	-0.11	-0.19	-0.32	-0.04	0.08	0.06	-0.09	0.15	-0.06	-0.05
CPD 25	0.10	-0.03	0.27	0.24	0.31	0.00	0.06	0.03	0.03	0.19	0.14	-0.12	-0.12
CPD 50	0.11	0.03	0.28	0.18	0.25	-0.01	0.07	-0.02	-0.01	0.23	0.16	-0.17	-0.16
CPD 75	0.08	0.07	0.19	0.11	0.15	-0.01	0.07	-0.01	0.01	0.15	0.15	-0.21	-0.19
CPD 90	0.07	0.02	0.03	0.03	0.01	0.03	0.06	-0.07	-0.05	-0.03	0.06	-0.20	-0.18
computation time	0.28	0.19	0.57	0.15	0.29	0.02	0.05	0.02	0.04	0.39	0.12	-0.02	-0.04

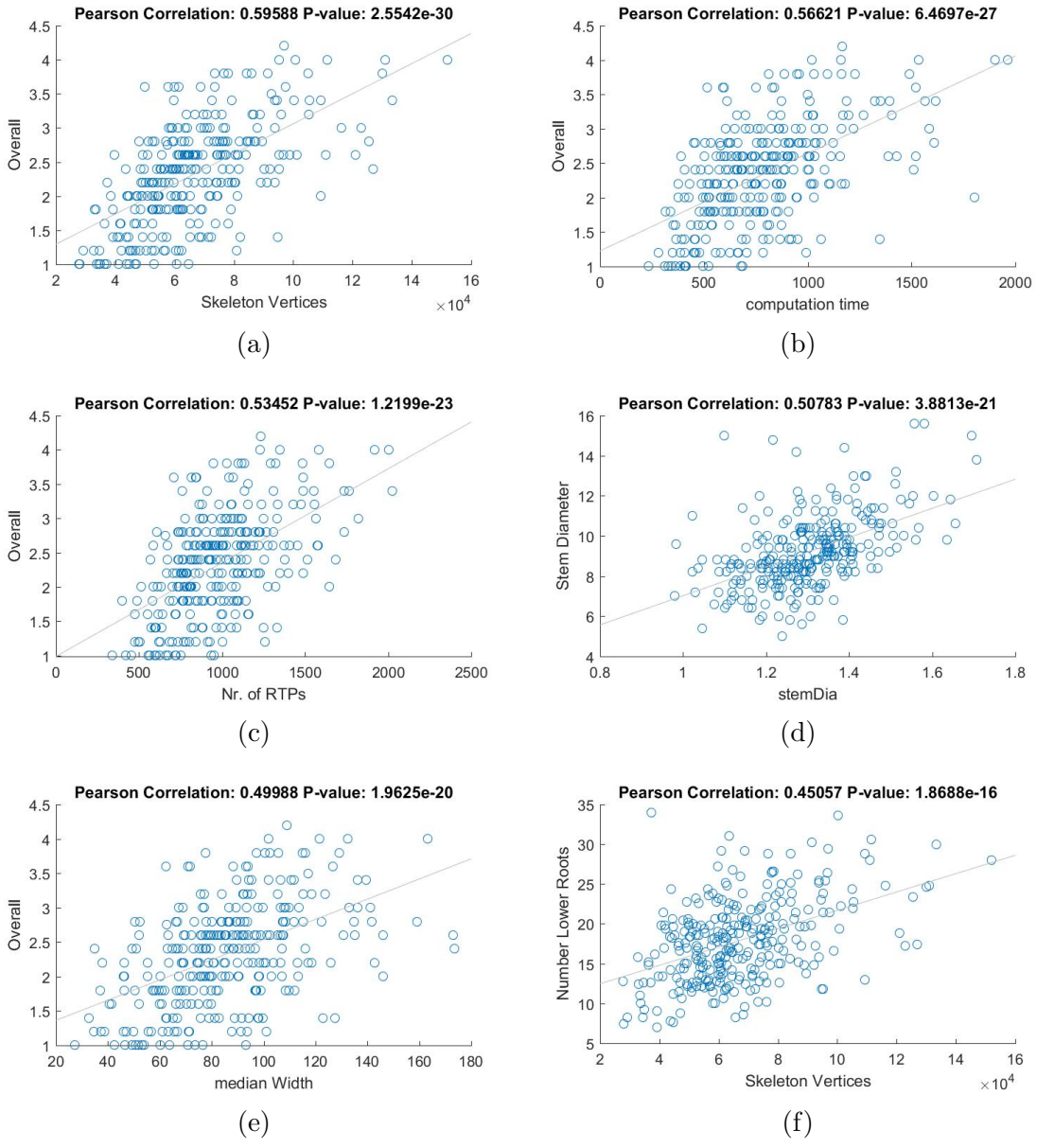

Figure 6.21: Best Pearson correlation values obtained between DIRT features from the front facing camera and the manual features for 2016 image dataset. The traits were averaged over plots before correlation analysis.

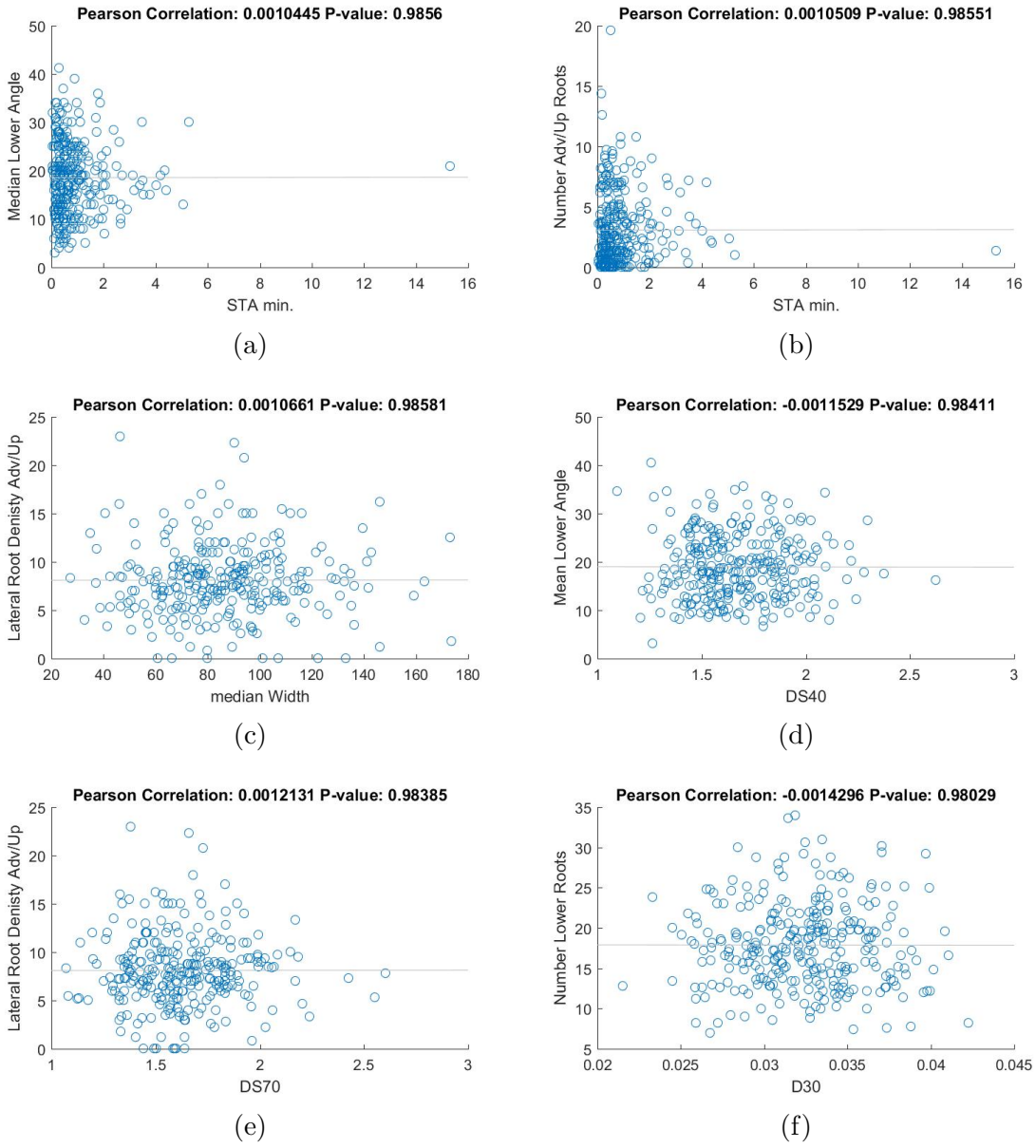

Figure 6.22: Trait combinations with least correlation between DIRT features from the front facing camera and the manual features for 2016 image dataset. The traits were averaged over plots before correlation analysis.

Table 6.15: Pearson correlation values between the automatically extracted DIRT features of 2016 trait data and the manually extracted features. The mean feature values from all the cameras, averaged over plots, are used in the correlation analysis.

Feature Names	SD	TR	OC	NS	ND	NUR	LRDU	MDUA	MEUA	NLR	LRDL	MDLA	MELA
Skeleton Vertices	0.22	0.22	0.60	0.16	0.32	-0.08	0.03	0.04	0.05	0.46	0.17	-0.04	-0.06
stemDia	0.58	0.41	-0.01	0.02	-0.01	-0.01	-0.09	0.16	0.16	-0.04	0.02	0.04	0.03
avg. Root Density	0.00	0.06	-0.15	-0.11	-0.14	-0.19	-0.11	0.15	0.15	-0.06	-0.01	0.02	0.04
STA range	0.01	0.02	0.15	0.07	0.11	-0.01	0.03	-0.01	0.01	0.20	0.04	0.00	0.00
STA dom. angle 1	0.03	0.12	-0.06	0.06	0.03	-0.00	0.01	-0.02	-0.02	0.03	0.12	-0.16	-0.18
STA dom. angle 2	0.01	-0.02	-0.09	0.00	-0.02	0.04	-0.07	0.05	0.05	-0.01	-0.01	-0.10	-0.12
STA 25% 1	0.09	0.11	-0.00	0.13	0.05	0.01	0.14	-0.06	-0.06	-0.00	0.17	-0.06	-0.05
STA 25% 2	0.05	0.06	0.01	-0.03	-0.04	0.09	0.07	-0.00	-0.01	-0.03	0.03	0.06	0.07
STA 50% 1	0.00	0.04	0.04	0.13	0.09	0.05	-0.01	-0.06	-0.07	0.02	-0.03	-0.01	0.00
STA 50% 2	-0.00	-0.02	-0.05	0.01	0.00	0.02	0.05	0.06	0.05	-0.09	0.01	0.20	0.23
STA 75% 1	0.07	0.02	0.09	0.07	0.05	0.03	-0.02	-0.09	-0.10	0.00	-0.02	-0.03	-0.01
STA 75% 2	0.03	-0.10	0.13	-0.01	0.03	0.05	0.03	-0.05	-0.05	-0.05	-0.04	0.13	0.16
STA 90% 1	-0.03	-0.06	0.02	0.01	-0.04	0.04	-0.00	-0.12	-0.14	-0.03	-0.07	0.00	0.03
STA 90% 2	-0.08	-0.14	-0.00	-0.11	-0.07	0.07	-0.02	-0.07	-0.08	-0.15	-0.08	0.22	0.24
RTA dom. angle 1	0.03	-0.07	0.02	0.03	-0.03	0.02	0.04	-0.09	-0.10	-0.06	-0.02	0.02	0.04
RTA dom. angle 2	-0.01	-0.10	0.06	0.04	0.04	0.04	0.02	-0.06	-0.06	-0.13	-0.02	0.18	0.21
STA min.	-0.04	-0.05	-0.20	-0.04	-0.10	-0.01	-0.04	-0.03	-0.04	-0.23	0.00	0.03	0.04
STA max.	-0.04	-0.03	0.01	0.06	0.05	-0.03	-0.00	-0.05	-0.03	0.05	0.06	0.05	0.05
STA median	-0.10	-0.12	-0.17	-0.05	-0.06	-0.06	-0.03	0.01	0.02	-0.14	0.04	0.06	0.06
RTA range	-0.12	-0.12	0.14	-0.12	0.02	-0.05	0.05	0.10	0.08	-0.01	0.02	0.38	0.40
RTA min.	-0.05	-0.01	-0.02	-0.06	-0.06	-0.03	0.00	0.01	0.00	-0.04	0.04	0.06	0.08
RTA max.	0.02	-0.13	0.25	0.13	0.15	0.20	-0.05	-0.05	-0.05	-0.00	-0.12	0.05	0.06
RTA median	0.02	-0.13	0.25	0.13	0.16	0.20	-0.06	-0.05	-0.05	0.00	-0.13	0.05	0.06
Nr. of RTPs	0.22	0.23	0.55	0.17	0.32	-0.09	0.05	0.04	0.06	0.44	0.18	-0.05	-0.08
TD median	0.11	0.04	-0.08	-0.04	-0.13	0.01	-0.16	-0.06	-0.08	-0.13	-0.15	-0.06	-0.05
TD mean	0.10	-0.14	-0.12	-0.06	-0.11	0.35	-0.02	-0.13	-0.13	-0.24	-0.19	0.04	0.06
DD90 max.	0.21	-0.02	0.12	0.04	0.05	0.35	-0.04	-0.18	-0.17	-0.11	-0.15	0.04	0.05
median Width	0.35	0.20	0.53	0.20	0.30	0.13	-0.00	-0.06	-0.06	0.26	0.01	-0.05	-0.06
max. Width	0.39	0.15	0.47	0.22	0.27	0.19	0.03	-0.09	-0.07	0.19	-0.04	-0.13	-0.15
D10	-0.07	-0.19	0.11	0.15	0.12	0.04	0.10	-0.00	0.01	0.02	-0.09	0.09	0.10
D20	-0.03	-0.15	0.11	0.15	0.12	0.10	0.08	-0.00	0.00	-0.03	-0.14	0.15	0.16
D30	0.01	-0.11	0.11	0.14	0.12	0.14	0.06	-0.00	-0.00	-0.05	-0.18	0.19	0.20

D40	0.04	-0.07	0.11	0.13	0.12	0.16	0.04	0.00	0.01	-0.06	-0.20	0.20	0.21
D50	0.06	-0.03	0.12	0.14	0.13	0.17	0.03	0.01	0.01	-0.04	-0.20	0.20	0.21
D60	0.09	-0.00	0.13	0.14	0.13	0.17	0.01	0.01	0.01	-0.02	-0.18	0.20	0.21
D70	0.12	0.04	0.13	0.11	0.11	0.14	-0.00	0.02	0.01	0.00	-0.17	0.20	0.21
D80	0.12	0.07	0.14	0.10	0.10	0.10	-0.01	0.03	0.02	0.04	-0.14	0.18	0.20
D90	0.13	0.10	0.17	0.10	0.09	0.05	0.00	0.04	0.04	0.11	-0.08	0.15	0.16
DS10	-0.08	-0.04	-0.13	-0.06	-0.08	-0.16	0.09	-0.06	-0.05	0.02	0.21	-0.24	-0.25
DS20	-0.13	-0.12	-0.18	-0.05	-0.12	-0.24	0.06	0.00	0.02	-0.00	0.19	-0.22	-0.22
DS30	-0.20	-0.17	-0.18	-0.08	-0.14	-0.20	0.05	-0.00	0.01	-0.01	0.16	-0.15	-0.15
DS40	-0.18	-0.18	-0.22	-0.13	-0.18	-0.15	0.04	-0.02	-0.01	-0.12	0.08	-0.05	-0.04
DS50	-0.21	-0.21	-0.26	-0.14	-0.20	-0.05	0.03	-0.01	0.01	-0.22	-0.01	-0.02	-0.01
DS60	-0.21	-0.22	-0.25	-0.09	-0.13	0.05	0.04	0.00	0.01	-0.23	-0.07	-0.02	-0.03
DS70	-0.12	-0.18	-0.19	-0.01	-0.06	0.14	0.04	-0.02	-0.01	-0.24	-0.12	0.06	0.04
DS80	-0.06	-0.16	-0.22	-0.08	-0.09	0.12	-0.04	-0.01	0.00	-0.30	-0.18	0.11	0.09
DS90	-0.03	-0.12	-0.22	-0.07	-0.09	0.17	-0.07	-0.01	-0.02	-0.33	-0.24	0.18	0.17
spatial root distr. X	0.01	-0.06	0.10	0.06	0.13	0.01	0.07	0.03	0.03	0.08	0.11	-0.05	-0.06
spatial root ditr. Y	-0.32	-0.16	-0.27	-0.08	-0.15	-0.23	-0.05	0.04	0.02	-0.15	0.05	-0.08	-0.07
CPD 25	0.14	0.05	0.33	0.23	0.35	-0.02	0.09	-0.03	-0.01	0.22	0.21	-0.13	-0.12
CPD 50	0.11	0.04	0.36	0.22	0.34	0.02	0.12	-0.05	-0.02	0.24	0.21	-0.21	-0.20
CPD 75	0.13	0.07	0.30	0.18	0.26	0.05	0.14	-0.08	-0.05	0.17	0.19	-0.25	-0.24
CPD 90	0.19	0.06	0.16	0.11	0.14	0.12	0.13	-0.16	-0.11	-0.02	0.08	-0.22	-0.19
computation time	0.31	0.24	0.57	0.16	0.30	-0.05	0.06	0.03	0.05	0.39	0.18	-0.04	-0.06

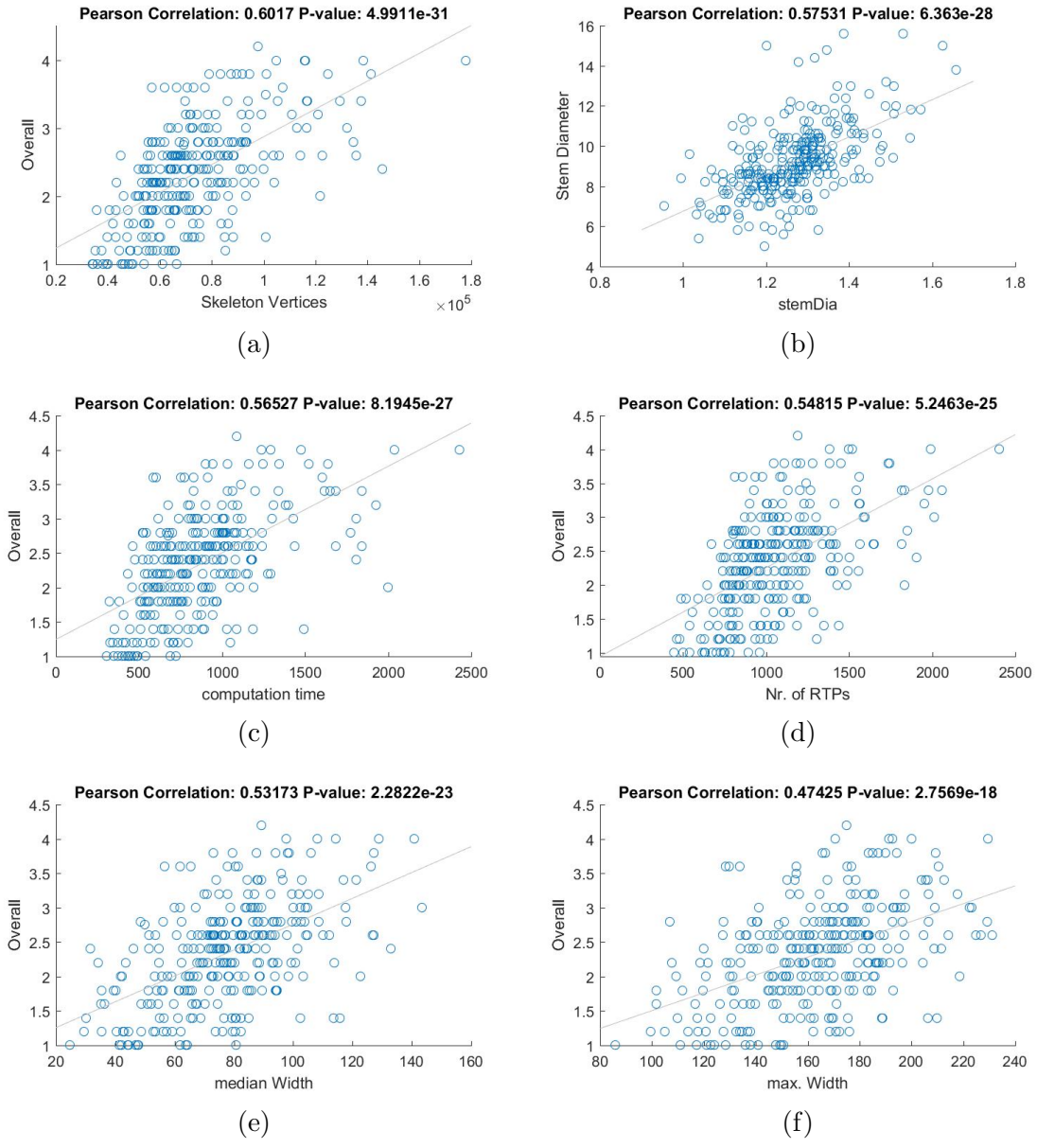

Figure 6.23: Best Pearson correlation values obtained between DIRT features from the combined mean features from all the cameras and the manual features for 2016 image dataset. The traits were averaged over plots before correlation analysis.

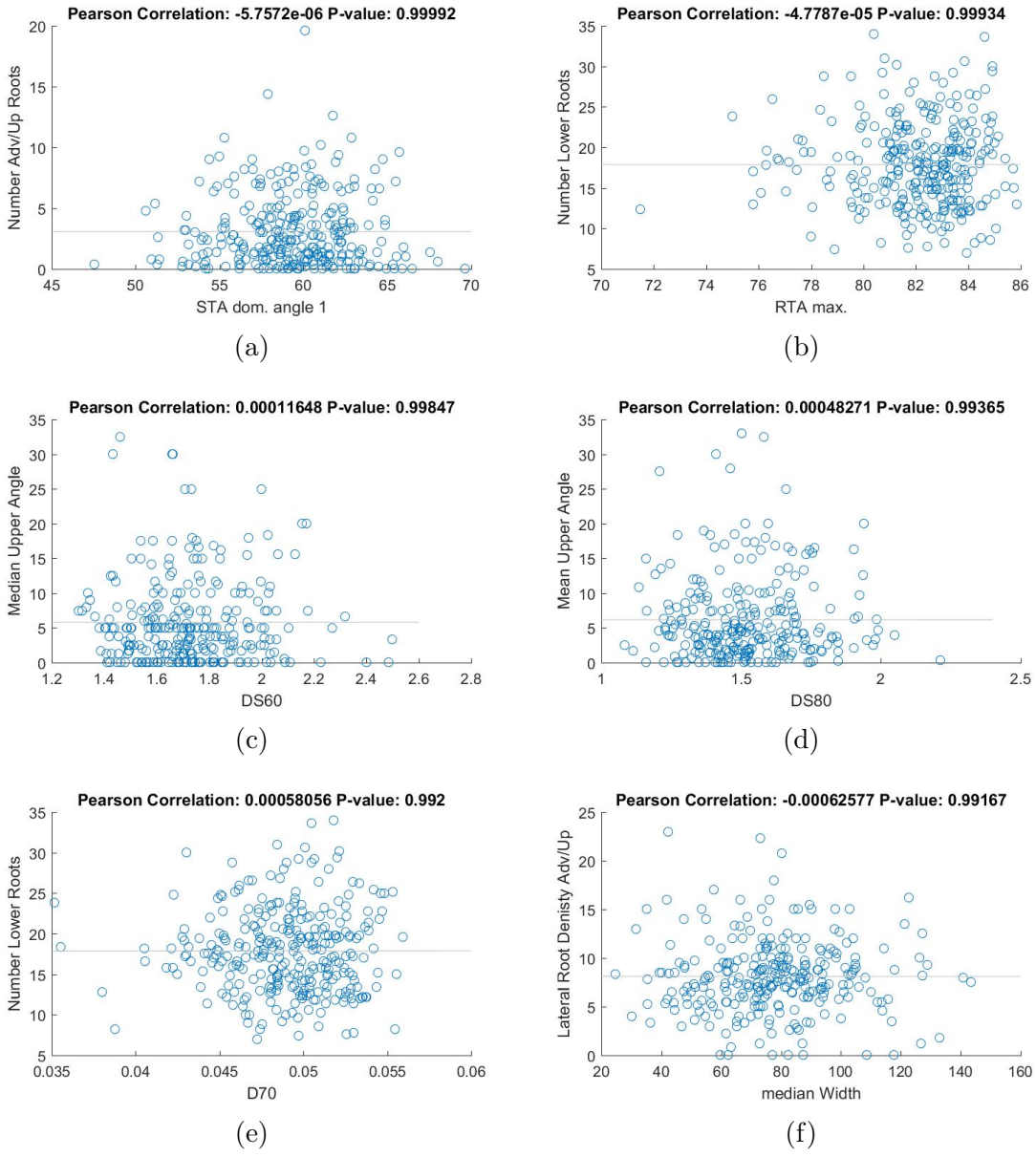

Figure 6.24: Trait combinations with least correlation between DIRT features from the combined mean features from all the cameras and the manual features for 2016 image dataset. The traits were averaged over plots before correlation analysis.

6.3 Average standard deviation of digital traits across cameras

The Tables 6.16 and 6.17 show the average standard deviation for each feature trait across all the cameras. The features Total root length, Depth, Maximum width, Network area, Convex area, Perimeter, Average radius, Volume, Surface area, Maximum radius and Lower Root Area are first converted from pixel units to the physical units before computing the average standard deviation of traits across the cameras. The physical unit for length used is millimeters, for area it is mm^2 and for Volume trait, we converted the feature value to mm^3.

From the Tables 6.16 and 6.17, we observe that the features have reasonable standard deviations across the cameras. For example, when a plant root is viewed from a different angle using a camera, it records new roots that may not be recorded when the images were taken at other angles. As a result a number of lateral roots can be observed which adds up to the total root length for the image taken from a specific angle. Specifically, the SD increases in cases where the plant root spreads in one plane instead of spreading equally in all directions. It is due to this observation of new roots when viewed at various angles, we also observe large variance for the convex area volume and surface area features.

We also observe that there is a significant increase in the standard deviation of the features for the data imaged in the years 2015 and 2016. This is because in the year 2015, we collected images from both soybean and cotton plant roots. These cotton plant roots have similar size compared to the soybean plant roots, with a much simpler root system architecture. Further, a majority of soybean plant roots imaged in 2015 have simpler root system architecture compared to the images taken in 2016.

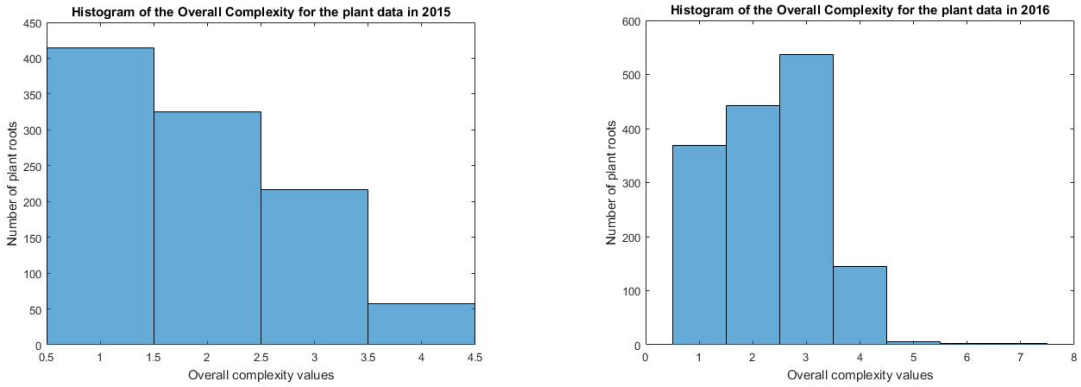

(a) (b)

Figure 6.25: Histograms of the overall complexity manual feature for the years 2015 and 2016.

The Figure 6.25 show the number of plant roots that were manually assigned various overall complexity values for the datasets of the years 2015 and 2016. From these figures, in case of simpler root architectures, all the cameras capture all the lateral roots, without having the problem of some front lateral roots obstructing the view of other lateral roots in the image. As a result, all the cameras identify many sub-roots of the plant root, resulting in the extracted features having lesser variance among the cameras.

Considering that these features have the physical units of mm, mm^2 and mm^3, we observe that these standard deviations are within reasonable limits for the corresponding features.

Table 6.16: Average SD of the traits across all the cameras for the data collected in the year 2015. The mean feature values averaged over plot from all the cameras are used in the correlation analysis.

Feature Names	Average Standard Deviation across cameras
Median no. of roots	0.82
Maximum no. of roots	3.82
Total root length	409.01
Depth	10.05
Maximum width	31.16
Width-to-depth ratio	0.24
Network area	270.62
Convex area	3238.71
Solidity	0.03
Perimeter	332.87
Average radius	0.08
Volume	3601.3
Surface area	2262.55
Maximum radius	0.47
LowerRootArea	292.73
radhist1	0.04
radhist2	0.05
radhist3	0.04
radhist4	0.03
radhist5	0.02
radhist6	0.02
radhist7	0.02
radhist8	0.02
radhist9	0.02
radhist10	0.02
orihist1	0.03
orihist2	0.06
orihist3	0.05
orihist4	0.05
orihist5	0.06
orihist6	0.03
holes	80.8

Table 6.17: Average SD of the traits across all the cameras for the data collected in the year 2016. The mean feature values from all the cameras are used in the correlation analysis.

Feature Names	Average Standard Deviation across cameras
Median no. of roots	1.65
Maximum no. of roots	7.15
Total root length	1008.68
Depth	13.14
Maximum width	28.32
Width-to-depth ratio	0.17
Network area	578.55
Convex area	3536.67
Solidity	0.03
Perimeter	808.52
Average radius	0.13
Volume	9546.53
Surface area	4689.29
Maximum radius	0.79
Lower Root Area	596.74
radhist1	0.02
radhist2	0.03
radhist3	0.03
radhist4	0.02
radhist5	0.01
radhist6	0.01
radhist7	0.01
radhist8	0.01
radhist9	0.01
radhist10	0.01
orihist1	0.02
orihist2	0.04
orihist3	0.03
orihist4	0.03
orihist5	0.03
orihist6	0.01
holes	535.4
radpca1	0.04
radpca2	0.03
radpca3	0.02
oripca1	0.07
oripca2	0.07
oripca3	0.03
Computation	12.46

Chapter 7

Summary and concluding remarks

In this study we designed a new multi-camera plant root phenotyping system which is capable of imaging the plant roots at hundreds of root per day. Additionally we implemented a reliable segmentation algorithm which can efficiently retrieve the root structure from the images. The segmentation program implemented is also capable of utilizing advanced CPU and GPU resources present on the PC to achieve faster segmentation rates without compromising on the quality of the segmentation process. We have extracted a variety of features, some are based on the size and appearance of the plant root, while other features extracted were intended to extract hidden structures or additional information about the plant roots. We are also comparing our methods and our extracted features and found to be faster, more similar to the manually extracted features than the current existing methods. We have also shown through various experiments that this system is much faster and is more suitable for high-throughput phenotyping as we optimized every step from the imaging process to the feature extraction process. Finally, we have shown that with the features from the

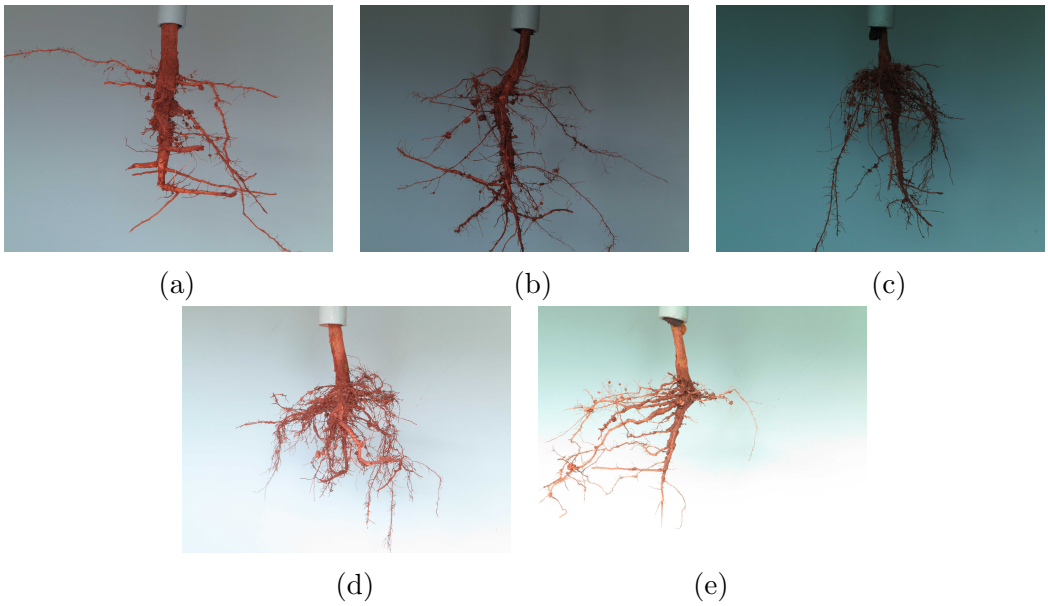

Figure 7.1: Images taken at different times of the day.

multi-camera high-thorughput phenotyping system, we can extract better correlated features than using single camera phenotyping systems. Our system is also much faster than the single camera systems that take images of plant roots from different perspectives with the help of a turn table.

Future directions in improving this system includes improving the segmentation process so that we no longer have the need to install advanced hardware to run the segmentation program. Here, we discuss one idea that may finally lead to the segmentation program become computationally less intensive. Consider the images shown in the Figure 7.1. These images, taken in 2016, show a lot of variation of background colors from image to image. Since, one of the faces of the experimental setup box is covered with cloth, there may be a chance for sunlight to enter into the box, which leads to several background colors in several images. Segmenting all these images requires EM algorithm to perform several iterations before retrieving

the plant root structure. Sometimes the segmentation may result in bad output due excessive light or too much darkness in the setup box. The kind of internal lights that we select also changes the background color. In such a case, instead of running EM on every image, we get the histograms of the red, green and blue channels of the images and cluster them into groups having similar histograms. For each of these groups, we run EM algorithm on one or two images in the group and save the parameters obtained from the output of the EM algorithm. When a new image of similar histogram arrives from the imaging box, we try to match the histogram of the new image with the histograms of the clusters. The cluster that has the most similar histogram will be identified and its stored parameters of the EM algorithm are retrieved Using these parameters, we proceed towards directly retrieving the plant root structure. This procedure eliminates the need for having a high-end hardware accelerated system and further improves the segmentation speed.

Future improvements in image feature extraction include new features such as the extraction of root angles from the images. This task may be challenging, because the angles determined from one image need not necessarily be the real root angle measured manually. This is because the angle at which the image is taken may change the measurement of root angle. Another improvement is, to explore better ways of merging the features from multiple cameras instead of using the mean across all the cameras. For example, for the image trait called maximum width, instead of taking mean across all the cameras for the maximum width, it would be better to take the maximum value across all the cameras. This will enable us to move closer to the manually extracted features and improve correlation.

Finally, with this current experimental setup and the software for phenotyping

traits from the images, we can also proceed towards analysis on genotype separability. This will also allow us to perform some experiments on variation of traits in genotype, identification of genotypes that contribute specific traits or even identify candidate genotypes for drought resistance.

Appendix A

Programming the Camera System

This section describes how cameras are mounted in the setup box and programmed so that these cameras take photos of the same plant root at different angles.

Controlling Canon PowerShot cameras remotely or by using USB requires a special software to be installed on the SD Card called CHDK (short form for Canon Hacker Development Kit). CHDK is a firmware enhancement program that allows user to perform enhanced operations by the user, which would not be possible otherwise. It allows user to perform variety of tasks such as remote control, control the camera through a USB interface, programmatically change focal length, aperture, exposure time, ISO speed, change modes of the camera such as macro mode, manual focusing and even taking pictures remotely and downloading them. The easiest way to install CHDK on a Canon camera is done by the tool called STICK [46]. Stick program easily installs CHDK on the SD card. We can always remove the CHDK installation by deleting the CHDK files on the SD card or by formating the SD card after backing up all the image data. After installing the CHDK on the SD cards of all the cameras that

we wish to control, we can check the CHDK installation by turning on the cameras. Immediately after turning the cameras on, we see a CHDK logo on the screen of the cameras. This confirms that the software has been installed successfully. For this study, we installed and collected data using CHDK version 1.3.

Before turning on, these cameras are mounted at specific positions in the experimental setup box. The power and USB cables are connected to the cameras. For an uninterrupted power supply, the power needs to be fed from a generator. The other end of the USB cables, each conencted to a different camera, are connected to a USB hub. A USB connector from the hub is connected to a PC, from which we control the cameras. After mounting the cameras, the cameras need to be turned on. A plant root is placed in the setup box for adjusting the cameras to focus the plant root. After turning on all the cameras, the cameras are started in "Play" mode, which are then initialized to "Rec" mode and camera parameters are set programmatically as discussed below. Adjustments are made so that the center of the root is seen in the white rectangle in the camera screens in all cameras. Once the cameras are adjusted, the cameras placed in a fixed position throughout the data collection and only plant root is replaced after imaging from all the cameras. We then take photos of each plant root by replacing the plant root in the setup box and typing the `shoot` command as described below. In order to successfully control the cameras from PC, the service named "gvfsd-gphoto2" needs to be turned off in Ubuntu OS. In case of controlling the cameras using windows, the service named "Windows Image Acquisition (WIA)" needs to be turned off. This section describes controlling the cameras using an Ubuntu 15.10 PC. Controlling the cameras now requires installing a program called chdkptp. It is a client program which is available for free [39].

We assume that the chdkptp is installed on `/chdk` directory. To start the client program, we open a terminal and type the following commands.

```
ubuntu@ubuntupc:~$ cd ./chdk/lua
ubuntu@ubuntupc:~/chdk/lua$ ../chdkptp-sample.sh -i
___> !mc=require('multicam')
___> !mc:connect()
```

`multicam` is a LUA mmodule in chdkptp that enables us to interface our PC with multiple Canon cameras simultaneously. In our study, we used 6 cameras to image a plant root. Hence, after running the `connect` command above, we see a message that all the 6 cameras are connected showing all the connected cameras' serial IDs.

Before starting to take photos of plant roots, we delete any previous photos in these SD card memory to get some space to store new photos. To delete any previous photos in the cameras, type the following command in the prompt:

```
___> !mc:delete()
```

The `delete` command deletes all the photos from all the cameras and starts the main script to process further commands. The delete is not implemented in the original version of chdkptp. This function, along with the functions described below were implemented as a part of the study. Before running the command we need to make sure the photos in the cameras are backed up (or downloaded to a pc). To download the existing photos from the cameras to the PC, we used the following command:

```
___> !mc:download('../day1_my_timestamp')
```

The `download` command above creates a folder named `day1_my_timestamp` inside the folder 'chdk' located in the home folder. The `download` command is implemented in this study such that when downloading the images from multiple cameras, the command creates sub-folders with the names equal to the unique numbers assigned to the cameras as described in 3. Hence, all the photos of 'camera 1' are found in the following location.

```
~/chdk/day1_my_timestamp/1/
```

Similarly for other cameras (2-6). After the `download` command had downloaded all the photos from all the cameras, the cameras are again ready to take further commands from the prompt. Since, we now have backed up the photos in the cameras, we can now safely delete the photos from the cameras using 'delete' command described above. If we cannot backup the images due to some reason and we also cannot delete the photos, we can type the following command and continue shooting the plant roots:

```
___> !mc:start()
```

The 'start' command starts the CHDK multi-camera interface script in each of the cameras so that these cameras can now take further commands on setting camera parameters and shooting. The 'start' command is not needed when 'delete' or 'download' commands are used already.

The following command turns the cameras into record mode which is needed to take photos. The command also sets aperture for Canon G1X cameras (aperture for Canon S110 cameras cannot be set using CHDK interface. It can only be set manually), ISO speed and exposure time for all cameras. Since, we are taking images

of plant roots at a shorter distance, this command also sets the capture mode of all cameras to 'Macro mode'. Finally, the command also creates necessary directories for the shoot command to download the newly imaged pictures to PC. Each time the `shoot` command is executed, the images are recorded and are downloaded in the folders created by this command. Before calling the `initc` command, we need to set the variable `download_folder` to a suitable location and then call the `initc` command.

```
___> !mc:initc(768, 800, 640, 512)
```

Since we started the chdkptp program in `/chdk/lua` directory, a folder called `newimages` will be created in the chdk folder and all the subsequent calls to `shoot` command results in downloading the images to `/chdk/newimages` directory.

The first value (768) in the command sets the aperture for Canon G1X cameras. The aperture value is given in APEX96 format. The second value sets the ISO speed to 800 for all cameras. Througnout the shooting, these parameters need not be changed. The third and the fourth values set the exposure time (or shutter speed) for Canon S110 and Canon G1X cameras respectively. The exposure time units are specified in APEX96 format. The conversions between APEX96 format to seconds for exposure time is given in the Table A.1. Depending on the sunlight, we can adjust the shutter speed. When sunlight is bright and when the setup box is not completely isolated from external lighting, then we need to increase the APEX96 value of the exposure times. When it is getting dark, we need to decrease the APEX96 values of the cameras. Once, the cameras are initialized to the parameters above, we have to restart the cameras if we want to change the camera parameters. Hence, we need to manually turn off and turn on the cameras and type the command `initc` command

again. Now if it is getting dark in the field, we may want to change the exposure time, by typing the following command:

```
___> !mc:initc(768, 800, 608, 448)
```

The above command changes the exposure time of Canon S110 cameras from 1/101 s to 1/80 s and that of Canon G1X from 1/40 s to 1/32 s. We now have a brighter image taken at dark lighting. When the day becomes too dark, decreasing the APEX96 values to too low would affect the quality of images. In such a case, we turn on the lamps to increase the lighting in the setup box. A suitable range of APEX96 values of exposure time for Canon S110 cameras is 640, 608, 576, 544 and a suitable range of APEX96 values of exposure time for Canon G1X cameras is 512, 480, 448, 416.

Usually after running the `initc` command, we check if all the cameras are focusing the center of the plant root. That is the center of the root should be present in the 'white' rectangle on the camera screens. Hence, we adjust the cameras until all the cameras (including the camera located at the bottom of the setup box) are focusing the center of the root. Once the camera adjustment is complete we start shooting each root.

Each plant root comes from a plot having a plot number (for example 1001). Each plot may have 5 or 10 plant roots. To shoot each root, we implemented a command for this study that takes the following syntax:

```
___> !mc:shoot(1001, 1)
```

The shoot command makes each camera take two photos of the same root. The first value for the command is the plot number and the second value is the plant

Table A.1: Table for converting exposure time in APEX96 format to exposure time in seconds.

Exposure time in APEX96 format	**Exposure time in seconds**
-576	64
-544	50.8
-512	40.32
-480	32
-448	25.4
-416	20.16
-384	16
-352	12.7
-320	10.08
-288	8
-256	6.35
-224	5.04
-192	4
-160	3.17
-128	2.52
-96	2
-64	1.59
-32	1.26
0	1
32	1/1.26
64	1/1.59
96	1/2.00
128	1/2.52
160	1/3.17
192	1/4.00
224	1/5.04
256	1/6.35
288	1/8.00
320	1/10.08
352	1/12.70
384	1/16.00
416	1/20.16
448	1/25.40
480	1/32.00
512	1/40.32
544	1/50.80
576	1/64.00
608	1/80.63
640	1/101.59
672	1/128.00
704	1/161.27
736	1/203.19
768	1/256.00
800	1/322.54
832	1/406.37
864	1/512.00
896	1/645.08
928	1/812.75
960	1/1024.00

number. The shot images from all the cameras are downloaded to the directory specified by `download_folder` variable. We may wish to write a simple python script that watches the folders for new images from these cameras. Once the script finds a new image, we can implement the script to segment the image. That way, we can find the segmented image as we are collecting the images in the field and retake a plant root again if we observe that the quality of the image is not good.

Once we take images of 4 roots in a plot, the photos of 5th root in the plot is taken as follows:

```
___> !mc:shoot(1001, 5)
```

Once the plot is completed, we go to another plot to take the images. The first root in the next plot is taken as follows:

```
___> !mc:shoot(1002, 1)
```

We continue imaging as new plant roots are dug from the field. The `shoot` command makes the cameras to shoot two times the same root. The cameras then rename the newly created images based on the plant root number and the plot number. Hence, the images generated by each camera from the command above are `I1002_11.JPG` and `I1001_12.JPG`.

Bibliography

[1] Tino Colombi, Norbert Kirchgessner, Chantal Andrée Le Marié, Larry Matthew York, Jonathan P. Lynch, and Andreas Hund. Next generation shovelomics: set up a tent and rest. *Plant and Soil*, 388(1):1–20, 2015.

[2] Wikipedia. Climate change and agriculture — wikipedia, the free encyclopedia, 2016. `https://en.wikipedia.org/w/index.php?title=Climate_change_and_agriculture`.

[3] Alexander Bucksch, James Burridge, Larry M. York, Abhiram Das, Eric Nord, Joshua S. Weitz, and Jonathan P. Lynch. Image-based high-throughput field phenotyping of crop roots. *Plant Physiology*, 166(2):470–486, 2014.

[4] Anjali S Iyer-Pascuzzi, Olga Symonova, Yuriy Mileyko, Yueling Hao, Heather Belcher, John Harer, Joshua S Weitz, and Philip N Benfey. Imaging and analysis platform for automatic phenotyping and trait ranking of plant root systems. *Plant physiology*, 152(3):1148–1157, 2010.

[5] Randy T Clark, Robert B MacCurdy, Janelle K Jung, Jon E Shaff, Susan R McCouch, Daniel J Aneshansley, and Leon V Kochian. Three-dimensional root

phenotyping with a novel imaging and software platform. *Plant physiology*, 156(2):455–465, 2011.

[6] CHDK. Chdk home. `http://chdk.wikia.com/wiki/CHDK`.

[7] CHDK. Chdk user manual. `http://chdk.wikia.com/wiki/CHDK_User_Manual`.

[8] CHDK. Chdk scripting cross reference page. `http://chdk.wikia.com/wiki/CHDK_Scripting_Cross_Reference_Page`.

[9] Michael P. Pound, Andrew P. French, Jonathan A. Atkinson, Darren M. Wells, Malcolm J. Bennett, and Tony Pridmore. Rootnav: Navigating images of complex root architectures. *Plant Physiology*, 162(4):1802–1814, 2013.

[10] Guillaume Lobet, Loc Pags, and Xavier Draye. A novel image-analysis toolbox enabling quantitative analysis of root system architecture. *Plant Physiology*, 157(1):29–39, 2011.

[11] Arthur P Dempster, Nan M Laird, and Donald B Rubin. Maximum likelihood from incomplete data via the em algorithm. *Journal of the royal statistical society. Series B (methodological)*, pages 1–38, 1977.

[12] Yugan Chen and Xuecheng Zhou. Plant root image processing and analysis based on 2d scanner. In *Bio-Inspired Computing: Theories and Applications (BIC-TA), 2010 IEEE Fifth International Conference on*, pages 1216–1220. IEEE, 2010.

[13] Qian Huang, Anil K Jain, George C Stockman, and Alvin JM Smucker. Automatic image analysis of plant root structures. In *Pattern Recognition, 1992. Vol. II. Conference B: Pattern Recognition Methodology and Systems, Proceedings., 11th IAPR International Conference on*, pages 569–572. IEEE, 1992.

[14] I. Janusch, W. G. Kropatsch, and W. Busch. Topological image analysis and (normalised) representations for plant phenotyping. In *Symbolic and Numeric Algorithms for Scientific Computing (SYNASC), 2014 16th International Symposium on*, pages 579–586, Sept 2014.

[15] Yan Hua Chen, Qian Zhang, Bao Guo Li, and Bao Gui Zhang. Characterizing wheat root branching using a markov chain approach. In *Plant Growth Modeling and Applications, 2006. PMA'06. Second International Symposium on*, pages 70–73. IEEE, 2006.

[16] Leo A. Goodman T. W. Anderson. Statistical inference about markov chains. *The Annals of Mathematical Statistics*, 28(1):89–110, 1957.

[17] Stefan Mairhofer, Susan Zappala, Saoirse R. Tracy, Craig Sturrock, Malcolm Bennett, Sacha J. Mooney, and Tony Pridmore. Rootrak: Automated recovery of three-dimensional plant root architecture in soil from x-ray microcomputed tomography images using visual tracking. *Plant Physiology*, 158(2):561–569, 2012.

[18] X. Zhou, X. Cao, C. Zhang, H. Yan, Y. Li, and X. Luo. A method of 3d nondestructive detection for plant root in situ based on cbct imaging. In *2014 7th International Conference on Biomedical Engineering and Informatics*, pages 110–115, Oct 2014.

[19] William E. Lorensen and Harvey E. Cline. Marching cubes: A high resolution 3d surface construction algorithm. *SIGGRAPH Comput. Graph.*, 21(4):163–169, August 1987.

[20] Ying Zheng, Steve Gu, Herbert Edelsbrunner, Carlo Tomasi, and Philip Benfey. Detailed reconstruction of 3d plant root shape. In *Computer Vision (ICCV), 2011 IEEE International Conference on*, pages 2026–2033. IEEE, 2011.

[21] Paramita Basu, Anupam Pal, Jonathan P Lynch, and Kathleen M Brown. A novel image-analysis technique for kinematic study of growth and curvature. *Plant Physiology*, 145(2):305–316, 2007.

[22] Loc Pags, Carole Bcel, Hassan Boukcim, Delphine Moreau, Christophe Nguyen, and Anne-Sophie Voisin. Calibration and evaluation of archisimple, a simple model of root system architecture. *Ecological Modelling*, 290:76 – 84, 2014. Special Issue of the 4th International Symposium on Plant Growth Modeling, Simulation, Visualization and Applications (PMA12)Special Issue of PMA12.

[23] Norbert Kirchgeßner, Hagen Spies, Hanno Scharr, and Uli Schurr. Root growth analysis in physiological coordinates. In *Image Analysis and Processing, 2001. Proceedings. 11th International Conference on*, pages 589–594. IEEE, 2001.

[24] Elena Balestri, Davide de Battisti, Flavia Vallerini, and Claudio Lardicci. First evidence of root morphological and architectural variations in young posidonia oceanica plants colonizing different substrate typologies. *Estuarine, Coastal and Shelf Science*, 154:205 – 213, 2015.

[25] Yinjiang Jia, Zhongbin Su, and Hongmin Sun. Research on the model construction of soybean root system based on l-system. In *World Automation Congress (WAC), 2010*, pages 195–199. IEEE, 2010.

[26] Yao Fang, Wang Wenyong, Zhong Shaochun, Tian Ye, and Ye Linan. Modeling and research on growth of virtual plant wheat roots. In *2009 International Forum on Information Technology and Applications*, pages 264–267. IEEE, 2009.

[27] Bi Kun, Huang Feifei, Zhao Xin, and Wang Cheng. Image collection filed of plant roots based on hypoid mirror. In *Proceedings of the 2011 Fourth International Conference on Intelligent Computation Technology and Automation - Volume 02*, ICICTA '11, pages 563–567, Washington, DC, USA, 2011. IEEE Computer Society.

[28] D. G. Lowe. Object recognition from local scale-invariant features. In *Computer Vision, 1999. The Proceedings of the Seventh IEEE International Conference on*, volume 2, pages 1150–1157 vol.2, 1999.

[29] L Dupuy, Thierry Fourcaud, Alexia Stokes, and F Danjon. A density-based approach for the modelling of root architecture: application to maritime pine (pinus pinaster ait.) root systems. *Journal of Theoretical Biology*, 236(3):323–334, 2005.

[30] Nobuyuki Otsu. A threshold selection method from gray-level histograms. *Automatica*, 11(285-296):23–27, 1975.

[31] VR Pantalone, GJ Rebetzke, JW Burton, and TE Carter. Phenotypic evaluation of root traits in soybean and applicability to plant breeding. *Crop Science*, 36(2):456–459, 1996.

[32] Christopher N Topp, Anjali S. Iyer-Pascuzzi, Jill T. Anderson, Cheng-Ruei Lee, Paul R Zurek, Olga Symonova, Ying Zheng, Alexander Bucksch, Yuriy Mileyko,

Taras Galkovskyi, Brad T Moore, John Harer, Herbert Edelsbrunner, Thomas Mitchell-Olds, Joshua S. Weitz, and Philip N. Benfey. 3d phenotyping and quantitative trait locus mapping identify core regions of the rice genome controlling root architecture. *Proceedings of the National Academy of Sciences USA*, 110:E1695–E1704, 2013.

[33] Taras Galkovskyi, Yuriy Mileyko, Alexander Bucksch, Brad Moore, Olga Symonova, Charles A. Price, Christopher N. Topp, Anjali S. Iyer-Pascuzzi, Paul R. Zurek, Suqin Fang, John Harer, Philip N. Benfey, and Joshua S. Weitz. Gia roots: software for the high throughput analysis of plant root system architecture. *BMC Plant Biology*, 12(1):116, 2012.

[34] Corinna Cortes and Vladimir Vapnik. Support-vector networks. *Machine Learning*, 20(3):273–297, 1995.

[35] Christopher J.C. Burges. A tutorial on support vector machines for pattern recognition. *Data Mining and Knowledge Discovery*, 2(2):121–167, 1998.

[36] Christopher M. Bishop. *Pattern Recognition and Machine Learning (Information Science and Statistics)*. Springer-Verlag New York, Inc., Secaucus, NJ, USA, 2006.

[37] Larry Matthew York. Near final image box schematic, 03-august-2016 private communication. private communication, 2016.

[38] Larry Matthew York. Imaging box, 27-july-2016 private communication. private communication, 2016.

[39] CHDK. Chdk scripting cross reference page. https://github.com/simonswine/chdkptp.

[40] Michael E. Tipping. Sparse bayesian learning and the relevance vector machine. *J. Mach. Learn. Res.*, 1:211–244, September 2001.

[41] Cambridge in Color. Local contrast enhancement. http://www.cambridgeincolour.com/tutorials/local-contrast-enhancement.htm.

[42] Michael Reichmann. Contrast enhancement. https://luminous-landscape.com/contrast-enhancement/.

[43] Wikipedia. Image sensor format — wikipedia, the free encyclopedia, 2016. https://en.wikipedia.org/w/index.php?title=Image_sensor_format.

[44] Tom Dempsey. Compare digital camera sensor sizes: 1-type, 4/3, aps-c, full frame 35mm. http://photoseek.com/2013/compare-digital-camera-sensor-sizes-full-frame-35mm-aps-c-micro-four-thirds-1

[45] Wikipedia. 35 mm equivalent focal length — wikipedia, the free encyclopedia. https://en.wikipedia.org/wiki/35_mm_equivalent_focal_length.

[46] Dave Mitchell. Simple tool for installing chdk (stick). http://www.zenoshrdlu.com/stick/stick.html.